1971

Mechanism of vapors sorption on Fiberglas-E

Rodney Jau-wei Huang
Iowa State University

71-26,859

HUANG, Rodney Jau-wei, 1941-
MECHANISM OF VAPORS SORPTION ON FIBERGLAS-E.

Iowa State University, Ph.D., 1971
Engineering, civil

Mechanism of vapors sorption on Fiberglas-E

by

Rodney Jau-wei Huang

A Dissertation Submitted to the

Graduate Faculty in Partial Fulfillment of

The Requirements for the Degree of

DOCTOR OF PHILOSOPHY

Major Subject: Soil Engineering

Approved:

Signature was redacted for privacy.

In Charge of Major Work

Signature was redacted for privacy.

Head of Major Department

Signature was redacted for privacy.

Dean of Graduate College

Iowa State University
Of Science and Technology
Ames, Iowa

1971

Mechanism of vapors sorption on Fiberglas-E

by

Rodney Jau-wei Huang

An Abstract of

A Dissertation Submitted to the

Graduate Faculty in Partial Fulfillment of

The Requirements for the Degree of

DOCTOR OF PHILOSOPHY

Approved:

Signature was redacted for privacy.

In Charge of Major Work

Signature was redacted for privacy.

Head of Major Department

Signature was redacted for privacy.

Dean of Graduate College

Iowa State University
Of Science and Technology
Ames, Iowa

1971

Mechanism of vapors sorption on Fiberglas-E

Rodney Jau-wei Huang

Under the supervision of T. Demirel
From the Department of Civil Engineering
Iowa State University of Science and Technology

The mechanism of interaction of water vapor and benzene vapor with Fiberglas-E was investigated using sorption isotherm, sorption rate and infrared absorption experiments. E-glass, as received was the cleanest available, treated with deionized water when manufactured. Test samples were cut into 2 cm long fibers or ground into powder and screened to pass a No. 200 or a No. 400 sieve. The latter was further compressed into a pellet.

The surface free energies of wetting were computed from the adsorption isotherm data yielding values from -235 erg/cm^2 to -254 erg/cm^2 and -71.1 erg/cm^2 to -72.4 erg/cm^2 for water and benzene adsorption respectively, depending upon temperature, surface geometry and sample treatment. Less affinity for benzene adsorption resulting in smaller work of adhesion suggests that actual adhesion of hydrocarbons is impossible in the presence of bulk water.

The BET method was used to obtain the specific surface of E-glass. The surface areas so obtained were found to be ten times greater than the areas calculated from geometry. It was believed that the E-glass surface consists of fine micropores of about 23 Å in size. This should account for the great reduction of tensile strength when exposed to a moise environment. The increase in surface area and micropore size during

subsequent runs supports the proposition that the glass suffers loss of strength with age when exposed to moist atmosphere.

The isosteric heat of adsorption computed using the Clausius-Clapeyron equation gave good agreement with that computed from the BET parameters for the first layer of adsorbed molecules. The heat of adsorption reaches the heat of liquefaction beyond two to three layers of adsorbate on E-glass fibers. The computed entropies of adsorption indicate that the state of adsorbed phase is between that of solid and liquid at low coverage. The mobility of the adsorbate increases with coverage until it reaches the liquid stage.

Sorption isotherm, sorption rate and infrared absorption data suggest that the hysteresis of the sorption isotherm is due to the formation of hydroxyl groups which diffuse into the glass at a rate of 10^{-17} cm^2/sec at ordinary temperatures; and also to attractive forces existing in fine internal capillaries. The activation energy of adsorption of water vapor by E-glass was found to be quite high. This may be due to a combination of adsorption, solubility and diffusion. A mechanism by which the water vapor diffuses into E-glass has been hypothesized.

The changes in the heat of adsorption and the variations in the frequencies and the intensities of infrared bands of adsorbed species as the surface coverage increases, were attributed firstly to the surface heterogeneity and secondly to the mutual adsorbate interactions.

TABLE OF CONTENTS

	Page
INTRODUCTION	1
THEORY AND REVIEW OF LITERATURE	3
Adsorption Thermodynamics	3
Thermodynamical Adhesion	11
Adsorption Kinetics	18
Infrared Absorption Spectrophotometry	21
MATERIALS	26
Fiberglas-E	26
Distilled Water	30
Benzene	30
Mercury	30
METHODS OF INVESTIGATION	33
Adsorption Apparatus	33
IR Absorption Apparatus	37
Preliminaries	42
Meniscus correction to mercury levels in the manometer	42
Gravity and temperature correction for manometers	42
Electrobalance calibration	44
Buoyancy correction to the electrobalance	44
Berenyi's correction factor f	44
Procedures	48
Determination of sorption isotherms	48
Determination of sorption rates	50
Determination of infrared spectra	51

	Page
Errors	52
Experimental error in determining p/p_o	52
Experimental error in determining q	53
Experimental error in determining dq/dt	54
Experimental error in determining absorbance A	54
PRESENTATION AND DISCUSSION OF RESULTS	57
Sorption Isotherms	57
Specific Surfaces	63
Surface Free Energy Change of Wetting	71
Adsorption Energy Change And Microstructural Analysis	77
Adhesion	91
Heats of Adsorption	93
Entropies of Adsorption	105
Kinetics of Sorption	109
Infrared Absorption	127
CONCLUSIONS	139
BIBLIOGRAPHY	144
ACKNOWLEDGMENTS	154
APPENDIX	155
Mathematical Formulation of Multimolecular Adsorption Isotherm	155
Definition of Adsorptive Enthalpy	160
Adsorption Isotherm Data	163
E-glass-water vapor system	163
E-glass-benzene vapor system	175
Geometric Surface Area Calculations of Fiberglas-E	180
Radius measurement from microscope photo	180
Surface area calculation	181

	Page
Adsorption Energy Change Data	181
E-glass-water vapor system	181
E-glass-benzene vapor system	183
Heats of Adsorption and Entropies of Adsorption Data	184
E-glass-water vapor system	184
E-glass-benzene vapor system	190
Sorption Rate Data	193

LIST OF FIGURES

Figure No.		Page
1	Model for Young's equation	13
2	Schematic representation of the contact angle formed by a liquid drop on a solid surface, e.g., modified model for Young's equation	14
3	Internal reflection effects: (a) Single reflection and (b) multiple reflection	24
4	Relative functions of the glass-making oxides in Fiberglas-E	28
5	Qualitative analysis of the distilled water used by infrared spectroscopy	31
6	Qualitative analysis of the benzene used by infrared spectroscopy	32
7	Schematic layout of adsorption apparatus	34
8	Gravimetric adsorption apparatus	35
9	Beckman IR-4 infrared spectrometer	38
10	Wilks model 38B high vacuum heatable reflectance chamber: (a) Optical layout (b) perspective layout	39
11	Schematic layout of absorption apparatus	41
12	Capillary depression of the apex of a mercurial column in a glass tube	43
13	Buoyancy correction for RG Cahn balance used	45
14	Berenyi's correction factor, f, for water vapor	46
15	Berenyi's correction factor, f, for benzene vapor	47
16	Relative error, $\Delta A/A$, plotted against A	56

Figure No.		Page
17	Sorption isotherms for water vapor sorbed on E-glass (adsorption cycle-dotted points, desorption cycle-dashed lines)	58
18	Adsorption isotherms for benzene vapor on E-glass pellet	62
19	BET plots for water vapor adsorbed on E-glass	64
20	BET plots for benzene vapor adsorbed on E-glass pellet	65
21	End view of Fiberglass-E through Zeiss Ultraphot II (M.P. = 1000)	68
22	Side view of Fiberglass-E through Zeiss Ultraphot II (M.P. = 800)	69
23	Free energy change plot for the adsorption of water vapor on E-glass	72
24	Free energy change plot for the adsorption of benzene vapor on E-glass pellet	73
25	Spreading pressure versus relative humidity plot for water vapor adsorbed on E-glass	78
26	Spreading pressure versus relative humidity plot for benzene vapor adsorbed on E-glass pellet	79
27	Adsorption energy change of E-glass fiber upon adsorption of water vapor	81
28	Adsorption energy change of E-glass powder upon adsorption of water vapor	82
29	Adsorption energy change of E-glass pellet upon adsorption of benzene vapor	83
30	Typical curve of $-\Sigma\Delta F$ versus p/p_o for micro-structural analysis	85

Figure No.		Page
31	Characteristic curve for the adsorption of water vapor on E-glass (ϵ vs. φ)	96
32	Characteristic curve for the adsorption of benzene vapor on E-glass pellet (ϵ vs. φ)	97
33	Characteristic curve for the adsorption of water vapor on E-glass (ϵ vs. t)	98
34	Characteristic curve for the adsorption of benzene vapor on E-glass pellet (ϵ vs. t)	99
35	q_f versus p for isosteric heat of adsorption computation (water vapor adsorbed on E-glass)	100
36	q_f versus p for isosteric heat of adsorption computation (benzene vapor adsorbed on E-glass pellet)	101
37	Isosteric heat of adsorption and isosteric entropy of adsorption (water vapor adsorbed on E-glass): (a) E-glass fiber and (b) E-glass pellet	103
38	Isosteric heat of adsorption and isosteric entropy of adsorption for benzene vapor adsorbed on E-glass pellet	104
39	Adsorption isotherm equilibrium curves for water vapor E-glass systems at $p/p_o = 1$, 20°C	110
40	Adsorption rate of water-E-glass system using the modified Bangham equation	112
41	Semi-log plot of adsorption rate of water on E-glass surface versus time	113
42	Semi-log plot of sorption rate of water versus amount of adsorption on E-glass	114
43	Dependence of the sticking probability of water vapor upon E-glass surface on temperature	116

Figure No.		Page
44	Full log plot of sorption rate of water on E-glass surface versus time	117
45	Amount of water sorbed on E-glass versus $t^{1/2}$ at a series of temperatures (IR-activated)	120
46	Amount of water sorbed on E-glass versus $t^{1/2}$ at a series of temperatures (non IR-activated)	121
47	m_D versus reciprocal of temperature for water vapor adsorbed onto E-glass	122
48	Logarithm of diffusion coefficient of water into glass versus reciprocal of temperature	126
49	Internal reflection spectrum of Fiberglas-E taken with KRS-5 plate, $\theta = 45^\circ$	128
50	Appearance of peaks at 3400 cm^{-1} due to adsorption of water on E-glass	131
51	Effect of surface hydroxyl groups on adsorbed benzene	133
52	Relationship between shift of the absorption band of surface free hydroxyl groups, $\Delta\nu$, and surface coverage on adsorption of water and benzene	134
53	Plot of $\Delta\nu_{oH}$ against ΔQ_a	137
54	Thermodynamical sorption model at equilibrium	161

LIST OF TABLES

Table No.		Page
1	Berenyi's correction factor f	5
2	Chemical composition, bond strength and durability of Fiberglas-E	27
3	The physical properties of E-glass fiber	29
4	Limit of precision in determining absorbance A	55
5	BET area determination of E-glass by adsorbing water vapor	66
6	BET area determination of E-glass by adsorbing benzene vapor	67
7	Surface free energy change for the adsorption of water vapor on E-glass	74
8	Surface free energy change for the adsorption of benzene vapor on E-glass pellet	74
9	Comparison of surface free energy change and work of adhesion of different materials upon water adsorption	75
10	Comparison of surface free energy change and work of adhesion of different materials upon benzene adsorption	76
11	Determination of specific surface areas based on FB method	87
12	Comparison of the free energy of displacement for various materials	92
13	Average heat of adsorption of monomolecular water or benzene adsorbed on E-glass	94
14	Determination of activation energy of diffusion of water vapor into E-glass	123
15	Comparison of activation energy of diffusion of water vapor for various glass	124

Table No.		Page
16	Calculation of diffusion coefficient of water vapor into E-glass	125
17	Infrared spectra of E-glass using the vacuum frustrated internal reflectance technique with Beckman IR 4 spectrophotometer	127
18	Hydroxyl groups associated with alumina	129
19	Values of $\Delta\nu_{OH}$ and ΔQ_a for adsorbed water and adsorbed benzene on E-glass	135
20	Adsorption isotherm data for water on E-glass fiber, first run	163
21	Desorption isotherm data for water vapor on E-glass fiber, first run	164
22	Adsorption isotherm data for water vapor on E-glass fiber, second run	165
23	Desorption isotherm data for water vapor on E-glass fiber, second run	166
24	Adsorption isotherm data for water vapor on E-glass powder, first run	167
25	Desorption isotherm data for water vapor on E-glass powder, first run	168
26	Adsorption isotherm data for water vapor on E-glass pellet, first run	169
27	Desorption isotherm data for water vapor on E-glass pellet, first run	170
28	Adsorption isotherm data for water vapor on E-glass pellet, second run	171
29	Desorption isotherm data for water vapor on E-glass pellet, second run	173
30	Adsorption isotherm data for water vapor on E-glass pellet, third run	174

Table No.		Page
31	Adsorption isotherm data for water vapor on E-glass pellet, fourth run	175
32	Adsorption isotherm data for benzene vapor on E-glass pellet, first run	175
33	Adsorption isotherm data for benzene vapor on E-glass pellet, second run	178
34	Adsorption isotherm data for benzene vapor on E-glass pellet, third run	179
35	Adsorption energy change of E-glass due to adsorption of water vapor	182
36	Adsorption energy changes of E-glass pellet due to adsorption of benzene vapor	183
37	Calculated film thickness of water vapor adsorbed on E-glass fiber	184
38	Calculated film thickness of water vapor adsorbed on E-glass powdered pellet	185
39	Calculated heats of adsorption for water vapor adsorbed on E-glass fiber	186
40	Calculated heats of adsorption for water vapor adsorbed on E-glass pellet	187
41	Gibbs free energy and entropy of adsorption for water vapor adsorbed on E-glass fiber	188
42	Gibbs free energy and entropy of adsorption for water vapor adsorbed on E-glass pellet	189
43	Calculated film thickness of benzene vapor adsorbed on E-glass pellet	190
44	Calculated heats of adsorption for benzene adsorbed on E-glass pellet	191
45	Gibbs free energy and entropy of adsorption for benzene adsorbed on E-glass pellet	192

Table No.		Page
46	Adsorption rate data for water vapor adsorbed on IR-activated E-glass pellet at 20°C	193
47	Adsorption rate data for water vapor adsorbed on non IR-activated E-glass pellet at 20°C	194
48	Adsorption rate data for water vapor adsorbed on IR-activated E-glass pellet at 18°C	195
49	Adsorption rate data for water vapor adsorbed on non IR-activated E-glass pellet at 18°C	196
50	Adsorption rate data for water vapor adsorbed on IR-activated E-glass pellet at 18.9°C	197
51	Adsorption rate data for water vapor adsorbed on non IR-activated E-glass pellet at 18.9°C	198

INTRODUCTION

The strength of pristine glass fibers is enormous--approaching a theoretical strength of one to four million psi. Exposure to atmospheric moisture results in rapid degradation of the glass fibers by one or two orders of magnitude. In general, the strength of silicate glasses is a function of the integrity of the surface. Griffith flaws are believed to be formed by reactions with moisture. These flaws initiate a fracture crack which is catastrophic because there is no ductile energy-absorbing deformation to reduce stress concentration at the crack tip. This leads to surface sensitive fracture.

In glass-reinforced plastics, the organic matrix binds glass fibers together and protects their surfaces to produce the highest strength-to-weight ratio available in commercial materials. Glass-reinforced plastics may lose strength by water penetration at the glass-resin interface. Improved composites could be produced if the fiber-matrix bond is improved. Chromio and silane compounds often are used as "coupling agents" to improve the bond.

The surface of glass has been extensively studied by physical and chemical methods (6, 25, 64, 109). The chemical reactivity and physical properties of the surface are important to many applications. The structure of glass surface, however, remains a mystery despite a large body of literature on the subject. Qualitative statements made are based on indirect evidence obtained from property changes with surface modification. Because of the lack of periodicity of glasses, diffraction techniques cannot be applied. The resonance techniques, such as infrared absorption, and the surface adsorption or adhesion techniques may help to give a better picture of glass surface structure. This is the objective of the present study.

E-glass was chosen as the material for this investigation because of its wide scale applications in various industrial fields, for example, in aeronautical and space vehicles and submarines.

The present study consists of an investigation of the thermodynamics and kinetics of sorption isotherms and of the infrared spectra of surface films.

THEORY AND REVIEW OF LITERATURE

Adsorption Thermodynamics

According to the potential theory, adsorption occurs because the adsorbent exerts a strong attractive force upon the gas in its vicinity. The attraction forces are so great that many adsorbed layers can form on the surface. Polanyi (99) defined the adsorption potential at a point near the adsorbent, as the work done by the adsorption forces in bringing a molecule from the gas phase to that point, and expressed it by the compensating compressional increase in the free energy:

$$\epsilon_i = \int_{\delta_x}^{\delta_i} V dp \ . \tag{1}$$

Here ϵ_i is the adsorption potential at a point where the density of the adsorbed gas is δ_i, δ_x is the density in the gas phase, and $V = M/\delta$, where M is the molecular weight of the adsorbate. To evaluate this integral, Polanyi assumed perfect gas behavior in the gas phase and incompressible behavior in the adsorbed phase leading to the evaluation of the adsorption potential as merely the work of compressing an ideal gas isothermally from p_x to p_o (the vapor pressure of the liquid):

$$\epsilon_i = \int_{p_x}^{p_o} \frac{RT}{p} dp = RT \ \ln \frac{p_o}{p_x} \tag{2}$$

where R is the gas constant, T is the absolute temperature, and p_o and p_x are the saturation and equilibrium vapor pressures respectively at given temperature. The potential thus calculated corresponds to a potential surface contour above the surface of the adsorbate enclosing a volume φ_i between itself and the surface of the adsorbent. Potential theory states that there exists a relationship between ϵ_i and φ_i:

$$\epsilon_i = f(\varphi_i) \tag{3}$$

and this relationship is temperature independent, i.e.

$$\left(\frac{\partial \epsilon}{\delta T}\right)_{\varphi} = 0, \text{ or } \frac{d\epsilon_i}{dT} = 0 \tag{4}$$

The curve representing Equation 3 is called the characteristic curve and can be obtained experimentally from adsorption data.

The theory has been sufficiently successful to indicate these assumptions are fulfilled with a fair degree of accuracy (87, 56, 88, 63).

A large number of variables affect adsorption such as surface area, surface roughness, capillarity, and the nature of the interaction between adsorbent and adsorbate. Berenyi (15, 16) considerably improved the theory by applying a correction to φ_i.

$$\varphi_i = q/f \cdot \delta_b \tag{5}$$

where q is the weight adsorbed, δ_b is the density of the liquid at boiling temperature, and f is a correction factor which is the sum of individual correction factors for compressibility and thermal expansion [see Table 1 (18, p. 103)].

If the surface area changes during the course of adsorption, the adsorbed volume no longer remains constant at the point of constant potential. But the thickness of an adsorbed layer is controlled by the

Table 1. Berenyi's correction factor f

(a) Compressibility Correction, f_c

T/T_b	p_x = 0.1	1	10	100	1000 mmHg
0.6	1.01	1.02	1.03	--	--
0.8	1.01	1.02	1.03	1.04	

(b) Thermal Expansion Correction, f_t

T/T_b	f_t
0.6	1.16
0.8	1.10

(c) Total Correction, f

T/T_b	p_x = 0.1	1	10	100	1000 mmHg
0.6	1.17	1.18	1.19	--	--
0.8	1.11	1.12	1.13	1.14	--

molecular diameter of the adsorbed gas, and is not a function of minor changes in potential. The thickness will be less sensitive to changes in surface roughness, which also changes surface area, than the adsorbed volume will be. Hence one must plot ϵ vs t rather than ϵ vs φ as the characteristic curve when surface changes may occur. The thickness may be obtained from the pressure, compressibility, liquid density, weight adsorbed and surface area. Therefore,

$$t = \varphi_i/\Sigma \qquad (6)$$

where Σ is the specific surface area of adsorbent.

A precise surface area measurement is needed to obtain the adsorbed film thickness, a significant parameter in the potential theory. The Brunauer-Emmett-Teller (BET) theory of multimolecular adsorption was used for surface area determinations in the present work. This theory has been widely employed for surface area determinations since it was proposed in 1938, (32, 104, 110, 53). Brunauer et al. (21) assumed that the forces chiefly responsible for the binding energy of multimolecular adsorption are the same as those responsible for condensation. This is the basic assumption of the theory of multimolecular adsorption from which they derived the following isotherm equation for adsorption on a free surface (an independent derivation of the equation is presented in the Appendix):

$$\frac{p}{V(p_o - p)} = \frac{1}{V_m C} + \frac{C - 1}{V_m C} \frac{p}{p_o} \qquad (7)$$

In Equation 7, V is the volume of vapor adsorbed at pressure p, V_m the volume of vapor adsorbed when the surface of the adsorbent is covered by a monomolecular layer of adsorbate and p_o the saturation pressure. The constant C is approximately given by the equation:

$$C = e^{(E_1 - E_L)/RT} \qquad (8)$$

where E_1 is the average heat of adsorption of the first layer and E_L is the heat of liquefaction. When the amount of vapor adsorbed is expressed in terms of mass, Equation 7 becomes:

$$\frac{p}{q(p_o - p)} = \frac{1}{q_m C} + \frac{C - 1}{q_m C} \frac{p}{p_o} \qquad (9)$$

where q is the mass of vapor adsorbed at pressure p and q_m is the mass adsorbed at monolayer coverage of the adsorbent surface. Brunauer and his co-workers (20) developed a more general isotherm equation which considers factors limiting the number of layers that can be adsorbed, and also includes capillary condensation. At low value of relative pressures their more general equation reduces to Equation 7 or 9. Therefore, according to BET theory, physical adsorption in the low pressure range may be characterized by the two parameters q_m and C. Values of these parameters can be determined if a plot of

$$\frac{p}{q(p_o - p)} \quad \text{versus } p/p_o$$

from the experimental data gives a straight line as predicted by Equation 9.

When the area, s, occupied by one molecule of the adsorbate on the solid surface is known, the specific surface, Σ, of the solid can be calculated from the parameter q_m of the BET equation by

$$\Sigma = N \cdot q_m \cdot s/M \tag{10}$$

where N is Avogadro's constant, M is the molecular weight of the adsorbate, and q_m is expressed for one gram of the adsorbent. Assuming closest packing, Brunauer (18, p. 287) gave the following expression for the area covered by a molecule of adsorbate:

$$s = (4)(0.866)\left(\frac{M}{4N\delta\sqrt{2}}\right)^{2/3} = 1.091\left(\frac{M}{N\delta}\right)^{2/3} \tag{11}$$

The coefficient 1.091 is called the packing factor; its value for an adsorbate may vary from one adsorbent to another depending on the packing and on the variation of adsorbent pores (80). Equation 10 then can be used to determine specific surface areas of adsorbents once the corss-sectional area of the adsorbate molecule is known.

When a molecule of adsorbate is adsorbed on the solid surface, heat evolves and surface energy of the system reduces. Parameter C includes the average heat of adsorption for the first layer, E_1. The values calculated by Equation 8 are less than measured heats of adsorption but are of the same order of magnitude (19). Harkins and Jura (59) found that the heat of adsorption decreases as the thickness of the water film increases, but that at the thickest films that could be measured the heat of adsorption is still greater than the heat of liquefaction of water. The heat of adsorption in the last layer is always greater than the heat of liquefaction, since the adsorbate loses energy by the disappearance of free liquid surface. Clampitt and German (23) rederived Equation 8 and arrived at:

$$C = e^{\left[(E_1 - E_L) + (\Delta H_s - E_L)\right]/RT} \qquad (12)$$

where ΔH_s is the heat of vaporization of the surface layer. The correction term $(\Delta H_s - E_L)$ accounts for the differences in the heat of vaporization of successive layers.

The heat of adsorption is not solely a function of adsorbates; it is also a function of temperature of the system, as well as of the type of adsorbent. The heat of adsorption may be obtained, more reasonably, by applying the Clausius-Clapeyron equation (62, 41).

$$\left[\frac{\partial \ln p}{\partial (1/T)}\right]_t = \frac{-\Delta H^*}{R} \tag{13}$$

where t refers to any appropriate coordinate and ΔH^* is the isosteric heat of adsorption. By keeping q_f, the weight of adsorbed gas on a unit area of adsorbent constant, the following integrated form can be obtained (67):

$$(\ln p_1/p_2)_{q_f} = \Delta H_a/R \ (1/T_2 - 1/T_1) \tag{14}$$

where p_1 and p_2 are equilibrium vapor pressures at temperatures T_1 and T_2. The value, ΔH_a, obtained is called the isosteric heat. The adsorptive free energy and adsorptive entropy changes may be calculated for the transfer of one mole of adsorbate from the gas phase to the adsorbed phase (see the Appendix). The free energy change for this process is:

$$\Delta G = \epsilon_i = -RT \ \ln p_o/p \tag{15}$$

The enthalpy change for the same process is given by $\Delta H = \Delta H_a - \Delta H_l$, where ΔH_a, the isosteric heat, is the enthalpy change for the transfer of one mole of vapor to the surface, and ΔH_l for the transfer to the liquid (see the Appendix). The entropy change for the transfer of one mole of liquid to the adsorbed phase is therefore given by

$$\Delta S = -\frac{(\Delta G - \Delta H)}{T} \tag{16}$$

Adsorption of molecules from a gas on to a surface is always accompanied by a drop in entropy. The study of the magnitude of this decrease may enable us to draw some very important conclusions about the freedom of movement of the adsorbed molecules.

The entropy change on adsorption is the sum of changes in the translational, rotational, and vibrational entropies of the molecules (108, p. 150).

$$\Delta S = \Delta S^{tr} + \Delta S^{rot} + {}_aS^{vib} \tag{17}$$

The translational entropy change per mole of a gas in its standard state (760 mm, T) to a mobile adsorbed film in its standard state (θ_s,T) is calculated to be:

$${}_gS_s^{tr} - {}_aS^{tr} = -\Delta S_s^{tr} = R/2\ln M + R/2\ln T + 2.30 \tag{18}$$

or to a localized adsorbed film where the translational entropy change is simply the loss of all the translational entropy of the gas:

$$-\Delta S_s^{tr} = {}_gS_s^{tr} = 3/2R\ln M + 5/2R\ln T - 2.31 \tag{19}$$

where the subscripts g, s and a indicate gaseous, standard and adsorbed states, respectively.

The rotational entropy change can be calculated on the basis of how the molecule rotates in the adsorbed phase. Hence,

$$\Delta S^{rot} = R\left[\ln 1/\pi\sigma \left\{ \frac{8\pi^3(I_A^a + I_B^b + .. + I_G^g)}{h^2}^{1/n} kT\right\}^{n/2} + n/2\right] \tag{20}$$

where a+b+ . . +g=n; I_A, I_B, ...I_G are the moments of inertia of the molecule and σ is the symmetry factor, and h is the Plank's constant. In the above expression, the degeneracy of the lowest energy state is omitted because it is not affected by the process of adsorption; the symmetry number is retained because it depends on the ability of the molecule to rotate and this may alter on adsorption.

The vibration of the adsorbed molecule with respect to the surface contributes to the entropy of adsorption--if the film is mobile and the vibration is that of a harmonic oscillator in one degree of freedom, for which the frequency does not change with temperature, the entropy contribution, ${}_aS^{vib}$ is given by:

$$ {}_aS^{vib} = \frac{Nhv}{(e^{hv/kT} - 1)T} - R\ln(1 - 3^{-hv/kT}) \tag{21} $$

where v is the frequency of the vibration. If the adsorbed film be localized, the entropy of vibration would be described by:

$$ {}_aS^{vib} = 2\left[\frac{Nhv_{\parallel}}{(e^{hv_{\parallel}/kT} - 1)T} - R\ln\left(1 - 3^{-hv_{\parallel}/kT}\right)\right] + $$

$$ \frac{Nhv_{\perp}}{(e^{hv_{\perp}/kT} - 1)T} - R\ln(1 - 3^{-hv_{\perp}/kT}) \; . \tag{22} $$

Thermodynamical Adhesion

In the formation of a joint, the surface concerned is first wetted by the liquid adhesive. Subsequently the adhesive solidifies and the strength of the joint will depend on the molecular attraction at the adhesive-adherend interface, and also on the contact angle that the adhesive makes at the ends of the joint. The thermodynamics of the solid-liquid interface is based on two equations, that of Young (124) for the contact angle and that of Dupré (36) for the work of adhesion (Figure 1). If γ_s is the free energy of the solid surface, γ_l the free surface energy of the liquid, γ_{sl} that of the solid-liquid interface, and θ the equilibrium contact angle, and if the solid is insoluble in the liquid,

$$\gamma_s = \gamma_{sl} + \gamma_l \cos \theta. \tag{23}$$

The work of adhesion, that is the work required to separate 1 cm^2 of solid-liquid interface, is

$$W_a^* = \gamma_s + \gamma_l - \gamma_{sl}. \tag{24}$$

Substituting γ_{sl} from Equation 23 into Equation 24:

$$W_a^* = \gamma_l (1 + \cos \theta). \tag{25}$$

It is clear that this model suffers a serious defect. As pointed out by Bangham and Razouk (8), it neglects the presence on the free solid surface of a film of vapor in equilibrium with the saturated vapor at pressure p_o (saturation pressure of the liquid, Figure 2). Therefore, the equilibrium relation becomes:

$$\gamma_s = \gamma_{sv}o = \gamma_{sl} + \gamma_{lv}o \cos \theta = \gamma_s o + \pi \tag{26}$$

where π is defined as the spreading pressure, and it is the surface free energy change corresponding to immersion in vapor.

Bangham (7, 8) was first to show that the Gibbs adsorption equation could be used to determine the surface free energy changes that occur during adsorption of vapors on solid surface i.e.,

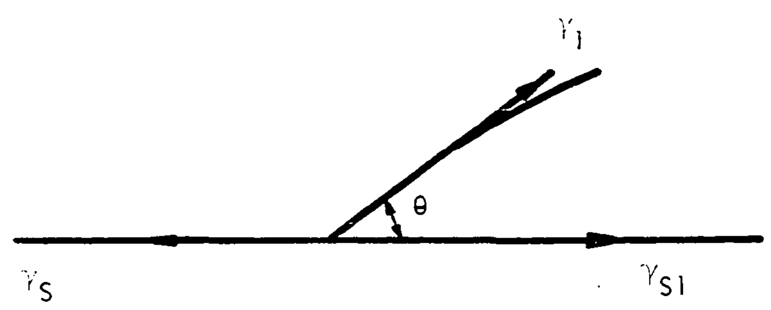

Figure 1. Model for Young's equation

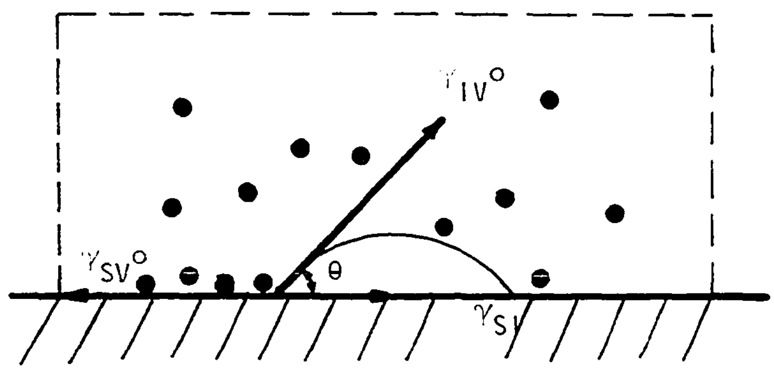

Figure 2. Schematic representation of the contact angle formed by a liquid drop on a solid surface, e.g., modified model for Young's equation

$$\Delta F = -\int_{p=0}^{p=p_o} \Gamma d\mu \tag{27}$$

in which $d\mu = RTd(\ln p)$, and Equation 27 becomes

$$\Delta F = -RT \int_{p=0}^{p=p_o} \frac{\Gamma}{p}\, dp \tag{28}$$

where Γ is the surface concentration, and μ the chemical potential. The free energy change ΔF will be referred to as the free energy of immersion and the symbol ΔF was chosen to differentiate it from the adsorptive free energy ΔG. Using the Gibbsian adsorption equation, Boyd and Livingston (17) derived a similar equation for the free energy of immersion of a non-porous wettable surface ($\theta = 0$) in a saturated vapor.

$$\Delta F = \gamma_{sl} - \gamma_s{}^o + \gamma_{lv}{}^o = -\frac{RT}{M\Sigma}\int_o^{p_o} \frac{q}{p}\, dp \tag{29}$$

In considering the differential free energy change upon the transfer of vapor from gas onto the solid surface, Demirel and Enüstün (33) arrived at

$$\Delta F = -\frac{RT}{M\Sigma}\int_o^1 \frac{q}{p/p_o}\, d(p/p_o) \tag{30}$$

which is more convenient when relative vapor pressure is employed. ΔF given by Equations 27-30 may be interpreted as the free energy change accompanying the process of transferring saturated vapor onto a unit area of solid surface; the process is terminated when the equilibrium pressure reaches p_o.

The work of adhesion W_a, work required to separate 1 cm^2 of solid-liquid interface in vacuum leaving a perfectly naked solid surface, becomes:

$$W_a = \gamma_s o + \gamma_{lv}{}^o - \gamma_{sl} = W_a{}^* - \pi \quad (31)$$

If the adsorbent is a mass of non-interacting fine powder wettable by the liquid, capillary condensation in the contact zones of the particles theoretically fills the voids with the liquid before the final saturation pressure is attained. In such cases, since $\theta = 0$ and liquid surfaces disappear:

$$\pi = \Delta F = \gamma_{sl} - \gamma_s o \quad (32a)$$

i.e., ΔF should be the free energy of immersion of a unit area of solid surface in the bulk liquid, which is called the "free energy of wetting."

If capillaries do not fill and therefore liquid surfaces do not disappear with $\theta = 0$ and $\gamma_{sl} = \gamma_{lv} o$, thus

$$\pi = \Delta F = \gamma_{sl} - \gamma_s o + \gamma_{lv} . \quad (32b)$$

Therefore for wettable adsorbents π and ΔF are synonymous.

Bartell et al. (34) extended this view in the case of porous solids; they also showed that the validity of this point of view does not depend upon the degree of compression of the powder (27). Some investigators (17, 71) calculated ΔF by an extrapolation of the adsorption isotherms to saturation pressure and identified it with the free energy of immersion in saturated vapor, assuming that no capillary condensation takes place. The assumption of no capillary condensation, and the steepness of the adsorption isotherm near the saturation pressure, introduce uncertainties in the free energy of immersion determined in this manner. It has been shown by Carmen et al. (23) and Craig et al. (27) that by using a compressed powder as adsorbent an adsorption isotherm of type IV is obtained instead of usual type II and, therefore, the isotherm can be extrapolated to saturation with certainty.

Zisman (125) states that when spreading occurs, the specific surface free energy of the liquid is usually less than that of the solid. Therefore, every liquid having a low specific surface free energy always spreads freely on a specularly smooth, clean, high energy surface at ordinary temperature unless the film adsorbed by the solid converts it into a low energy surface having a critical surface tension less than the surface tension of the liquid. Harkins (59) has developed conditions for spreading in terms of an initial spreading coefficient S. S equates the work of adhesion minus the work of cohesion:

$$S = \gamma_s o + \gamma_{lv} o - \gamma_{sl} - 2\gamma_{lv} o = \gamma_s o - (\gamma_{lv} o + \gamma_{sl}). \tag{33}$$

For spreading $S > 0$. So, a spontaneous spreading over a surface can occur only when it results in a reduction in the free energy of the system, i.e., when the adhesion of liquid for solid exceeds the cohesion of the liquid. For complete spreading or wetting of the solid, however, the contact angle must be zero. It has been shown by Kline (74) that clean surfaces and increased surface area favor adhesion.

The stability of a coupling sized glass fiber decreases appreciably when subjected to the action of water. It is believed that this is a result of stripping i.e., displacement of size coupling by water at the glass fiber surface. To assess the tendency of a given adsorbent to stripping, Hallberg (55) studied the process of stripping taking place in the capillary structure of the bituminous mixtures and showed that the quantity called the adhesion tension $\gamma_{sw} - \gamma_{sb}$, where γ_{sw} and γ_{sb} are solid-water and solid-binder interfacial tensions, respectively, is the driving force for adhesion i.e., the reverse process of stripping. Demirel and Enüstün (33) calculated the adhesion tension from the adsorption data. The adhesion tension is given by

$$\gamma_{sw} - \gamma_{sb} = \Delta F_w - \Delta F_b \tag{34}$$

where ΔF_w and ΔF_b are the free energies of wetting of the same solid by water and hydrocarbon, respectively. This quantity has in fact a fundamental importance. It is the free energy change accompanying stripping. Therefore, it should measure the competition between water and binder for covering the solid surface and define the state of equilibrium whenever attained. This free energy change corresponds to the displacement of binder in the capillaries and its joining the bulk of the binder.

Adsorption Kinetics

In most physico-chemical processes the study of adsorption can be divided into two parts: thermodynamics as already described and kinetics. For an adsorbent surface where mechanical adhesion is important the rate of wetting (adsorption rate) may be a determining factor. The adsorption process consists of five distinct steps:

1. migration of the molecule to the surface,
2. adsorption of the molecule,
3. movement of the molecule along the surface,
4. desorption of the molecule, and
5. migration of the molecule away from the surface.

Apparently steps two and four are very rapid (in the order of 10^{-13} sec. Therefore the kinetics of adsorption and desorption steps may be immeasurably fast. McBain (84) in 1919 wrote:

> True adsorption is nearly instantaneous. Any lag, at present, can be accounted for by the time required for the dissipation of the heat evolved, or the comparative inaccessbility of a portion of the surface of an adsorbing medium.

Therefore, the measured overall adsorption must be accounted for by the other steps--by migration of the molecule to the surface and motion of the molecule along the surface. Since almost the entire surface of a good adsorbent is internal, the motion of the molecule to the surface will be affected by pore size, pore length, and effective pore size after adsorption has taken place. In other words the treatment of adsorption kinetics is similar to a diffusion problem corresponding to diffusion into a pore.

Theories of adsorption rates based upon diffusion have been developed by McBain (83), Damköhler (28), Wicke (123) and Barrer (10). An equation for the rate of adsorption on a free surface developed by Langmuir serves as the starting point for diffusion analysis (77). The experimentally observed rate is equal to the difference between the rates of condensation on the surface and evaporation from the surface. At constant pressure,

$$\frac{d\theta}{dt} = k_1(1 - \theta) - k_2\,\theta \qquad (35)$$

where θ is the fraction of the surface covered by the adsorbed gas, and k_1 and k_2 are rate constants. Integrating, with boundary conditions $\theta = 0$ when $t = 0$, gives:

$$\theta = \frac{k_1}{k_1 + k_2} \left[1 - e^{-(k_1 + k_2)t} \right] \qquad (36)$$

when $t = \infty$, $\theta = \theta_e$ where θ_e is the fraction of the surface covered at equilibrium. This gives the relationship

$$\theta_e = \frac{k_1}{k_1 + k_2} \qquad (37)$$

from which it follows that

$$\theta = \theta_e(1 - e^{-kt}) \qquad (38)$$

where $k = k_1 + k_2$. Because $\theta = V/V_m$ and $\theta_e = \frac{V_e}{V_m}$ we can write

$$V = V_e(1 - e^{-kt}), \text{ or} \qquad (39)$$

$$\ln \frac{V_e}{V_e - V} = kt \qquad (40)$$

here V_m is the volume adsorbed at saturation, V is the volume adsorbed at time, t, and V_e is the volume adsorbed at equilibrium. Plotting the first term versus time should give a straight line.

Adsorption on the walls of a capillary reduces the effective diameter of the capillary. The rate of adsorption increases with pressure, but the effect of reduction in the capillary diameter usually overcomes the effect of increased pressure. Therefore, capillarity affects the simple Langmuir adsorption process.

Bangham and Sever (9) expressed the rate of capillary condensation in a gas-glass system by

$$\log \frac{V_e}{V_e - V} = kt^{1/m} \quad . \qquad (41)$$

They concluded that the long continued sorption of gases by glass was an absorption rather than an adsorption process. The amount of gas taken up was many times greater than that required for a complete monolayer on the glass surface. Some of the tests required weeks or months to reach complete equilibrium. This sort of behavior is not associated with adsorption process. It seems probable that capillary condensation and diffusion are responsible for the slow process.

Infrared Absorption Spectrophotometry

The methods of investigation of adsorption phenomena described so far give no direct information about the changes produced in the molecules by adsorption forces.

Infrared spectroscopy has been found of the greatest value in the structural analysis of molecules. Its application to the study of surface chemistry has provided one of the most direct means of observing the interactions and perturbations that occur at the surface during adsorption, and of determining the structure of the adsorbed species (79). Infrared spectra give direct information on molecular vibrations and changes in the spectra show the effect of the surroundings on the molecule. Under suitable conditions, the shapes of the vibration bands are affected by the rotation of the molecule as a whole, and thus they give information on the rotational motions of the molecules. When a molecule is adsorbed, the surface forces cause a change in the symmetry and therefore in vibrations of the molecule, and any quantitative measure of this change can be directly related to the nature of the adsorption.

If the molecule is adsorbed physically, it is subjected only to weak intermolecular forces of the van der Waals type and thus the symmetry it possesses in gas phase is only slightly perturbed. Accordingly, the infrared spectrum is altered only slightly, and small frequency shifts are observed. During the chemisorption process, however, the symmetry of the adsorbed species is completely different from that of the gaseous molecule. The surface bond is very strong, and the adsorption may be dissociative in nature. In this case, a complete new infrared spectrum is observed, and band shifts and intensities are far removed from those of gaseous adsorbate.

Folman and Yates (43) demonstrated the utility of infrared spectroscopy in explaining adsorption phenomena. They found that the adsorption of gases upon a porous glass body had caused an initial contraction of the glass rod under investigation; this was followed by an expansion. The expansion-contraction effects were thought to be the result of a specific interaction between the adsorbate and the surface in particular through the hydroxyl groups on the surface. In other studies involving porous glass, Folman and Yates (44, 45) revealed that OH groups exist on the surface of the glass even after degassing at 450°C. Kozirowski and Folman (75) showed that methylation of the OH groups reduces the Young modulus of the porous glass by 10% and the bulk modulus by 22%.

When the infrared investigation is extended to the study of surface problems, the adsorbent must be included in the infrared beam in addition to adsorbed molecules. This may lead to the loss of infrared radiation due to scattering and absorption by the opaque adsorbent, making transmission techniques almost useless. Fahrenfort (42) was first to propose and develop the internal reflection spectroscopy utilizing a single reflection for measuring the spectra of bulk materials which could not easily be prepared for conventional measurements (Figure 3a). Harrick (60) proposed and developed internal reflection spectroscopy techniques utilizing multiple reflections, for studying surfaces and thin films (see Figure 3b).

Internal reflection spectroscopy technique consists of recording the optical spectrum of a sample material in contact with an optically denser but transparent medium (prism) and then measuring the wavelength dependence of the reflectivity of the interface. As shown in Figure 3a the light is first introduced into the denser medium. In the study of adsorption radiation from within the adsorbent at angles exceeding the critical angle at the surface, will be totally reflected through the denser material. The infrared beam will still be totally reflected when the surface of the adsorbent is covered with a substance of lower refractive index, provided the frequency of the radiation does not correspond to an absorption frequency of the adsorbed material. When this happens, radiation will be absorbed and a spectrum closely resembling a normal transmission spectrum of the adsorbate will be obtained. In this technique the reflectivity is a measure of the interaction of the evanescent wave with the sample material and the resulting spectrum is also a characteristic of the sample material. Increasing the number of internal reflections serves to increase the chance of the interacting with a point of contact (see Figure 3b), the

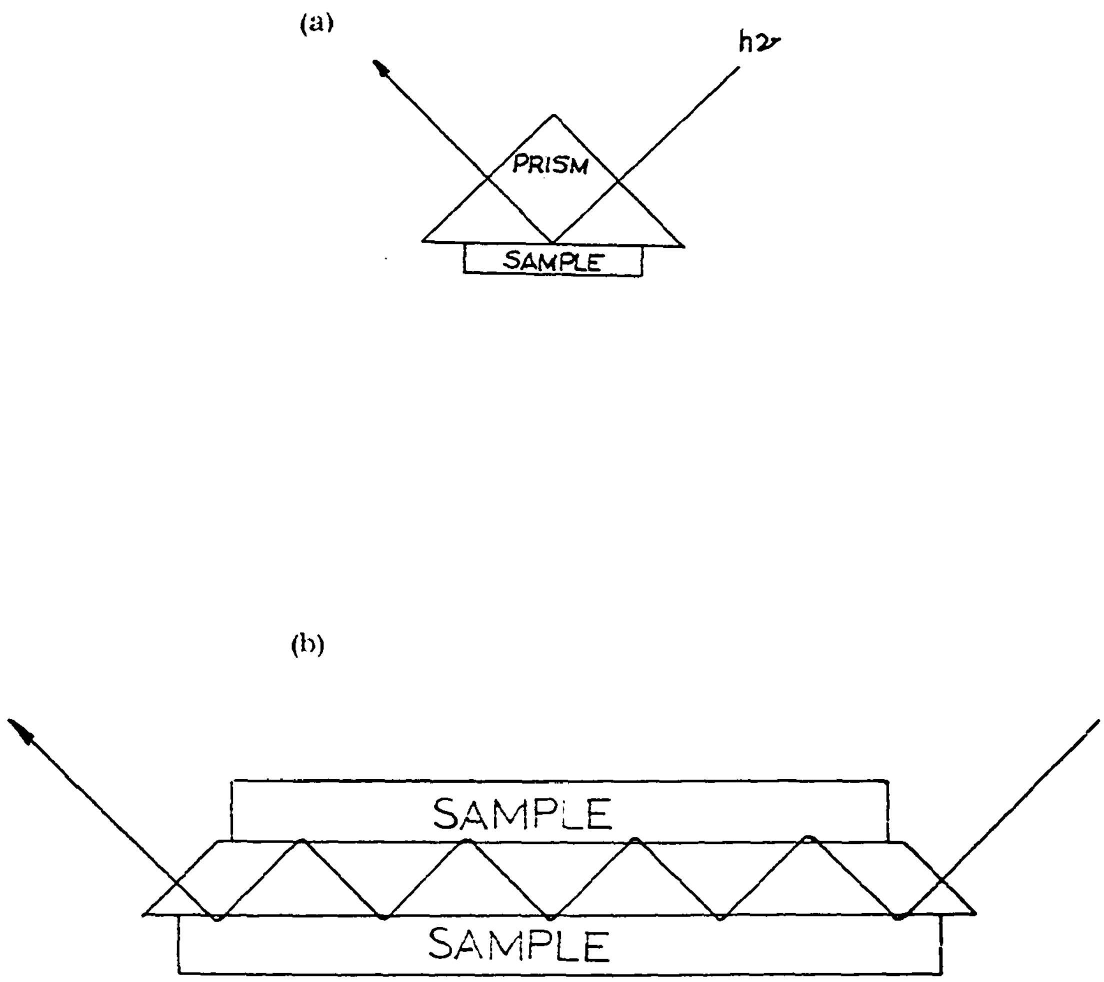

Figure 3. Internal reflection effects: (a) Single reflection and (b) multiple reflection

total effect being identical with increasing the sample thickness in transmission spectroscopy.

MATERIALS

Fiberglas-E

The Fiberglas-E was provided as the cleanest available, treated with deionized water without protective coating by research laboratories of Owens-Corning Fiberglas Corporation. Fibers are ordinarily treated with sizing agents at the time of formation. E-glass which is used for such purposes as textile yarn, reinforcement of plastics, and filament winding, has high tensile strength and high modulus of elasticity, but poor acid resistance. According to the producer, it is composed of a random network of various vitreous oxides--mainly, silica. Its chemical composition, bond strength and durability are shown in Table 2. SiO_2, Al_2O_3 and B_2O_3 which possess high single bond strength--above 89 Kcal, are the glass formers which incidently have high viscosity and low thermal expansibility. The rest of the constituents which are called the glass modifiers are used to control workability, durability and probability of devitrification. The very small alkali content is to prevent excessive destruction weathering when exposed to atmospheric moisture. Relative functions of glass-making oxides in Fiberglas-E can be best recognized as shown in Figure 4.

The expanding technology of glass fibre was primarily prompted by the discovery that glass wool and its products are excellent thermal, acoustic insulating materials in addition to their highest strength to weight ratios if not weathered.

Selected physical properties of E-glass fiber are summarized in

Table 2. Chemical composition, bond strength and durability of Fiberglas-E (6)

Constituent	Ed (Kcal)[a,b]	Coordination No.[b]	f_s(Kcal)[c,b]	Wt, %
SiO_2	424	4	106	54.0
Al_2O_3	402	4	100	15.0
CaO	257	8	32	17.3
MgO	222	6	37	5.0
Na_2O	120	6	20	0.5
B_2O_3	356	4	89	8.0
F_2				0.2

Reagent[d]	Wt, % loss
Water	1.1
0.02N H_2SO_4	6.8
0.01N NaOH	3.5

[a]Dissociation energies.

[b]Based on the data of Rawson (102, p. 24-25).

[c]Single bond energies.

[d]One gram of fiber boiled in 300 cc of the indicated solution for one hour.

Table 3. One of these properties, strengths of fiber glass deserve most attention. The strength of glass fiber is enormous when the surface is pristine. Glass usually fails in tension, showing brittle, conchoidal

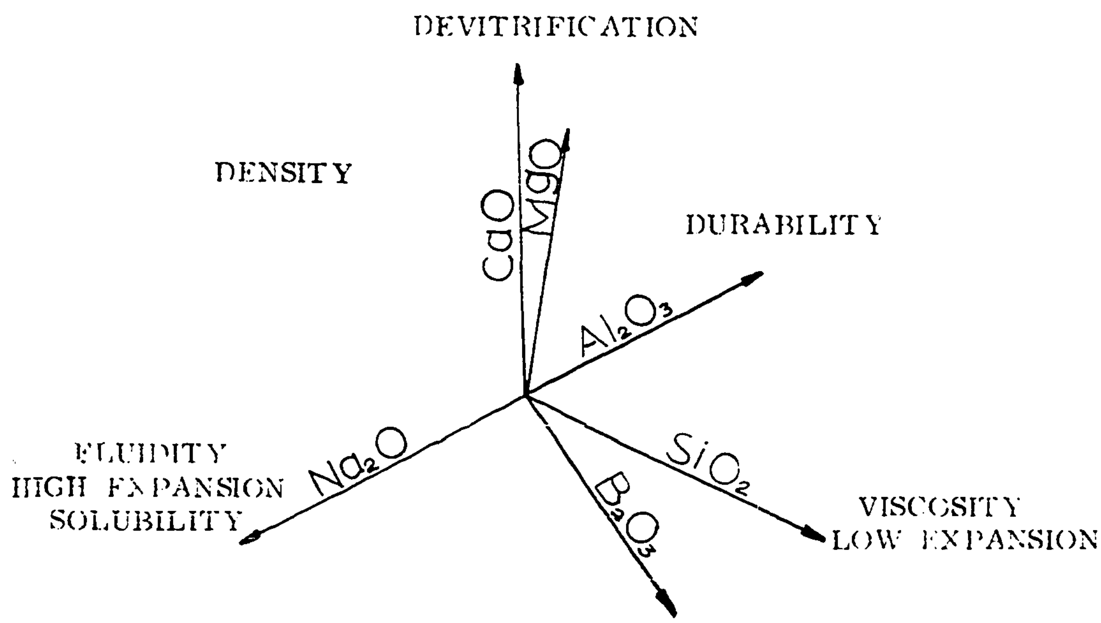

Figure 4. Relative functions of the glass-making oxides in Fiberglas-E

Table 3. The physical properties of E-glass fiber (26)

Properties	Unit	Value
Thermal expansion from 0-300°C	$10^{-7}/°C$	60
Softening point	°C	830
Young's modulus	psi x 10^6	10.5
Dielectric constant at 20°C		6.4
Refractive index at sodium D line		1.548
Density	gm/cm^3	2.60
Strength*	psi	
Protected in vacuum		up to 2,000,000
In air		250,000
In plastic		150,000

*Theoretic strength of untreated glass fiber = 1,000,000 - 4,000,000 psi.

fracture normally originating at a surface flaw. Because of the tendency of the glass surface to develop stress-concentrating flaws, there is a strong dependence of glass strength on the surface area of the sample under test. Since the stress concentration varies inversely with the square root of the depth of the flaw, the limited flaw depth possible with fine fibers can also explain high measured strengths obtained (113, p. 83). Reactions with the atmosphere cause rapid weakening by one or two orders of magnitude. In glass-reinforced plastics, the organic matrix binds glass fibers together and protects their surfaces to produce the highest strength-to-weight ratio available in commercial materials.

Distilled Water

The distilled water used as the adsorbate was obtained from a steam operated SLH-2 Barnstead still which produces, when fresh, practically carbon dioxide free distilled water with a pH approaching 7. For the adsorption experiments, this distilled water was triple distilled just before introducing into the apparatus. The purity of the distilled water used was verified qualitatively by an infrared spectrum using a Beckmen IR-4 spectrophotometer as shown in Figure 5.

Benzene

The benzene used was purified by 4A linde molecular sieve and stored over sodium wire prior to adsorption experiments. It was obtained through the courtesy of Dr. Thomas J. Barton, Assistant Professor of Chemistry, Iowa State University, Ames, Iowa. The purity of the benzene used has also been verified qualitatively by infrared absorption spectrophotometry as shown in Figure 6.

Mercury

The C.P. grade triple distilled mercury was used in the mercury diffusion pump and manometers.

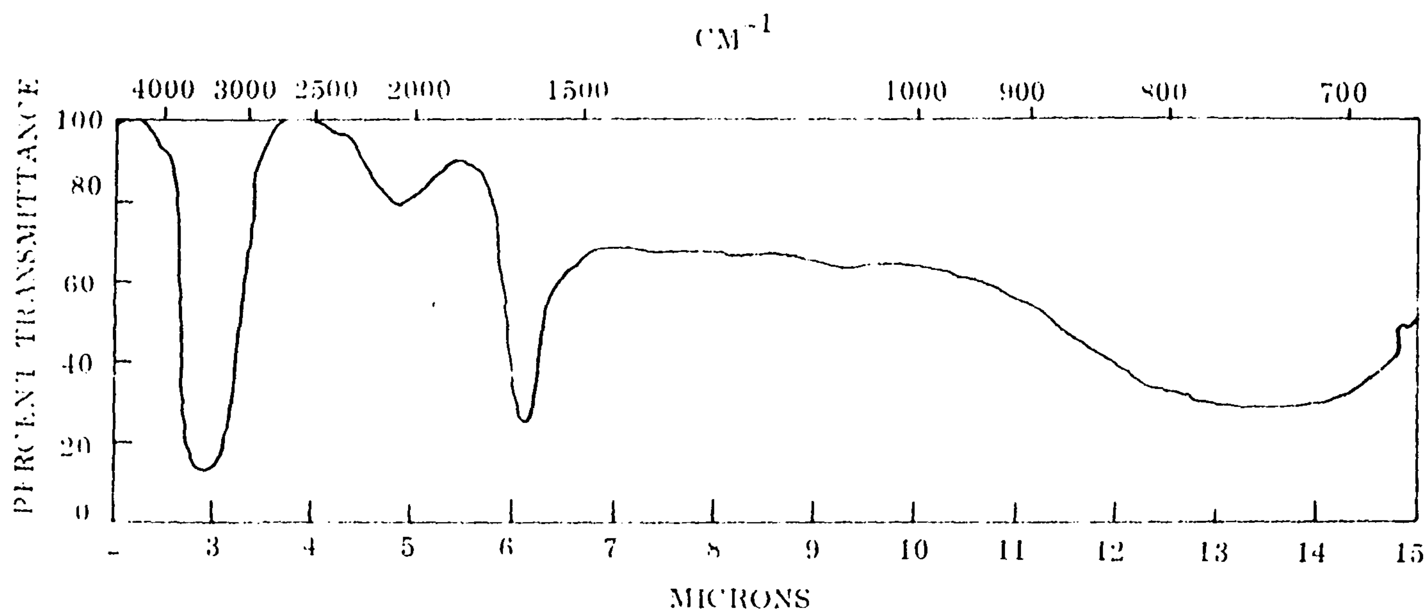

Figure 5. Qualitative analysis of the distilled water used by infrared spectroscopy

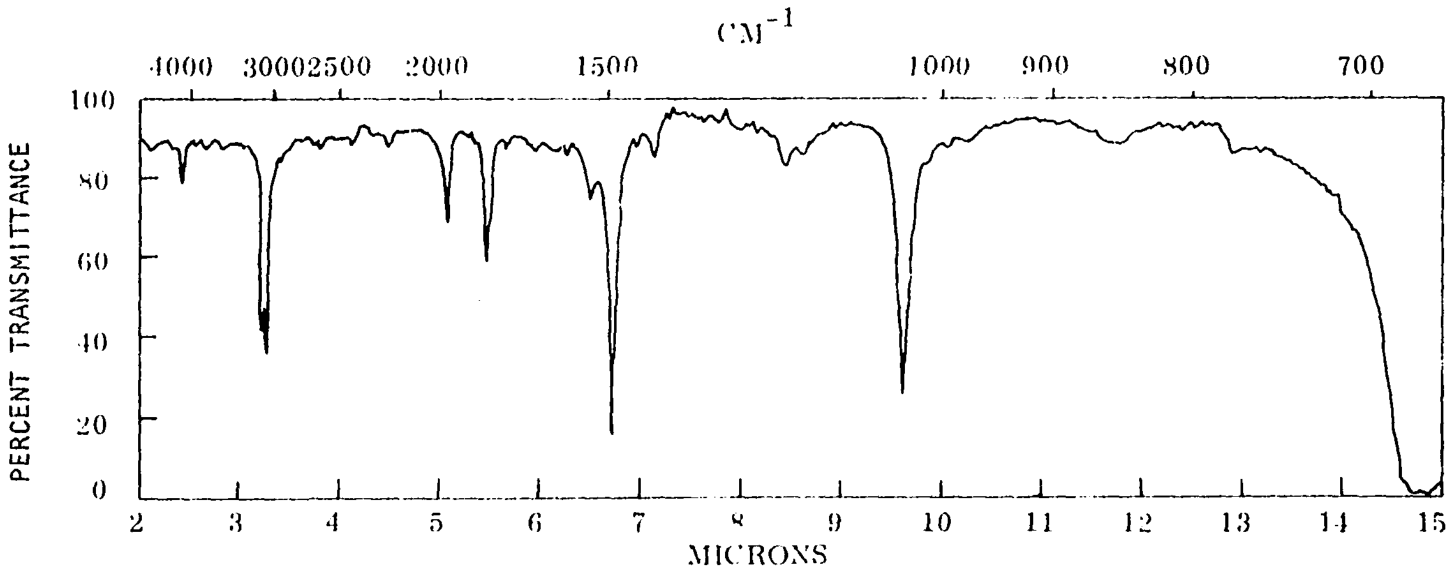

Figure 6. Qualitative analysis of the benzene used by infrared spectroscopy

METHODS OF INVESTIGATION

The adsorption isotherms and adsorption rates were determined by the gravimetric method (18). The infrared absorption spectrophotometry was conducted using the vacuum internal reflection technique (60).

Adsorption Apparatus

The adsorption apparatus was constructed and used for earlier investigation on calcium montmorillonite - H_2O system (110). Some modifications were made in the method of pressure readout.

The apparatus, Figures 7 and 8, consisted of a Cahn RG electrobalance system comprised of a beam balance (Mb), control unit (BC), and vacuum flask (VC), connected to a Sargent model SR recorder (R). The electrobalance coupled with the automatic recorder was used to measure the sample weight to microgram sensitivity. Changes in the sample weight cause the beam to deflect momentarily; this motion changes the phototube current which is amplified and applied to the coil attached to the beam. The coil is in a magnetic field, so the current passing through it exerts a moment on the beam, restoring it to balance. The current is an exact measure of the sample weight. A signal is sent to the control unit where it is amplified and the final signal is fed to the automatic recorder. The instrument was calibrated prior to the test, and a buoyance correction was applied. Room temperature was maintained at 22 $\pm$ 0.25°C throughout the investigation while the experiment was in progress.

A capacitance manometer (CM) coupled with a pressure sensing head (SH) was used to avoid mercury contamination and to maintain a pure adsorbent-

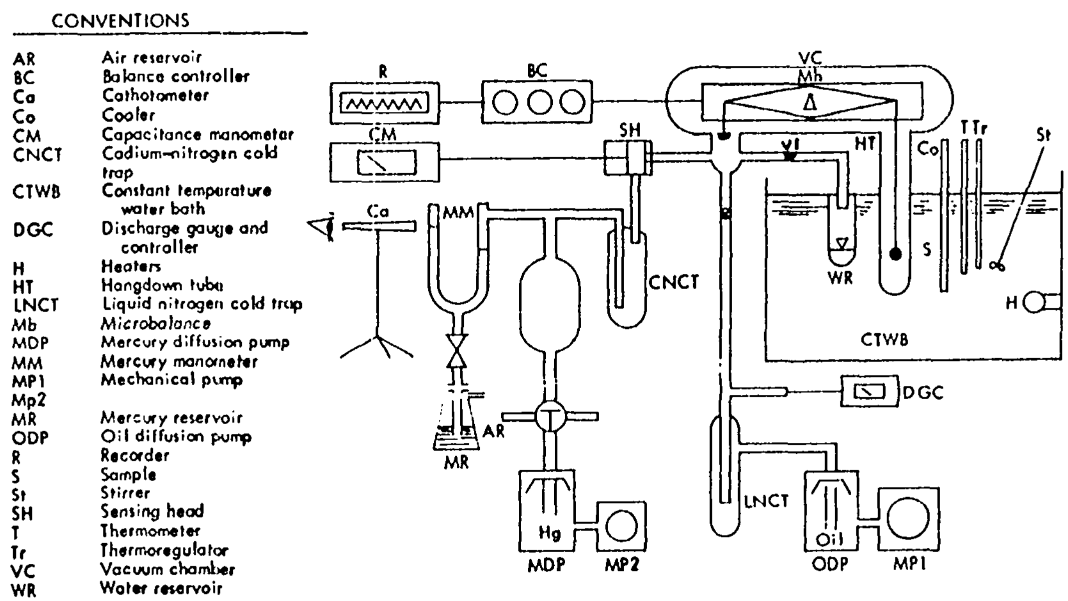

Figure 7. Schematic layout of adsorption apparatus

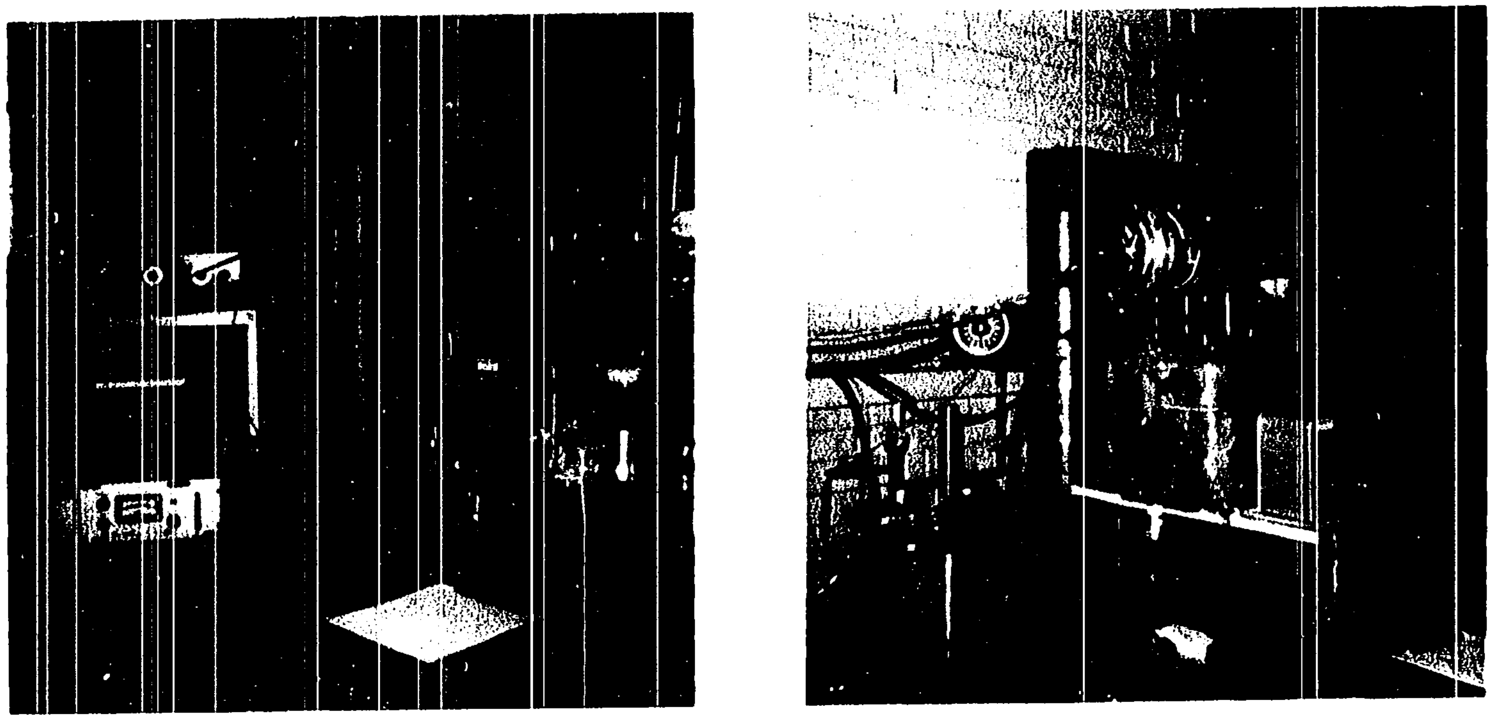

Figure 8. Gravimetric adsorption apparatus

adsorbate system. It operated as a null indicator for system pressure. The true pressure was read from the mercury manometer (MM) with a vernier micrometer slide cathotometer (Ca). The pressures read to one micron of mercury.

The vacuum train was a portable unit consisting of a fore pump (MP1), an air-cooled oil diffusion pump (ODP), a liquid nitrogen cold trap (LNCT) and a Cenco vacuum discharge gauge (DGC), all mounted on a rolling cart. The rotary mechanical fore pump and the VMF oil diffusion pump and a liquid nitrogen trap provided a high vacuum of 10^{-6} mm of mercury. Flex-pand bellows were connected wherever vibration could be transmitted. A cadmium-nitrogen cold trap (CNCT) was used in the manometer system to condense water, mercury, and oil vapors to prevent contamination of the capacitance manometer and to achieve a pure high-vacuum system in the reference leg of the mercury manometer.

The sample (S) was suspended from an arm of the microbalance into a pyrex glass hang-down tube (HT) which was immersed in the constant temperature bath (CTWB). Water or benzene was distilled into the system from a mercury sealed adsorbate reservoir (AR) which was also immersed in the constant temperature bath. The immersed heaters (H) - a continuous heater, and an intermittent electronic relay circuit heater, were two 100-watt light bulbs with variable transformer voltage control. A thermal regulator (Tr) with an "All Temp" cooler (Co) or a tap water cooling coil, controlled the bath to maintain the adsorption temperature. The variation in the thermoregulated temperature was not more than $\pm$ 0.01°C throughout the entire testing period and was $\pm$ 0.002°C when readings were taken with a

Beckman thermometer (T). The Beckman thermometer was calibrated against an N.B.S. certified thermometer.

All the valves used in the system were Teflon stem--viton "O" ring sealed Pyrex stopcocks purchased from the Scientific Glass Apparatus, Inc.

IR Absorption Apparatus

The IR absorption apparatus used was a Beckman IR-4 spectrophotometer compatible with a Wilks model 38B evacuable reflectance attachment. The Beckman IR-4 spectrophotometer combines double-beam and double-monochromator coupled with collimating mirrors which act as order sorters and cancel most of the aberrations. Figure 9 shows the optical arrangement of the system. Radiation from the Nernst glower (N) is received by a single mirror (Ml) and split into sample and reference beams by the rotating sector wheel, Cl. The beams are recombined by a second chopper, C2, synchronized with the first. After passage through the double monochromator (Pl, P2), the beam is condensed onto the thermocouple (T), which has a lens window. The amplified signal from the thermocouple positions the optical attenuator (A) in the radiation path so that the radiation from the reference and sample beams is equal in intensity. The position of the attenuator determines the position of the recorder pen.

A Wilks model 38B evacuable multiple reflectance attachment was used as a sample cell in the spectrometer. Figure 10 shows the optical layout and the actual cell mounted in the Beckman IR-4 spectrophotometer. The body of the cell consists of a stainless steel cylinder. The internal reflection element, KRS-5, is mounted in a stainless steel block suspended

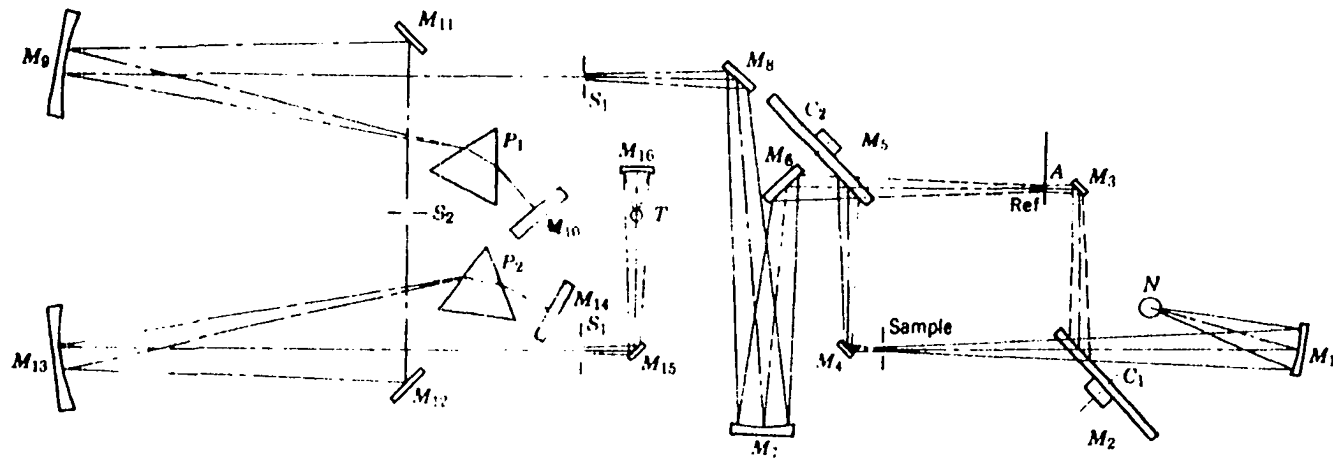

Figure 9. Beckman IR-4 infrared spectrometer

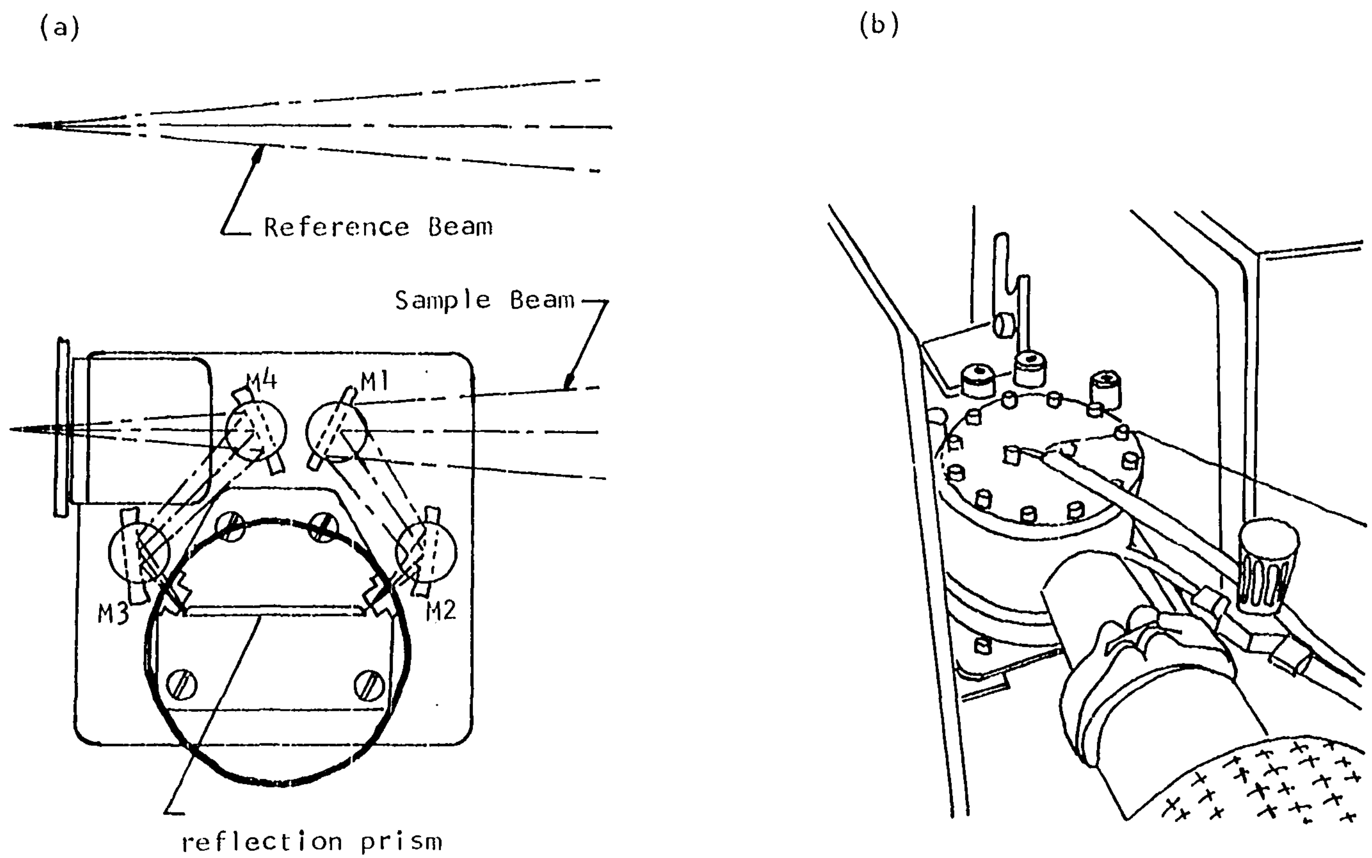

Figure 10. Wilks model 38B high vacuum heatable reflectance chamber: (a) Optical layout (b) perspective layout

from the cylinder lid. The block was tapped through the lid to accept two 85 watt Hotwatt heaters and a thermocouple well between the heaters. A high vacuum seal between the lid and cell body was accomplished by compressing a Viton "O" ring between the flat of the lid and the rim of the cell. The infrared windows, made of KRS-5, are 1.5 cm diameter plugs with a 2.5 mm flat flange; the vacuum seal is made also with Viton "O" rings. The window-plugs protrude into the cell and nearly contact the internal reflecting element. This design makes it possible to record the spectrum of molecules adsorbed on the sample surface which contact intimately the internal reflecting crystal and is in equilibrium with gas phase without interference of infrared absorption by the gas phase. The available cell used restricted the choice of angle of internal reflection to 45^{o}.

Figure 11 shows the complete schematic layout of the absorption apparatus. The apparatus consisted of a Beckman IR-4 spectrophotometer Sp, sample compartment where the vacuum chamber was located, the vapor source AR connected to a vacuum train. The vacuum train was a portable unit consisting of a fore pump MP, a Cenco water-cooled oil diffusion pump ODP, a liquid nitrogen cold trap LNCT and a Cenco vacuum discharge gauge DGC, all mounted on a rolling cart. The rotary mechanical pump and the Cenco oil diffusion pump provided a high vacuum of 10^{-6} mm of mercury. A cathotometer Ca was used to read the pressure from the mercury manometer MM. The pressures are accurate to $\pm$ 0.02 mm. A double cadmium trap was used to trap mercury vapor from the manometer. All the valves except one, a Hoke packless valve, used in the system were Teflon stem-viton "O" ring seated Pyrex stopcocks purchased from the Scientific Glass Apparatus, Inc.

CONVENTIONS

AR	Adsorbate reservoir
Ca	Cathotometer
CT	Cadmium trap
D	Detector
DGC	Discharge gauge and controller
E	Electronic
H	Heater
LNCT	Liquid nitrogen cold trap
M	Monochromator
MM	Mercury manometer
MP	Mechanical pump
MR	Mercury reservoir
ODP	Oil diffusion pump
RR	Recording readout
S1	Entrance slit
S2	Exit slit
SC	Sample compartment
So	Source
Sp	Spectrometer
Tb	Thermocouple and potensiometer
VC	Vacuum chamber

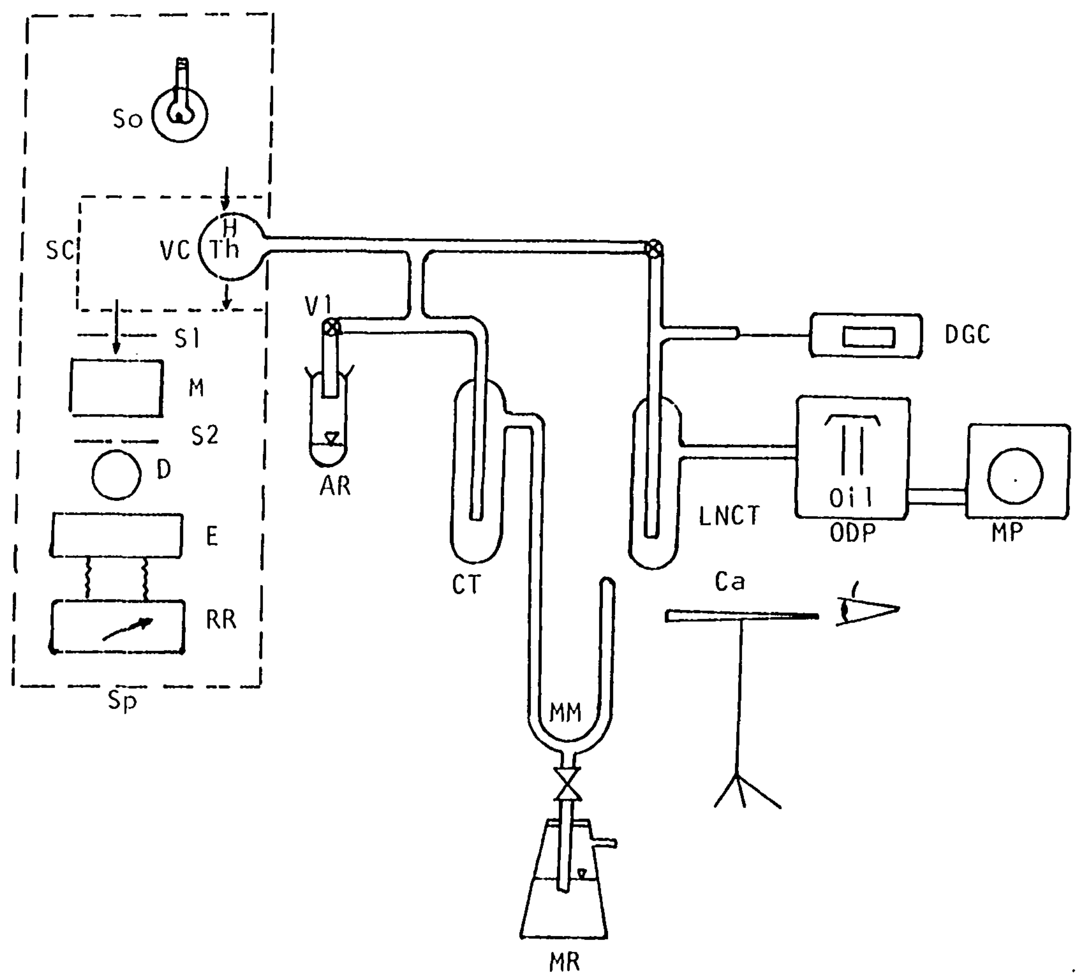

Figure 11. Schematic layout of absorption apparatus

The room temperature was maintained at 27 $\pm$ 2^{o}C throughout the investigation.

Preliminaries

Meniscus correction to mercury levels in the manometer

The mercury levels in each limb of the manometers for both the adsorption apparatus and the IR absorption apparatus were corrected for capillary depression of the apex of the mercury columns. After the inside diameter of the manometer limbs was determined, data from the International Critical Tables (93) were used to construct graphs of apex depression versus meniscus height. In case of diameter larger than 14 mm, the equation empirically derived by Huang et al. (68) was used to construct the calibration graph (Figure 12). The equation which reads

$$h = \left[(0.2936\gamma - 0.42325)\,\Delta h^2 + 0.225\gamma^3 - 0.325\gamma^2 + 0.009\gamma + 0.1306\right] \frac{\Delta h}{\Delta h^2 + \gamma^2},$$

produces all the data from the International Critical Tables, and it can be used for almost any size of manometer. The meniscus height was measured for each mercury level and the level reading corrected by adding the corresponding apex depression.

Gravity and temperature correction for manometers

Vapor pressure determinations were converted to the standard scale by the relationship: $h_o g_o \rho_o = hg\rho$, where h_o is the corrected manometer reading, g_o and g are standard, and local acceleration of gravity in cm/sec^2, and ρ_o and ρ are the density of mercury at 0^{o}C and at the test temperature in

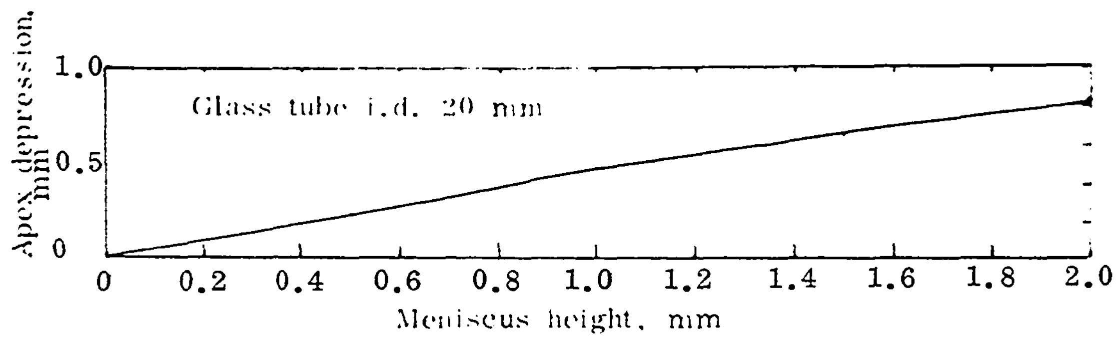

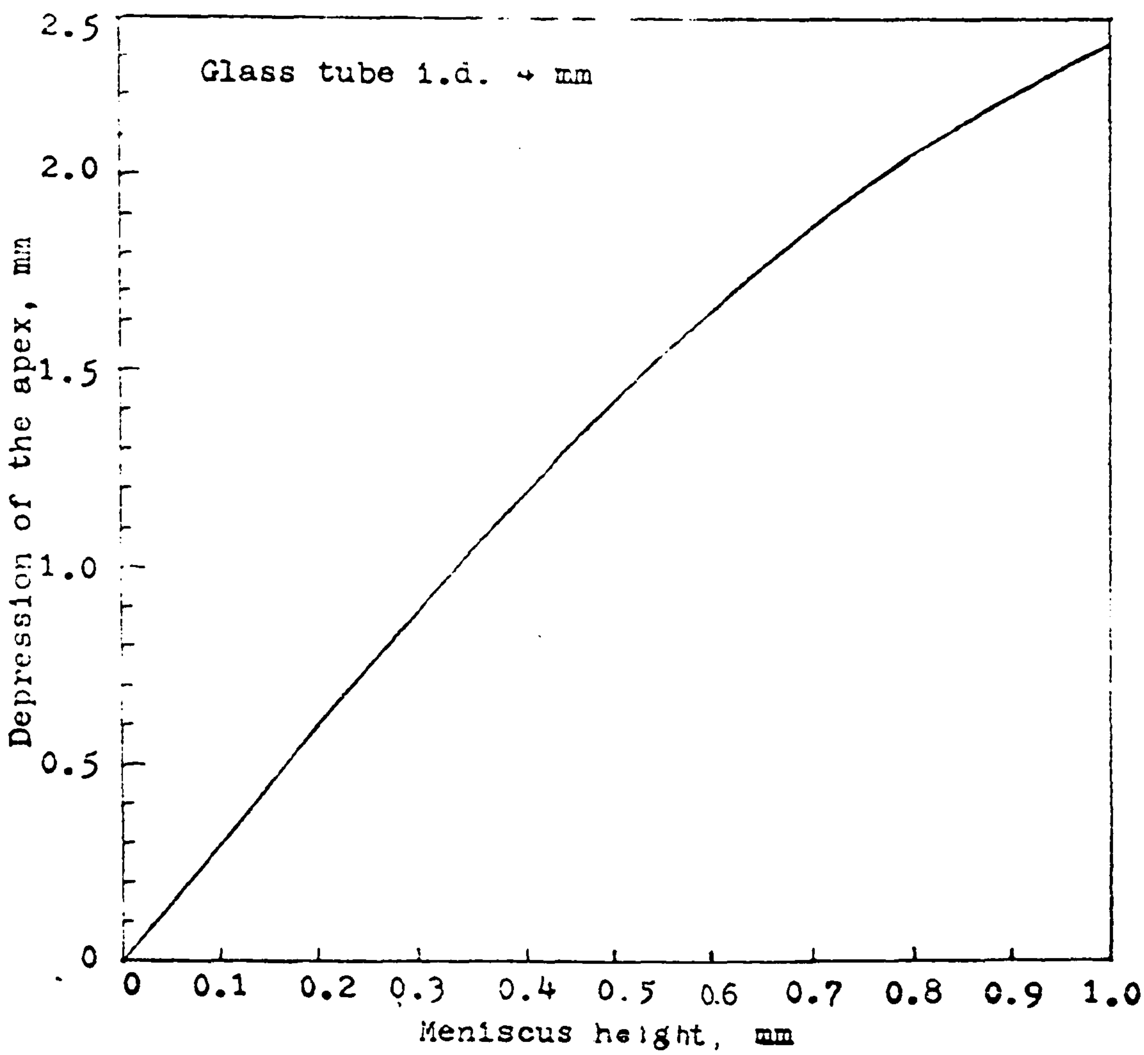

Figure 12. Capillary depression of the apex of a mercurial column in a glass tube

gm/cm^3, respectively. Values of $g_o = 980.665\ cm/sec^2$, and $\rho_o = 13.5951\ gm/cm^3$ were used. Values of ρ at test temperatures were obtained from the literature (122). The local value of the acceleration of gravity is $g = 980.297\ cm/sec^2$ (32). When these values are substituted in the above relationship, the following correction value was obtained:

$$h_o = 0.07535\ \rho h \qquad (42)$$

for both the adsorption apparatus and the absorption apparatus.

Electrobalance calibration

The electrobalance was calibrated based on the instruction manual supplied by the Cahn Instrument Company. The inert weight of 304 mg was made of 1 mm diameter platinum wire. After the calibration, the sample weight = substitution weight + mass dial reading + recorder reading.

Buoyancy correction to the electrobalance

The electrobalance readings were corrected for buoyancy force by running blank tests at various ranges of pressure. The weight used for blank tests was also made of platinum wire making the corrections for the balance mechanism alone possible. Figure 13 shows the calibration chart for buoyance correction for the balance. The weights measured were, thus, corrected accordingly.

Berenyi's correction factor f

The Berenyi's correction factor f was calculated using the ranges in Table 1 for each test temperature and pressure. They are presented in Figures 14 and 15 for water vapor and benzene vapor, respectively, and were used to calculate the correct adsorption volume according to Equation 5.

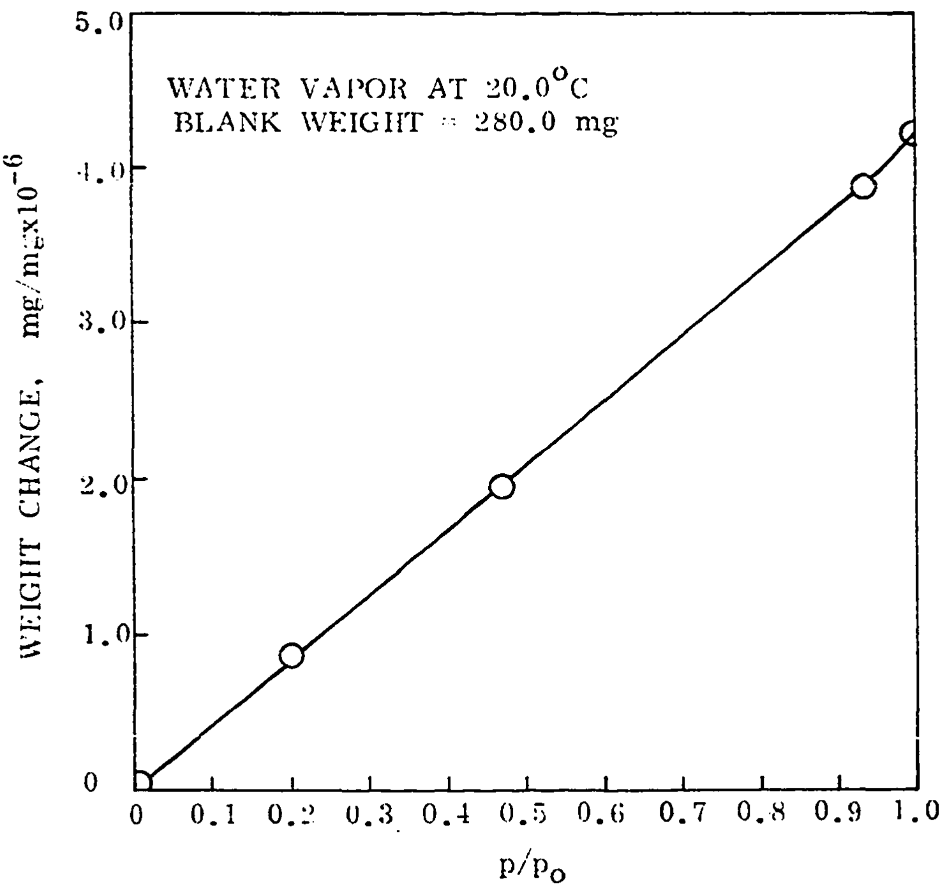

Figure 13. Buoyancy correction for RG Cahn balance used

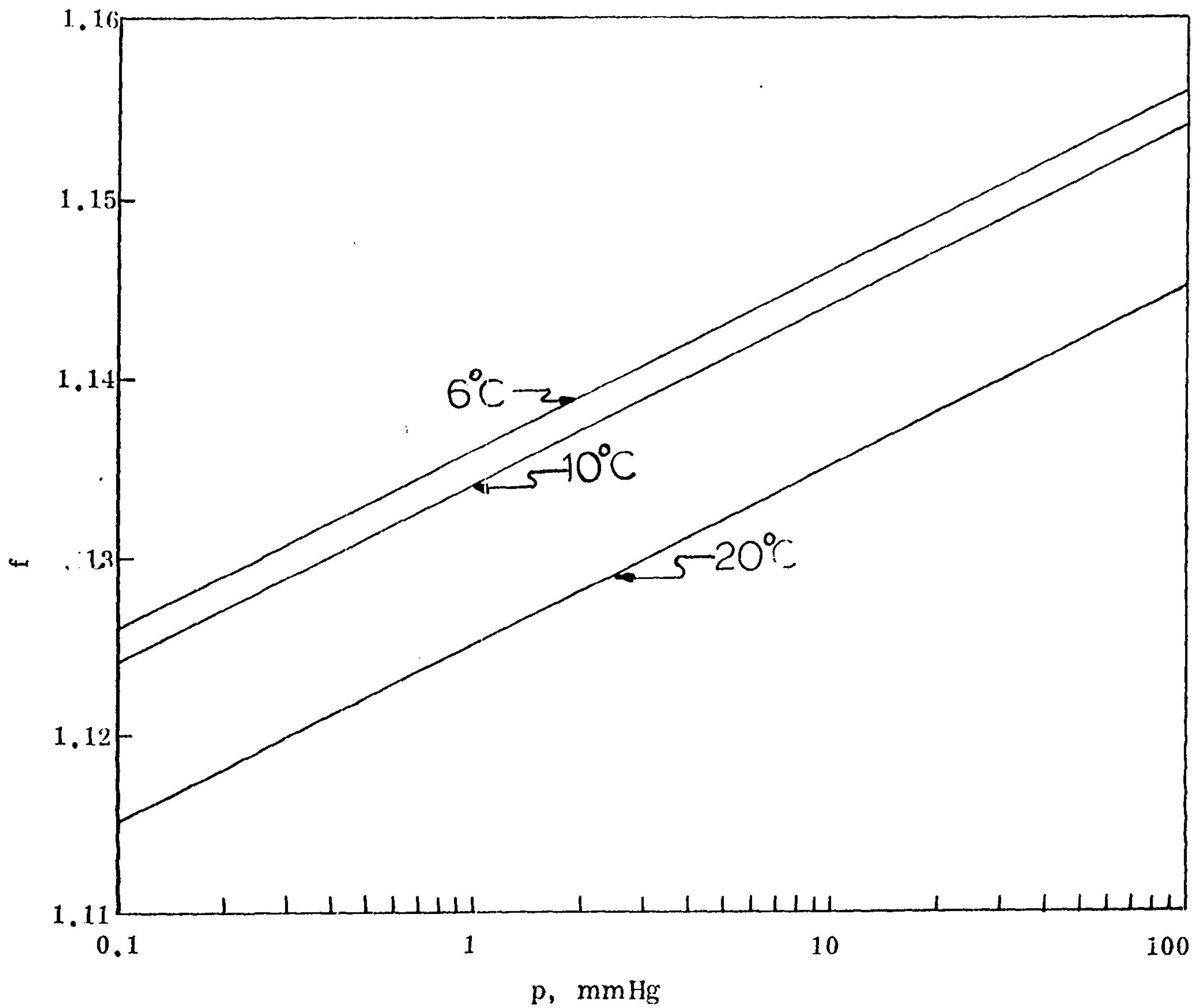

Figure 14. Berenyi's correction factor, f, for water vapor

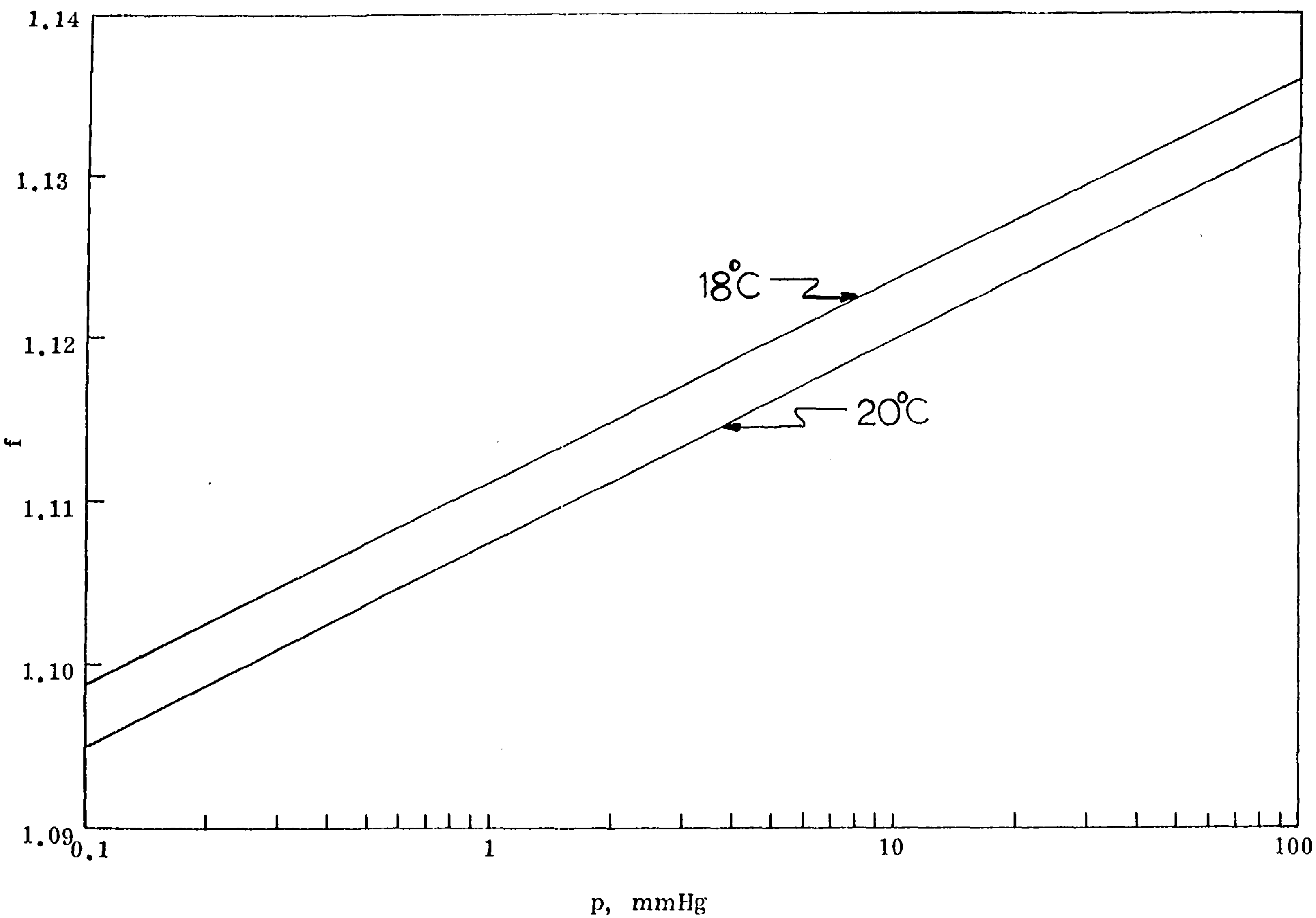

Figure 15. Berenyi's correction factor, f, for benzene vapor

Procedures

Determination of sorption isotherms

The sample in fiber form was prepared by wrapping about 280 mg of E-glass into a bundle with a nichromium wire. Other samples were ground in an acid cleaned ceramic vial with a SPEX No. 8000 Mixer/Mill and screened with SPEX nylon sieves to pass No. 200 and No. 400 sieves. A third category of sample was collected between No. 200 and No. 325 sieves after grinding. Just before testing, samples were heated to 110°C for 24 hours and cooled in a desiccator for one day. They were then introduced into the balance either in loose powder or compressed pellet or fiber form.

The sample and the system were evacuated for two weeks at room temperature which was maintained at 22°C throughout the investigation. The oil diffusion pump was started when the system reached a vacuum of 10^{-3} Torr; liquid nitrogen was introduced into the cold trap after the pressure reached 5×10^{-5} Torr. The hangdown tube containing the sample, and all parts of the adsorption system except the microbalance, were heated for 12 hours to about 300°C with a Bunsen burner. The sample was heated occasionally during degassing with an infrared heater. The adsorbate reservoir (either contains triple distilled water or purified benzene) was also degassed by pumping during the period of evacuation after the adsorbate had been frozen in liquid nitrogen. When the system reached 10^{-6} Torr (determined with a calibrated discharge gauge) the pumping valve was closed for two hours to determine if degassing was complete. The part of the system connected to the capacitance manometer was also pumped down at the same time. Finally the system was sealed and the capacitance manometer was calibrated. A reading of the automatic recorder was taken to determine the equilibrium weight in milligrams.

Water vapor or benzene vapor was transferred into the system from the adsorbate reservoir for the range of $p/p_o = 0$ to $p/p_o = 1$. The amount of adsorbate adsorbed on the sample was automatically registered on the recorder, and the actual vapor pressure was obtained by zeroing the capacitance manometer and a reading of the mercury manometer with the cathotometer. System equilibrium was attained when there was no increase in sample weight and no drop of system pressure. It was found that the equilibrium condition of adsorption on the sample in most cases was attained in about three to four hours after introduction of the vapor. Because of heterogeneous capillary condensation and slow glass wall adsorption the system sometimes required 24 hours to reach equilibrium. To eliminate uncertainties at least 24 hours were allowed between the vapor transfers. Readings were taken intermittently between four and eight hours and immediately prior to an additional transfer of vapor. In this manner, more and more vapor was introduced into the adsorption chamber until the saturation was reached.

In the vicinity of saturation the dew point technique was used to insure complete saturation. The high vacuum valve V1 was left open and after there was no additional rise in weight of the sample, a small amount of ice-water was introduced against the side of the hangdown tube containing the sample. This produced a small amount of dew on the hangdown tube, and the time for the dew to disappear was observed. At pressures below saturation the dew disappeared rapidly, whereas at saturation the time of disappearance sharply increased. The weight as recorded on the automatic recorder showed very little change in the weight of the sample, while the dew persisted on the side of the tube.

The desorption process was performed by cooling the adsorbate reservoir by means of a dewar flask containing ice water and opening valve V1 to distill small amounts of adsorbate into the adsorbate reservoir. Thus the desorption isotherm was obtained by condensing more and more vapor back into the adsorbate reservoir. This condensation process was performed by cooling with ice water to a p/p_o of about 0.15 then liquid nitrogen was used to bring p/p_o to zero. For the final removal of adsorbed vapor, the sample was pumped by using the vacuum train. As will be shown later, the pumping could not remove all of the adsorbate from E-glass; however, it could be and was removed by an infrared heater.

Determination of sorption rates

The same E-glass sample used in the adsorption isotherm determinations was used to determine the sorption rates at various temperatures using water vapor as adsorbate. After each balance calibration and evacuation, two different sample treatments were performed: one with infrared activated heating, and another without infrared activated heating. After this, valve V1 was opened and left open, and the weight increases due to adsorption were registered on the automatic recorder. Since the time for adsorption equilibrium was more than six hours, the recorder chart speed was selected to be one inch per hour.

For desorption rate study the process was reversed by freezing the adsorbate in the reservoir AR with liquid nitrogen. After the adsorbate reached liquid nitrogen temperature, valve V1 was opened, and the weights decreased due to desorption were automatically registered on the recorder. When desorption reached equilibrium, valve V1 was closed. The system was further evacuated by the vacuum train.

During the experiment, the thermostat, S (Figure 7) temperature was kept at the desired value (18 to 20°C) while the vacuum chamber, VC, was kept at room temperature (22°C).

Determination of infrared spectra

Three different forms of E-glass were used in obtaining infrared spectra. Firstly, the fiber was cut to the KRS-5 element longitudinal size and was packed on the two faces of the element. Secondly, the fiber was simply wrapped around the KRS-5 element. Thirdly, E-glass powder (-400 mesh) was spread evenly over the two faces of the element. The sample was then tightened in place and was placed in the vacuum chamber. The system was then sealed and evacuation was applied. The liquid nitrogen baths were placed around the adsorbate reservoir and cold trap. The diffusion pump was turned on when the system pressure reached 10^{-3} Torr. The adsorbate was degassed by repeated thawing, freezing and evacuation. Then infrared spectra were determined at various p/p_o values ranging from zero to 1 by using double beam and single beam operations. Patience is needed in focusing the reflection beam going through the internal reflectance element.

An infrared lamp was used to activate the system. At least two days of evacuation and one day of heating were allowed. One spectrum of E-glass under vacuum was taken prior to each adsorption cycle. The vapor was introduced from the adsorbate reservoir; a spectrum with SB and DB operations was subsequently taken. Pressure readings as well as room temperature were registered. More and more vapor was introduced in increments into the chamber and spectra determined until the saturation was reached. The desorption was performed in a manner similar to that used in the adsorption isotherm study by condensing the adsorbate into the reservoir with liquid nitrogen. The spectrum was taken at each desorption stage until the system reached vacuum again. The experiment was then terminated, and the adsorbate was changed for the next experiment.

Errors

Experimental error in determining p/p_o

The error in p/p_o for the adsorption isotherm study was determined as follows: The readings of the mercury manometer were made with a cathotometer, the reproducibility of which is $\pm$ 0.005 mm. The maximum error in the value of p_o due to temperature variations was estimated to be 0.02 mm. The error in p/p_o was obtained through the use of the following relationship (117, p. 20):

$$(\delta \frac{p}{p_o})^2 = (\delta \frac{p_o - \Delta p}{p_o})^2 = (\delta \frac{\Delta p}{p_o})^2$$

$$= (\frac{\partial \Delta p/p_o \delta \Delta p}{\partial \Delta p})^2 + (\frac{\partial \Delta p/p_o \delta p_c}{\partial p_o})^2 \qquad (43)$$

which gives:

$$\delta \frac{p}{p_o} = \pm \left[(\frac{\delta \Delta p}{p_o})^2 + (1 - \frac{p}{p_o})^2 (\frac{\delta p_o}{p_o})^2 \right]^{1/2} \qquad (44)$$

where $\delta \frac{p}{p_o}$, δp_o and $\delta \Delta p$ are the errors in p/p_o, p_o and the pressure difference, respectively. The error in p/p_o calculated by this expression was found to be $\pm$ 0.0004 for all pressure ranges.

The error in p/p_o for the infrared apparatus was also determined from the above equation. The readings of the cathotometer were found to be reproducible within $\pm$ 0.02 mm, and the maximum error in the value of p/p_o due to temperature variation was estimated to be $\pm$ 0.04 mm for all pressure ranges.

Experimental error in determining q

The automatic recording device had a reliability of 0.05% at the range selected. The error in grams of vapor adsorbed per gram of E-glass specimen was estimated to be a maximum of $\pm$ 3×10^{-6} gm/gm as determined from an average of five series of 20 recordings at selected equilibrium conditions.

Experimental error in determining dq/dt

The errors in determining sorption rate, dq/dt were determined according to Topping (117) as follows:

$$\frac{dq}{dt} = \frac{dq_o}{dt_o} \frac{(1 + \Delta q)}{(1 + \Delta t)} = \frac{dq_o}{dt_o} (1 + \Delta q)\ (1 - \Delta t + \Delta t^2 + \ldots)$$

$$\simeq \frac{dq_o}{dt_o} (1 + \Delta q - \Delta t). \qquad (45)$$

Thus the fractional error in dq/dt is approximately the difference of the fractional errors in q and t.

From the preceding discussion, Δq is about $\pm$ 3x10^{-6} gm/gm, and Δt is found to be about $\pm$ 0.01 min./min. Hence errors in dq/dt $\simeq - \Delta t + \Delta q = \pm 0.01 \pm 3\text{x}10^{-6} \simeq \pm 0.01$.

Experimental error in determining absorbance A

The error in determining absorbance A using Beckman IR 4 spectrophotometer are from the noises which are the keys to instrumental limits on precision. One of them is called source noise in which $\Delta I \propto I$. However this source of error is very small in Beckman IR 4 spectrometer. The other source of error is called Johnson noise which comes from the random motion of electrons in conductors in which ΔI = constant. Since

$$A = \log_e I_o/I$$

$$dA/A = \frac{-(\log e)\frac{dI}{I}}{A}$$

$$= \frac{-0.434}{A} dI/I \qquad (46)$$

Substituting Beer's Law, $I = I_0 10^{-abc}$, where a is absorptivity, b is path length, c is concentration and A = abc into the above equation, we obtain

$$\Delta A/A = -0.434\ (\Delta I/I_o)\ (1/A10^{-A}). \qquad (47)$$

To find A for $(\Delta A/A)_{min}$, we differentiate the above equation in respect to A:

$$\frac{d(\Delta A/A)}{dA} = \pm\ 0.434\ (\Delta I/I_o)\left(\frac{10^A/\ln 10}{A} - \frac{10^A}{A^2}\right)$$

and set it equal to zero. So, A = 0.4343 or %T = 36.8 for $(\Delta A/A)_{min}$.

Using $\Delta I/I = 0.005$ for the instrument used, the following table gives the limit of precision in determining absorbance.

Table 4. Limit of precision in determining absorbance A

%T	A	$\Delta A/A \times 100$, %
95	0.022	± 10.2
90	0.046	± 4.72
70	0.155	± 2.00
40	0.399	± 1.36
10	1.000	± 2.17
2	1.699	± 6.38

Figure 16 shows the relative error, $\Delta A/A$, plotted against A. As it can be seen from the Figure 16, one would not put the recording needle up to 100% T or down close to 0% T in order to prevent great uncertainty in determining A.

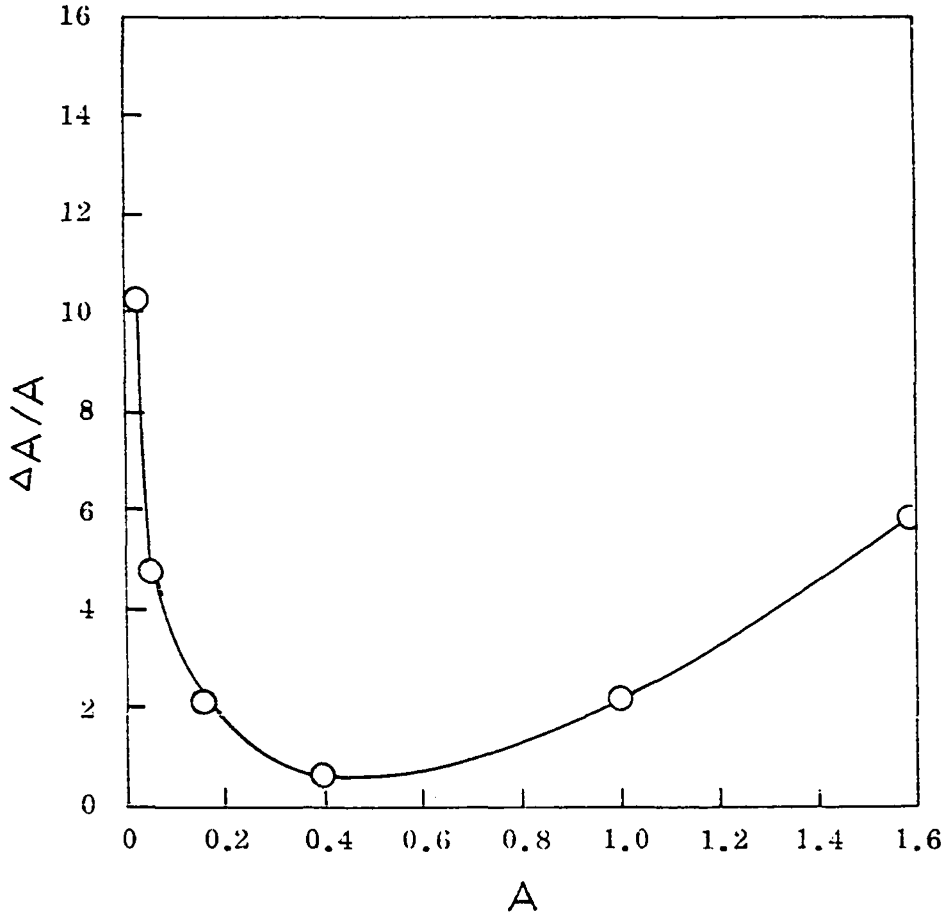

Figure 16. Relative error, $\Delta A/A$, plotted against A

PRESENTATION AND DISCUSSION OF RESULTS

Sorption Isotherms

The data for adsorption and desorption and the values of the functions for evaluation of Langmuir parameters, BET parameters and energy changes are presented in the Appendix (see Tables 20, 21, 22 and 23, for the water vapor sorption on E-glass fiber, Tables 24 and 25 for the water vapor sorption on E-glass powder, Tables 26, 27, 28, 29, 30 and 31 for the water vapor sorption on E-glass pellet and Tables 32, 33 and 34 for the benzene vapor sorption on E-glass pellet). The amount of vapor adsorbed, q, is expressed in gm per gm of the E-glass. The relative vapor pressure, p/p_o, is unitless and is expressed in a fraction. Included in the Tables also are the values of the function $\frac{p/p_o}{q}$ for the evaluation of the Langmuir parameters, the function $\frac{p/p_o}{q(1-p/p_o)}$ for evaluation of the BET parameters, and the function $\frac{q}{p/p_o}$ used to determine the free surface energy change.

The water sorption isotherms on various forms of E-glass at 6.00°C, 10.00°C and 20.00°C were obtained. Figure 17 is a plot of water vapor-E-glass sorption isotherms. The isotherms show equilibrium moisture contents for the E-glass as the relative water vapor pressure increases or decreases. In the low relative pressure region, the isotherm is concave to the pressure axis, whereas in the high relative pressure region it is convex to the pressure axis. In an intermediate relative pressure range the isotherm exhibits a somewhat linear portion, the length and slope of which Brunauer (18) states is dependent on the adsorbent, the adsorbate, and the temperature selected for the investigation. In a series of

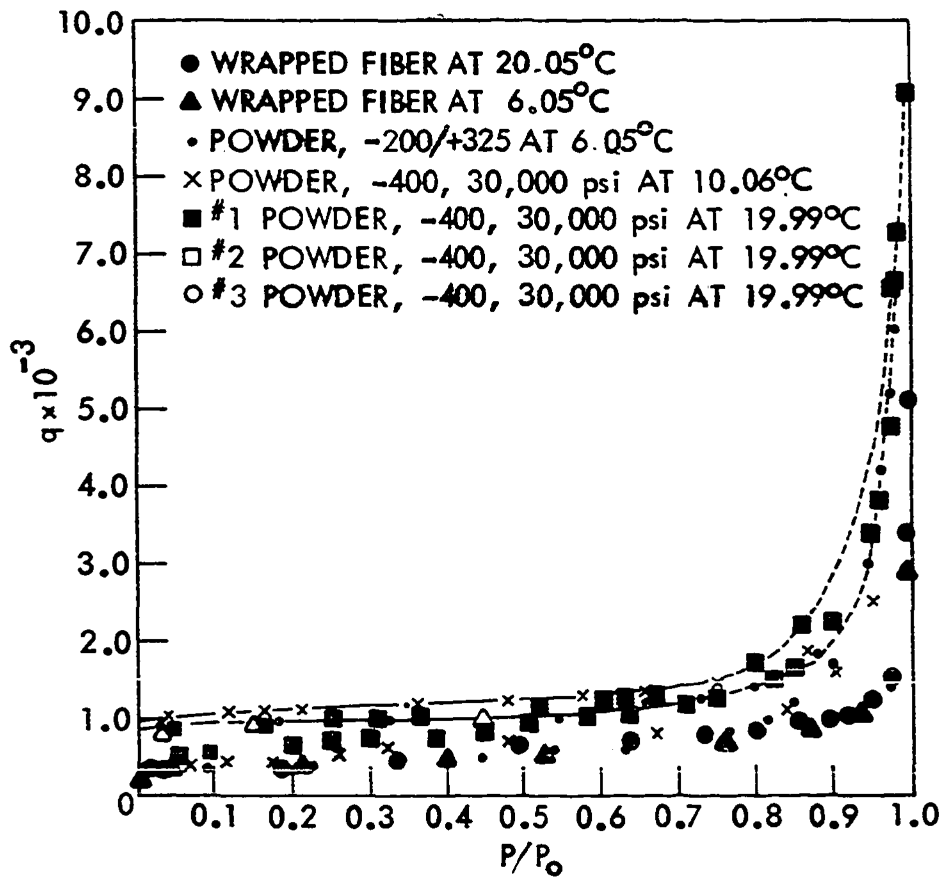

Figure 17. Sorption isotherms for water vapor sorbed on E-glass (adsorption cycle-dotted points, desorption cycle-dashed lines)

studies on the water vapor adsorption on clays, Orchiston (94, 95) points out that the multimolecular adsorption occurs on localized sites rather than being due to the formation of a mobile adsorbed layer. Using the Orchiston approach, the concave section of the isotherms explains the completion of the first layer on these sites. The convex section of the isotherm shows a running together of the cluster of water molecules around the active sites. In Figure 17 the weight adsorbed in the initial portions of the isotherms are nearly identical. At higher p/p_o values, because of the greater exposed surface area of the pulverized powder, the weight adsorbed by the powdered specimens is greater than the fiber specimens. The capillary spaces become filled with water as p/p_o approaches 1. Thus the weight adsorbed increases rapidly, reaching a limiting value corresponding to BET type IV isotherms (3, P. 584). The difference in the isotherms as well as in adsorbed weight is presumbly due to the difference in the average pore radius and the pore radii distributions.

Permanent hysteresis was always observed on desorption. In no case did the hysteresis loop come back to the origin. It is believed that the first monolayer of water was adsorbed so strongly that it formed OH bonds on the E-glass surface; thus it cannot be dehydrated simply by pumping. However, the samples could be dehydrated by infrared heating to close the hysteresis loop. This behavior has been reported by Razouk and his coworkers (103), Mikhail and Shebl (90) and Eqorov et al. (38) in their investigation of adsorption of water vapor on glass surfaces, silica and silica gels, respectively. According to Razouk and Salem (103), the adsorption of water vapor on glass surface is due partly to a chemisorbed monolayer which can not be removed by pumping at room temperature and partly to a physically adsorbed film which is estimated to be one molecule thick at 0.2 relative pressure and two molecules think at 0.8 relative pressure.

Physical adsorption on the surface of the adsorbent is usually completely reversible, whereas the hysteresis shown by the desorption branch may or may not be reversible. The data of the present study also suggest that the adsorption, rather than desorption branch is the true equilibrium curve.

According to Brunauer (18, p. 409) the adsorption process most probably causes a change in the pore volume which may be either reversible or irreversible. The pore volume change may result in different pore shapes. This may account for the differences between the successive adsorption curves and in the specific surface areas as will be explained later.

The first explanation for hysteresis was advanced by Zsigmondy (18, p. 394). He assumed that during adsorption the vapor does not wet the walls of the capillaries in which adsorption takes place. As the adsorption reaches saturation, the impurities are displaced and complete wetting takes place at saturation.

The hysteresis due to trapped gases or adsorbed water molecules should be eliminated or reduced by effective evacuation of the system prior to investigation. However, pore size, its distribution and bond formation probably remain as the chief causes of hysteresis.

McBain (85) proposed the "ink bottle" theory of hysteresis. He points out that as p/p_o increases, the condensed absorbate will occupy the narrowest cross-section and will extend to wider cross-section only as p/p_o increases. When the vapor is sufficiently close to saturation, the pore will be completely filled. On desorption, no evaporation will occur from filled pores until the relative vapor pressure has fallen to a value sufficient to cause evaporation from the largest orifice or passage leading to the larger enclosed cavity. The true equilibrium, according to this hypothesis, corresponds to the adsorption points since the liquid, contained in the body of the pore, is in equilibrium with the vapor only on the adsorption side. This is also in agreement with the "open pore" theory proposed by Foster (46).

Figure 18 presents a plot of benzene vapor-E-glass pellet adsorption isotherms. The shape of the curves looks the same as that of water adsorption isotherms. However, less affinity is found for benzene adsorption than for water adsorption. This is due to the stronger physical bonds formed with polar molecules on E-glass, i.e., H_2O, which causes higher initial heat of adsorption (11, 73). This will be discussed later in this report.

Several interesting facts concerning the rate of adsorption were observed during the investigation. The spontaneity and instantaneousness of adsorption was indicated by the automatic recording device attached to the electrobalance. As soon as a small increment of adsorbate vapor entered the system, the response of the pen was immediate. At low relative pressures, the slope of the line described by the marking pen was very steep, and the slope decreased as the relative vapor pressure approached saturation. During desorption studies, this trend was

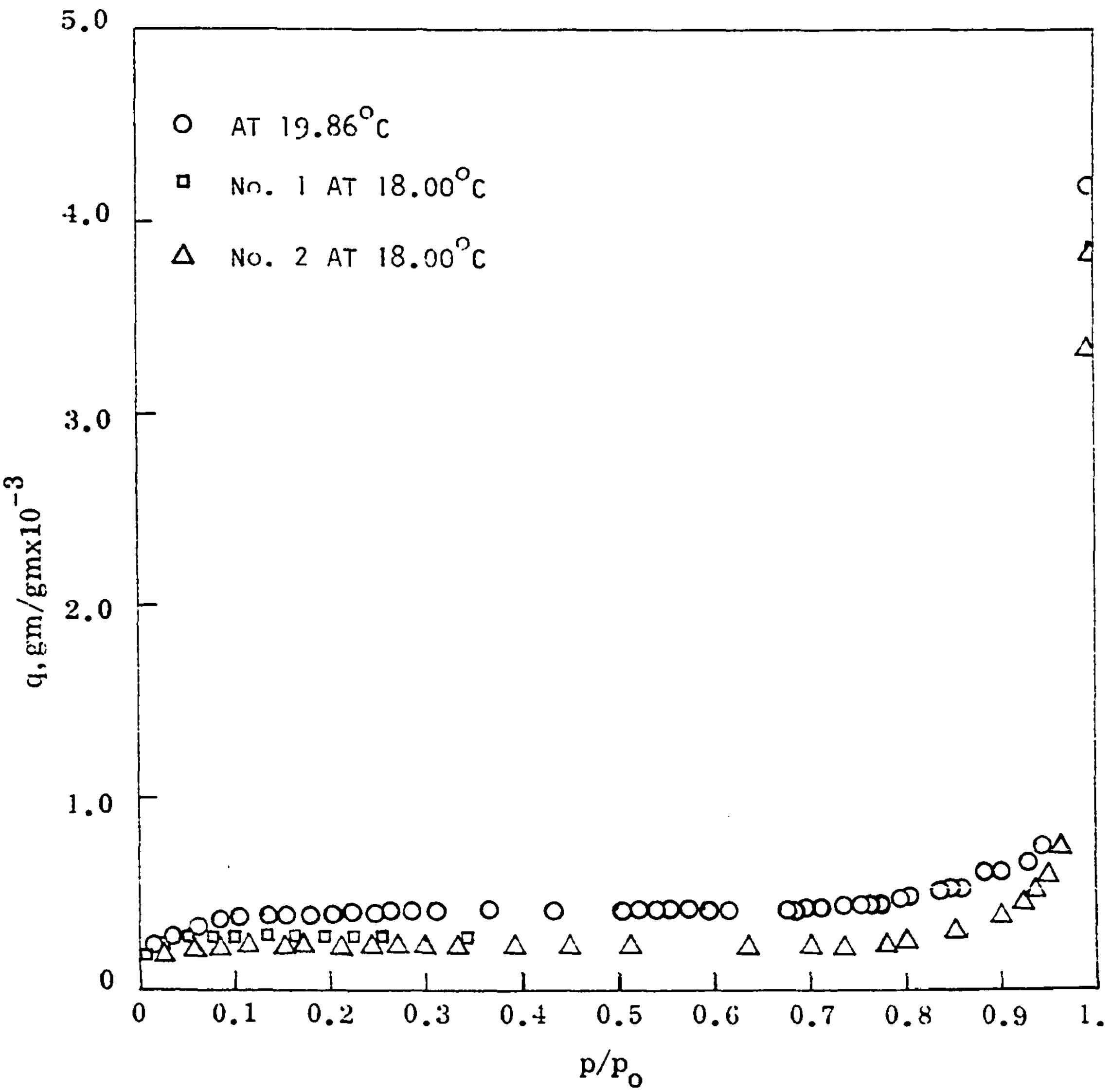

Figure 18. Adsorption isotherms for benzene vapor on E-glass pellet

reversed at high relative vapor pressures. These phenomena have been observed by various investigators (32, 104, 110) on the studies of water vapor-montmorillonite systems.

If it is assumed that only a small fraction of the impinging vapor molecules are reflected back elastically by the solid, the rate of adsorption on a free surface would be quite rapid. If, however, the adsorbent contains long, very narrow pores and the vapor must diffuse into them, the adsorption would take a longer time to reach equilibrium. If the incoming water molecules must displace previously adsorbed molecules already there, the rate of adsorption may become very slow. In our studies, equilibrium was reached in four hours after introduction of vapor and six to eight hours after removal of vapor for adsorption and desorption respectively. The mechanism which causes these long sorption rates will be further discussed later in the report.

Specific Surfaces

The values of the BET function, $\frac{p/p_o}{q(1-p/p_o)}$, tabulated in Tables 20, 22, 24, 26, 28, 30, 31, 32, 33 and 34 are plotted against the relative pressure, p/p_o, in Figures 19 and 20 for the water vapor and the benzene vapor sorption on various forms of Fiberglas-E.

Each of the plots in Figure 19 shows that a fairly straight line is obtained with sorption data in the p/p_o range of 0.01 to about 0.25 for the water sorptions. But each of the plots in Figure 20 shows a straight line only in the p/p_o range of 0.01 to 0.15 for the benzene adsorption. Generally, BET will have a straight line region between p/p_o value of 0.05 to 0.30 (3, p. 583).

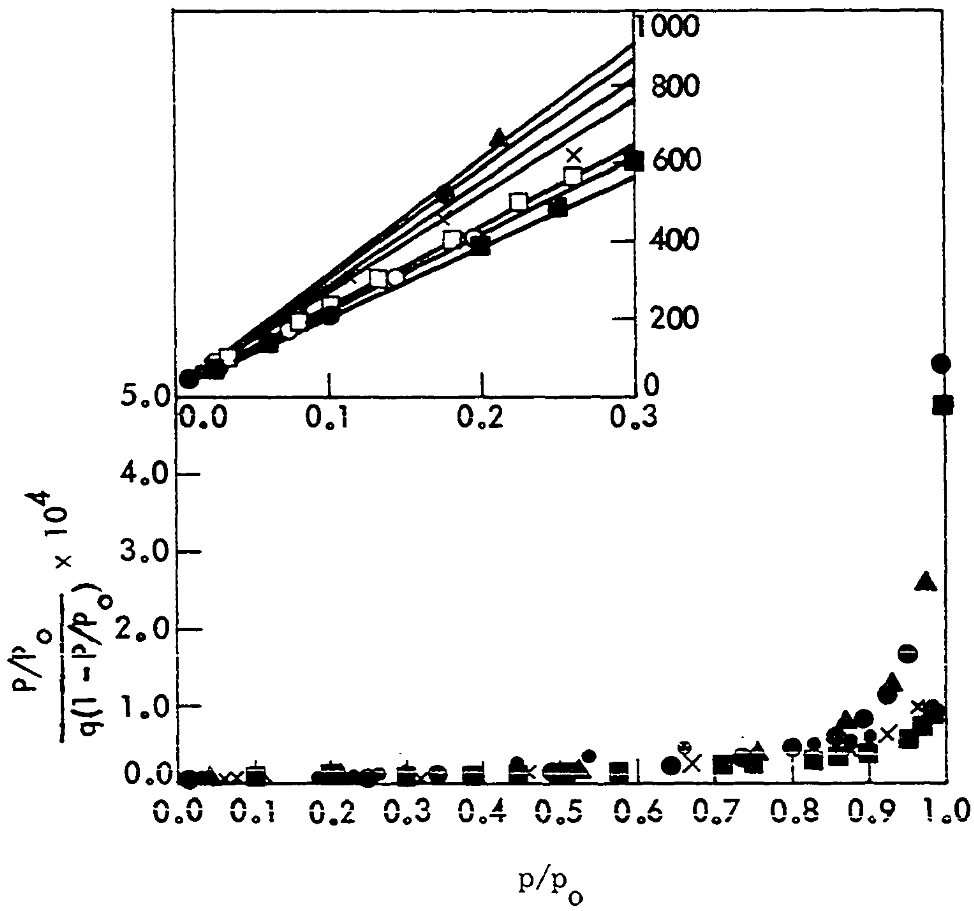

Figure 19. BET plots for water vapor adsorbed on E-glass

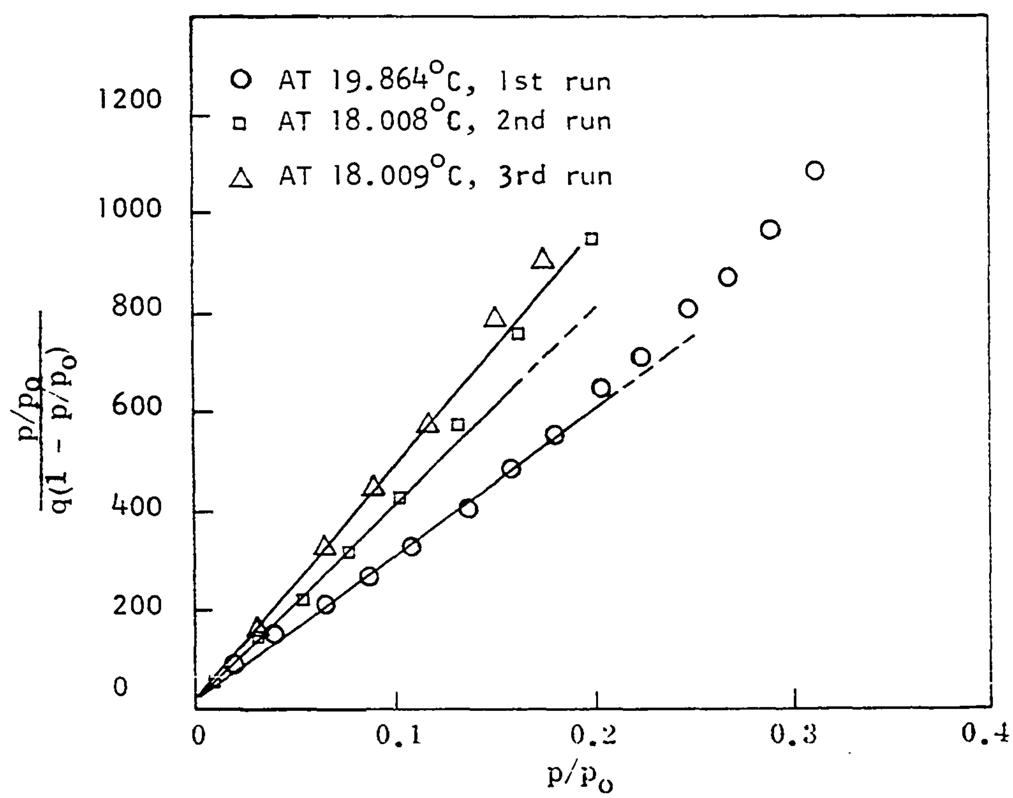

Figure 20. BET plots for benzene adsorption on E-glass pellet

The surface areas were calculated from the slope and intercept of the BET curves in the range of 0 to 0.25 in the case of water adsorption and of 0 to 0.15 in the case of benzene adsorption using a water molecule cross-section area of 10.8 A^2 and a benzene molecule cross-section area of 32.2 A^2 at the closest packed condition. Results are listed in Table 5 using water vapor adsorption. Results for the benzene vapor adsorption are listed in Table 6.

In case of water vapor adsorption, two determinations at different temperatures on the same fiber specimen were in agreement giving 1.21 m^2/gm. The 200-325 mesh powder fraction had slightly higher area. The 400 mesh compressed powder, i.e., pellet, specimen was tested four times in succession. The specific surface increased 38% after the first adsorption desorption cycle to 1.95 m^2/gm and then became fairly stable at a value about 25% greater than the original area.

Table 5. BET area determination of E-glass by adsorbing water vapor

Sample No.	Test No.	Iso-temp.	$q_m \times 10^{-14}$	C	$\Sigma, m^2/gm$	Specimen treatment
1	1	20.05	3.37	370	1.22	Fiber
1	2	6.05	3.35	370	1.21	Fiber
2	3	6.05	3.75	133	1.35	200-325 mesh powder
3	4	10.06	3.95	133	1.42	400 mesh compressed powder
3	5	19.99	5.39	93	1.95	400 mesh compressed powder
3	6	19.99	4.72	106	1.71	400 mesh compressed powder
3	7	19.99	4.95	101	1.78	400 mesh compressed powder

Table 6. BET area determination of E-glass by adsorbing benzene vapor

Sample No.	Test No.	Iso-temp.	$q_m \times 10^{-4}$	C	$\Sigma, m^2/gm$	Specimen treatment
3	B1	19.86	3.39	147	0.84	400 mesh pellet
3	B2	18.00	2.52	198	0.63	400 mesh pellet
3	B3	18.00	2.10	238	0.52	400 mesh pellet

The specific surface of the fiber determined by BET method is about ten times the specific surface calculated from the geometry of the fiber using a light microscope. (Figures 21 and 22 show pictures viewed from the end and from the side of the fiber. The calculation of the geometric fiber area is shown in the Appendix.) Surface roughness or porosity may be a factor in this anomaly. Chemical changes produced at the time of production by treating with water could cause an active surface. Water attack on freshly fractured surfaces could also occur on the first and subsequent sorption cycles on compressed samples. Weathering and corrosion of glass surface have well been recognized (109, p. 262). Glass fiber is attacked by atmospheric moisture adsorbed on the large surface area of the filament, alkalis pass from the glass to the water film forming an alkaline solution, which produces a secondary intensive destruction of the vitreous silicate. The fiber surface becomes hygroscopic and, after taking up more atmospheric moisture, electrically conductive (120, p. 424). Surface destruction of glass fiber is basically the same as that of a window-pane or a glass beaker, and the difference is only in the much larger specific surface of the fiber. For this reason

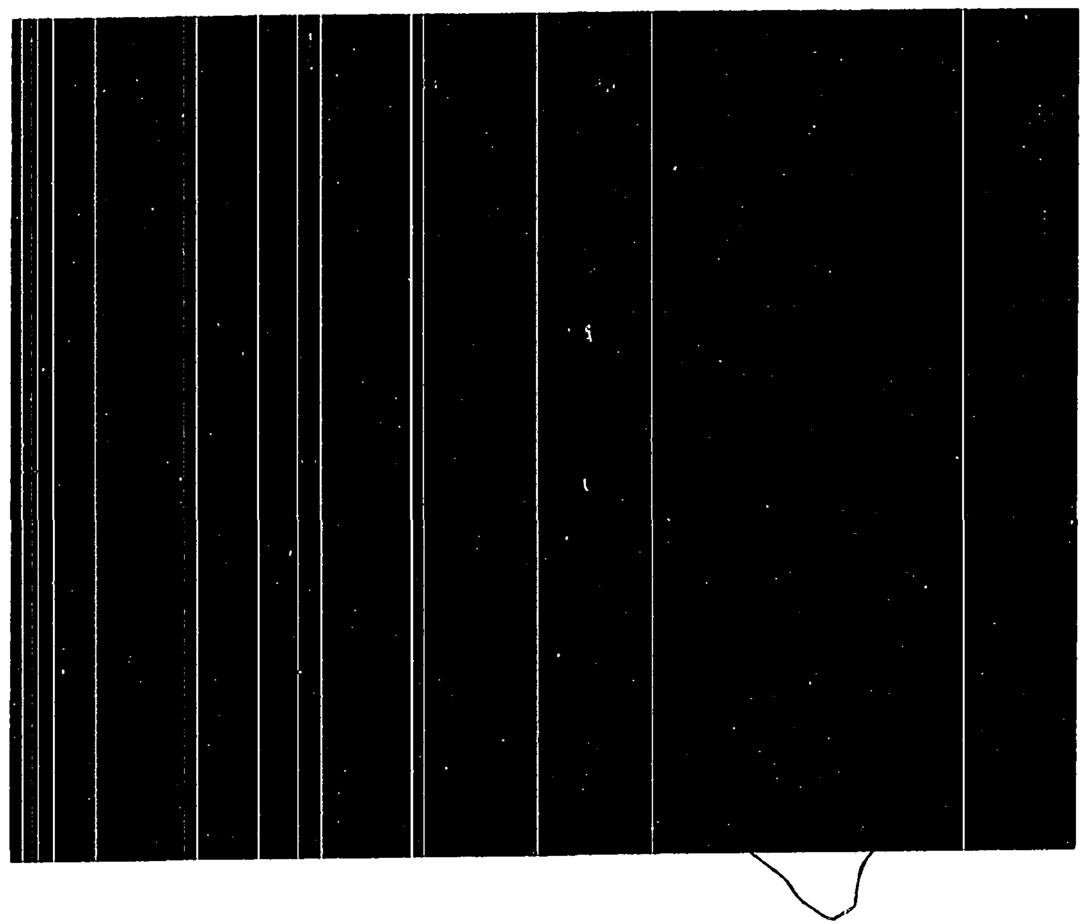

Figure 21. End view of Fiberglas-E through Zeiss Ultraphot II (M.P. = 1000)

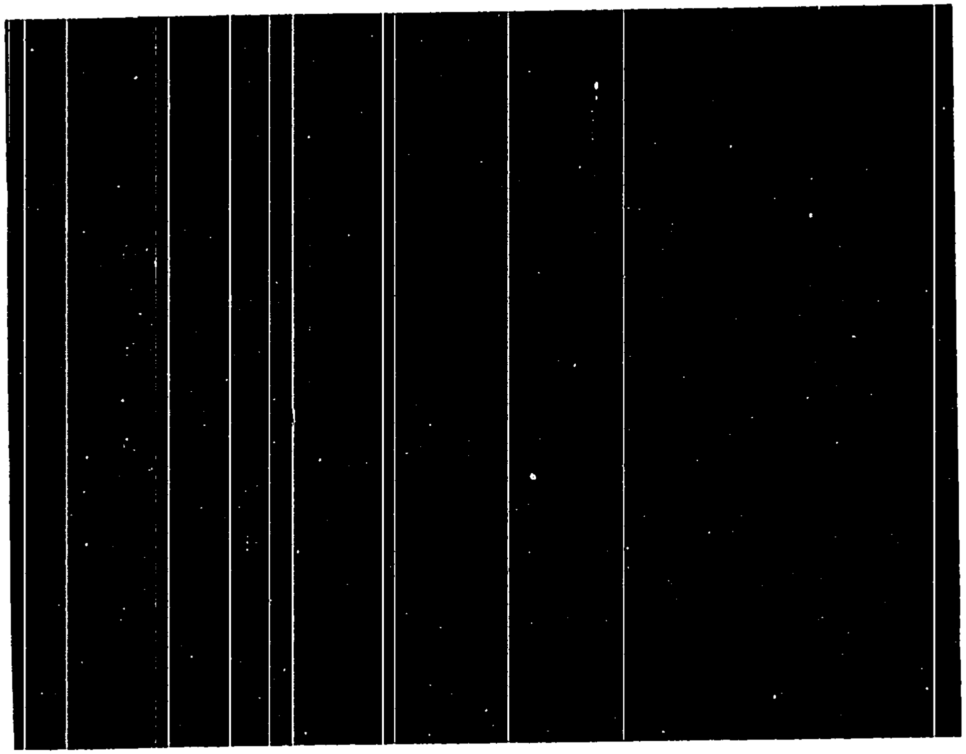

Figure 22. Side view of Fiberglas-E through Zeiss Ultraphot II (M.P. = 800)

the surface destructive process is more intensive on glass fiber than on ordinary flat glass.

The leaching of glass with strong reagents like cleaning solution is well known to increase the surface area. Pliskin (98) showed that boiling water leached 85% of the boron out of a thin film of Corning 7050 borosilicate glass. The surface destruction was also found on the E-glass surface after boiling in water (69, 28).

In a recent study of glass fiber surfaces by electron microscopy and gas adsorption, Donnet et al. (35) were able to trace the surface cracks which had followed an helicoidal path, representing the minimum energy line on a leached E-glass fiber. According to them E-glass fiber specific surface could reach 200 m^2/gm, if leached with 0.04% HF solution for 9 hours.

Little variation in specific surface was found for the fiber sample between two adsorption experiments while larger differences occurred with powders. This may be attributed to the presence of freshly fractured surfaces in powdered specimens, and to the effect of compression on the sample. Compression of finely pulvirized fibers could have caused some welding and could seal or close the pores. Water adsorption and subsequent dehydration could make the isolated pores accessible - also causing an increase in apparent surface area on the second determination.

Benzene adsorption on E-glass gave about half of the surface areas which were obtained from water adsorption (see Table 6). It may be assumed that portions of the micropores were sealed off and reduced by the adsorption of benzene vapor. The microstructures of glass have been studied by various investigators (103, 38, 40). Razouk and Salem in 1947 (103) found that the real surface is about two to three times greater than the geometric surface in the case of water-washed glass and about ten to twenty times in the case of acid-treated glass. Egorov et al. (38) found that the silica gel specific surface decreased from 695 m^2/gm to 178 m^2/gm when the heat treatment temperature was increased from 300°C to 900°C. According to Menzies (89), this was because the capillaries in the surfaces were sealed due to incipient fusion by heating glass. This sealing with modern day's understanding may be attributed to diffusion instead of incipient fusion. In study of microporous structure of silica gel using various vapors, Mikhail and Shebl (90, 91) found that specific surface of silica gels determined by water and nitrogen vapors was 796.8 m^2/gm while benzene vapor gave specific surfaces either 438.0 or 721.0 m^2/gm depending on the benzene orientation on the surface. The former value was the result of vertical orientation and later value was the result of flat orientation. They also pointed out that in very small micropores the molecular area of benzene increased. They used 25 $Å^2$/molecule for vertical orientation and 42 $Å^2$/molecule for flat orientation. In small micropores the molecular area was as high as 84 $Å^2$/molecule.

Surface Free Energy Change of Wetting

The values of the function $\frac{q}{p/p_o}$ versus p/p_o used to determine the free energy change of wetting were plotted in Figures 23 and 24 for the water and benzene adsorption data, respectively. The free energy change of wetting was determined from the area under the curve (graphical integration of Equation 30). The results obtained are tabulated in Tables 7

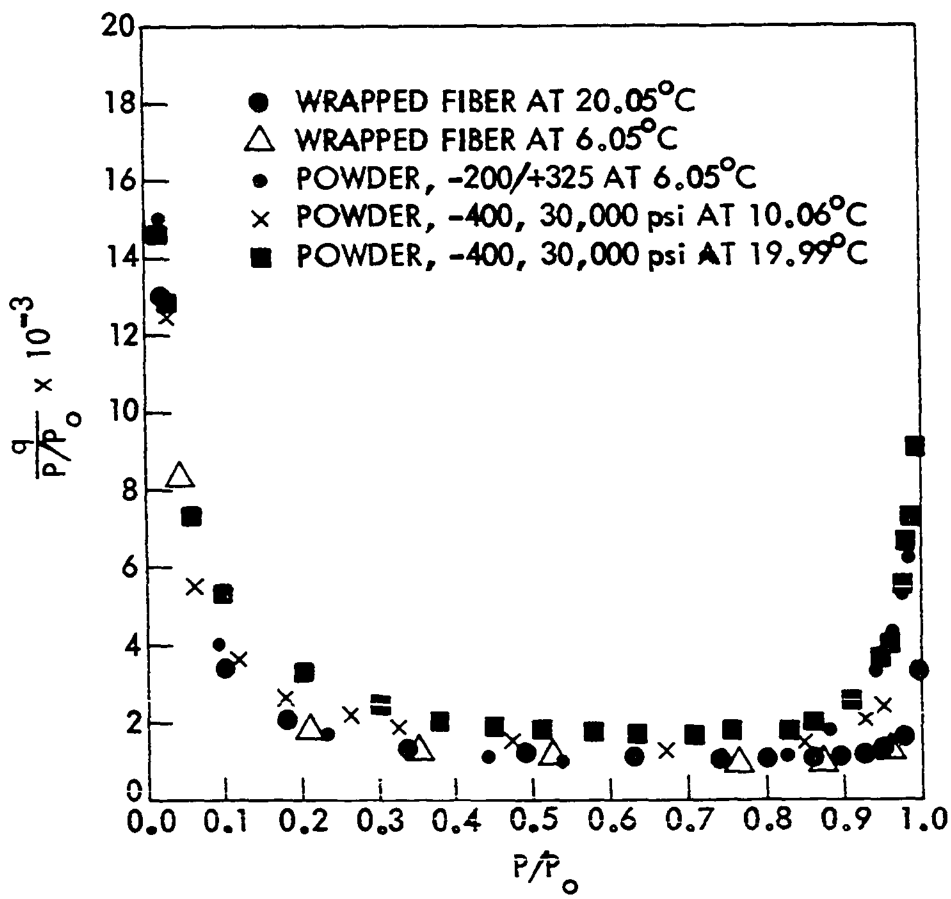

Figure 23. Free energy change plot for the adsorption of water vapor on E-glass

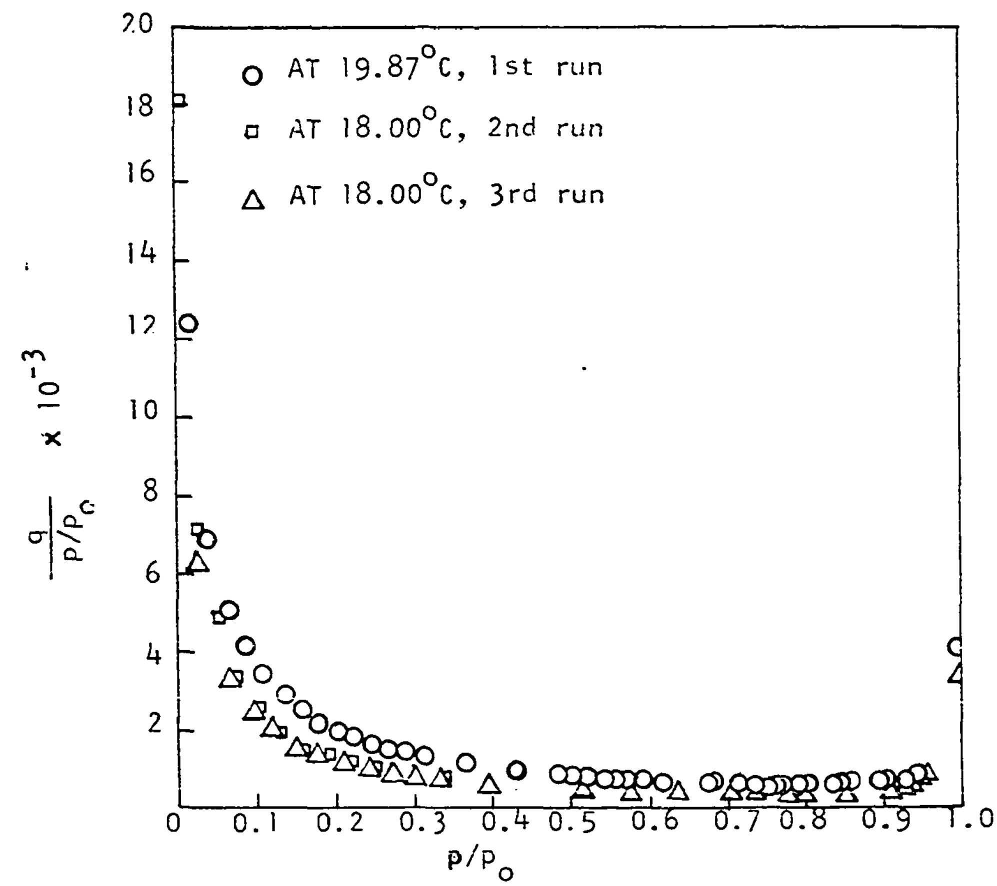

Figure 24. Free energy change plot for the adsorption of benzene vapor on E-glass pellet

and 8. The fibers have a lower surface free energy than the powdered specimens at the same temperature. Application of compression pressure seems to have no effect on the free energy change of wetting. This fact has been pointed out by Craig and his co-workers (27) on the investigation of the water adsorption on graphite.

Table 7. Surface free energy change for the adsorption of water vapor on E-glass

Sample No.	Test No.	Iso-temp.	Σ m^2/gm	ΔF erg/m^2	W_a^a erg/m^2
1	1	20.05	1.22	-246.85	319.6
1	2	6.05	1.21	-235.02	309.8
2	3	6.05	1.35	-241.22	315.9
3	4	10.06	1.42	-244.52	318.7
3	5	19.99	1.95	-253.69	325.4
3	6	19.99	1.71	-	-
3	7	19.99	1.78	-	-

[a]Calculated based on Equation 31.

Table 8. Surface free energy change for the adsorption of benzene vapor on E-glass pellet

Sample No.	Test No.	Iso-temp.	Σ m^2/gm	ΔF erg/m^2	W_a^a erg/m^2
3	b1	19.86	0.845	-72.36	101.2
3	b3	18.00	0.523	-71.11	100.1

[a]Calculated based on Equation 31.

The surface free energy of wetting and the work of adhesion computed here are reasonable when compared with those for water and benzene on

Table 9. Comparison of surface free energy change and work of adhesion of different materials upon water adsorption

Solid	$-\Delta F$ erg/cm^2	W_a erg/cm^2	Temp. °C	m^2/gm	Reference
Na-montmorillonite	40.5		23	749	Demirel (32)
Ca-montmorillonite	76.6		23	751	Demirel (32)
Graphite	64	136	25		Boyd and Livingston (17)
		385			Harkins and Boyd (58)
Silica (gel)	82.8			500	Bartell and Fu (12)
Mercury	101	174	25		Boyd and Livingston (17)
Tin	168	312	25		Loesser et al. (81)
TiO_2	196	340	25		Loesser et al. (81)
		640			Harkins and Boyd (58)
	300	370	25		Boyd and Livingston (17)
SnO_2	220	364	25		Loesser et al. (81)
	292	364	25		Boyd and Livingston (17)
		800			Harkins and Boyd (58)
Calcite	264		25	0.92	Demirel and Enüstün (33)
SiO_2 (Quartz)	316	388	25		Boyd and Livingston (17)
		720			Harkins and Boyd (58)
CaF_2		1170			Howard and Culbertson (66)
PbS		2750			Howard and Culbertson (66)

Table 10. Comparison of surface free energy change and work of adhesion of different materials upon benzene adsorption

Solid	$-\Delta F$ erg/cm^2	W_a erg/cm^2	Temp. °C	Σ m^2/gm	Reference
SiO_2	81	110	25		Boyd and Livingston (17)
$CaCO_3$	155		25	0.98	Demirel and Enüstün (33)
Mercury	119	148	25		Boyd and Livingston (17)
TiO_2	85	114	25		Boyd and Livingston (17)
Graphite	76	96	25		Boyd and Livingston (17)

various materials (Tables 9 and 10). E-glass has a larger surface free energy change when it adsorbs water vapor than montmorillonite, graphite, silica gel and TiO_2, but lower than calcite, SiO_2 (quartz), CaF_2 and PbS. The strong chemical bondings within the latter group contribute to this. Na-montmorillonite and Ca-montmorillonite swell upon adsorption of water, and thus reduce the free energy change. E-glass shows no similar swelling during water adsorption as evidenced by the fact that there is no break in the spreading pressure (calculated from Equations 30 and 32b) versus relative humidity plots (Figures 25 and 26).

It is important to note that at every p/p_o film pressure of benzene vapor on E-glass is only a fraction of that of water vapor on E-glass.

Adsorption Energy Change and Microstructural Analysis

As pointed out in Equation 30, the free energy change of adsorption may be expressed as:

$$\Delta F = -\frac{RT}{M\Sigma}\int_{o}^{p/p_o} \frac{q}{p/p_o}\, d(p/p_o). \tag{48}$$

Fu and Bartell (47), studying the surface areas of porous adsorbents, evaluated this equation and found that the change in free energy could be expressed by the relationship:

$$-\Sigma\Delta F = \alpha(p/p_o)^{\beta} \tag{49}$$

where $-\Sigma\Delta F$ is the decrease in the free energy per unit area, α and β are constants. When the values of $-\Sigma\Delta F$ were plotted against p/p_o a curve consisting of two portions was obtained by these authors; each portion could be represented by Equation 49. For a given adsorbate-adsorbent system, α and β remain constant so long as there is no change in the

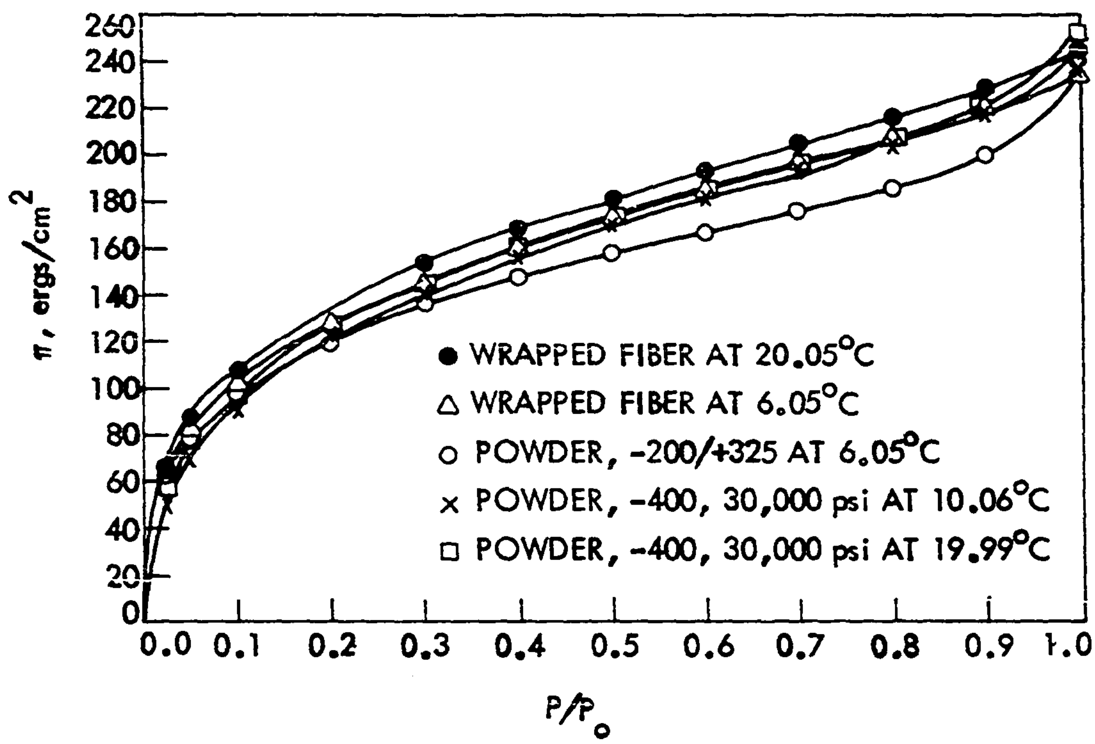

Figure 25. Spreading pressure versus relative humidity plot for water vapor adsorbed on E-glass

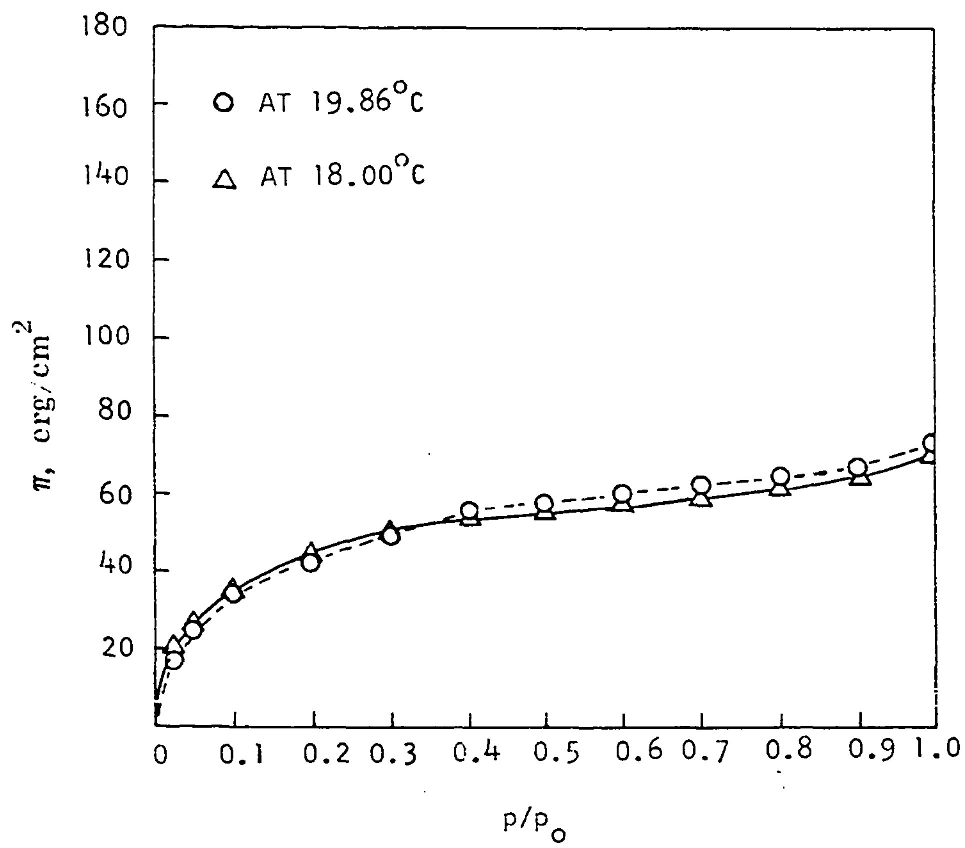

Figure 26. Spreading pressure versus relative humidity plot for benzene vapor adsorbed on E-glass pellet

mechanism of adsorption. If changes in the mechanism of adsorption, such as capillary condensation or swelling occur, values of α and β change to another set of constant values. The change in slope of the $-\Sigma\Delta F$ curve, observed by Fu and Bartell (47) was attributed to capillary condensation in the pores of the adsorbents. From the intersection of the two portions of the curve and from the proposed hypothetical process, they were able to derive an expression for the specific surface of rigid porous adsorbents which did not involve assigning a molecular area to the adsorbate. They tested their method with a variety of adsorbents and adsorbates; the specific surfaces obtained were found to be in very good agreement with those determined by the BET nitrogen adsorption method.

In the present study, the values of the integral $\int_0^{p/p_o} \frac{q}{p/p_o} d(p/p_o)$ for increasing increments of p/p_o, up to and including the saturation point, were determined by graphical integration. This was done with both water and benzene adsorption data for Fiberglas-E. The values of $-\Sigma\Delta F$ obtained are presented in the Appendix.

Plots of $\log(-\Sigma\Delta F)$ versus $\log(p/p_o)$ are presented in Figures 27, 28 and 29 for water and benzene adsorption runs. Each of the plots displays three straight line portions (implying equations of the type $-\Sigma\Delta F = \alpha(p/p_o)^\beta$ for various portions) rather than the two obtained by Fu and Bartell. Above a p/p_o of about 0.05 a linear plot is obtained to a p/p_o of 0.41 for water adsorption and 0.18 for benzene adsorption. There is then a transition to another linear portion which continues to a p/p_o of about 0.90. This is followed by another linear portion up to saturation. The portions of the plots below p/p_o of about 0.05 are not strictly

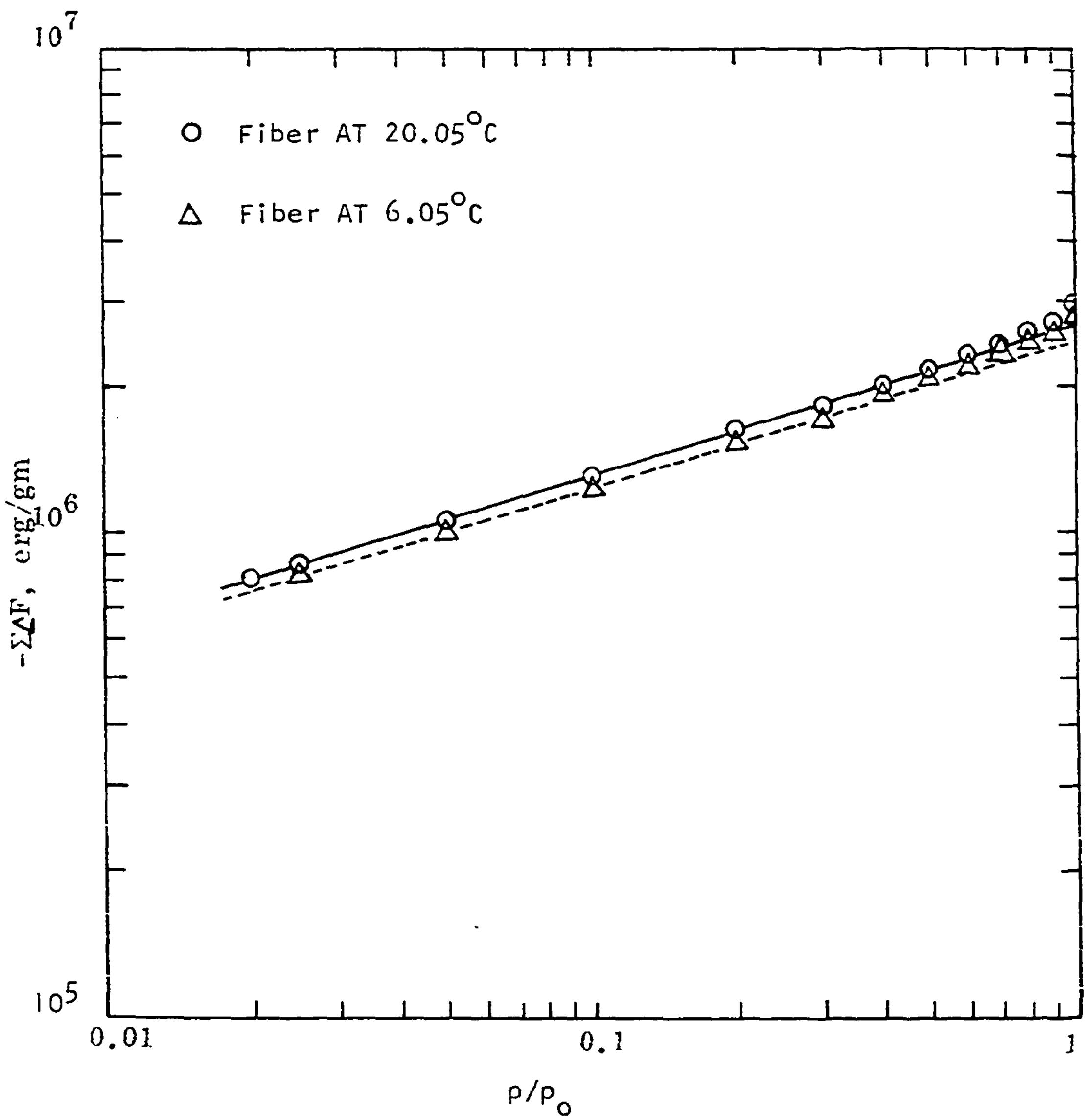

Figure 27. Adsorption energy change of E-glass fiber upon adsorption of water vapor

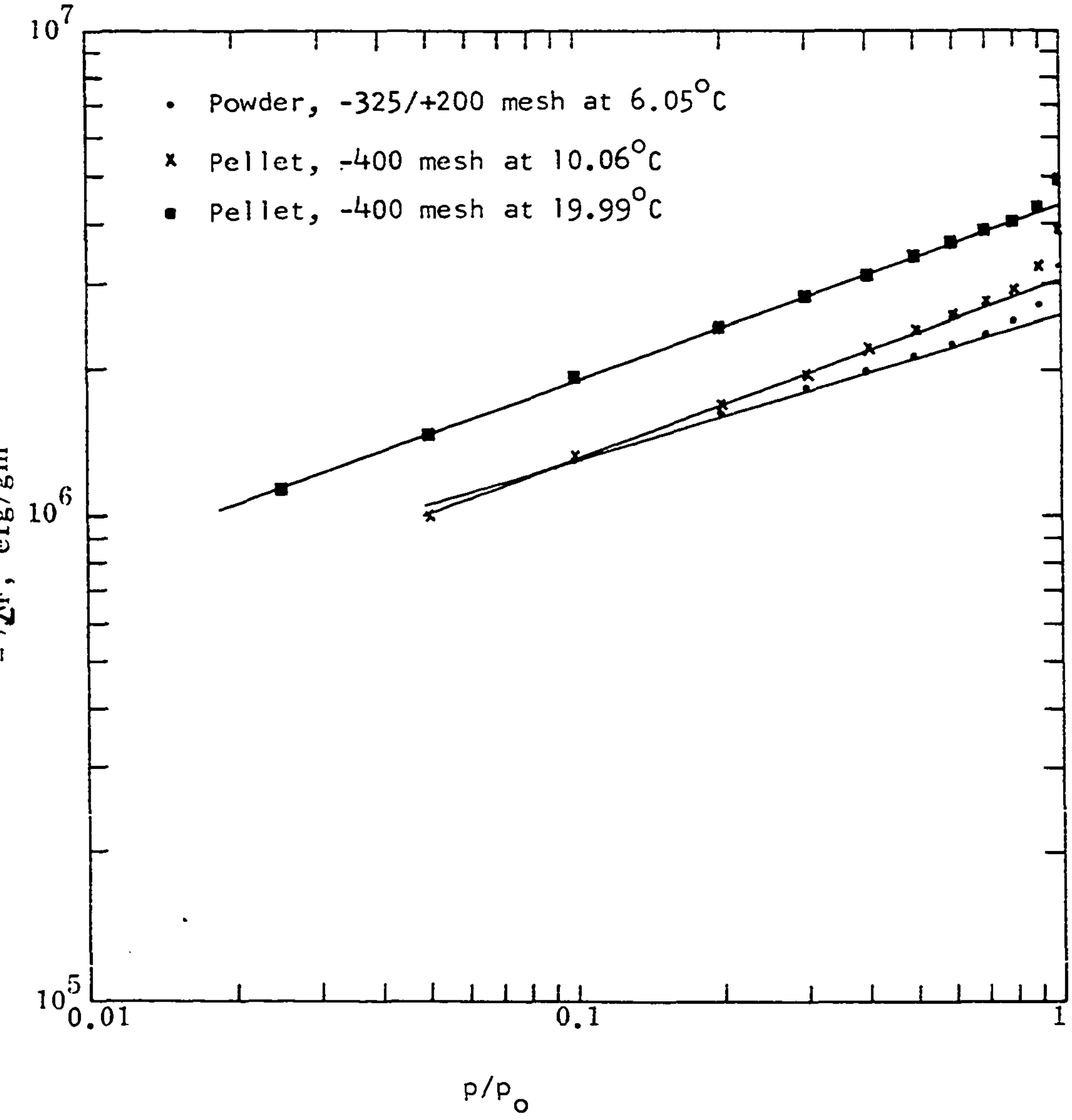

Figure 28. Adsorption energy change of E-glass powder upon adsorption of water vapor

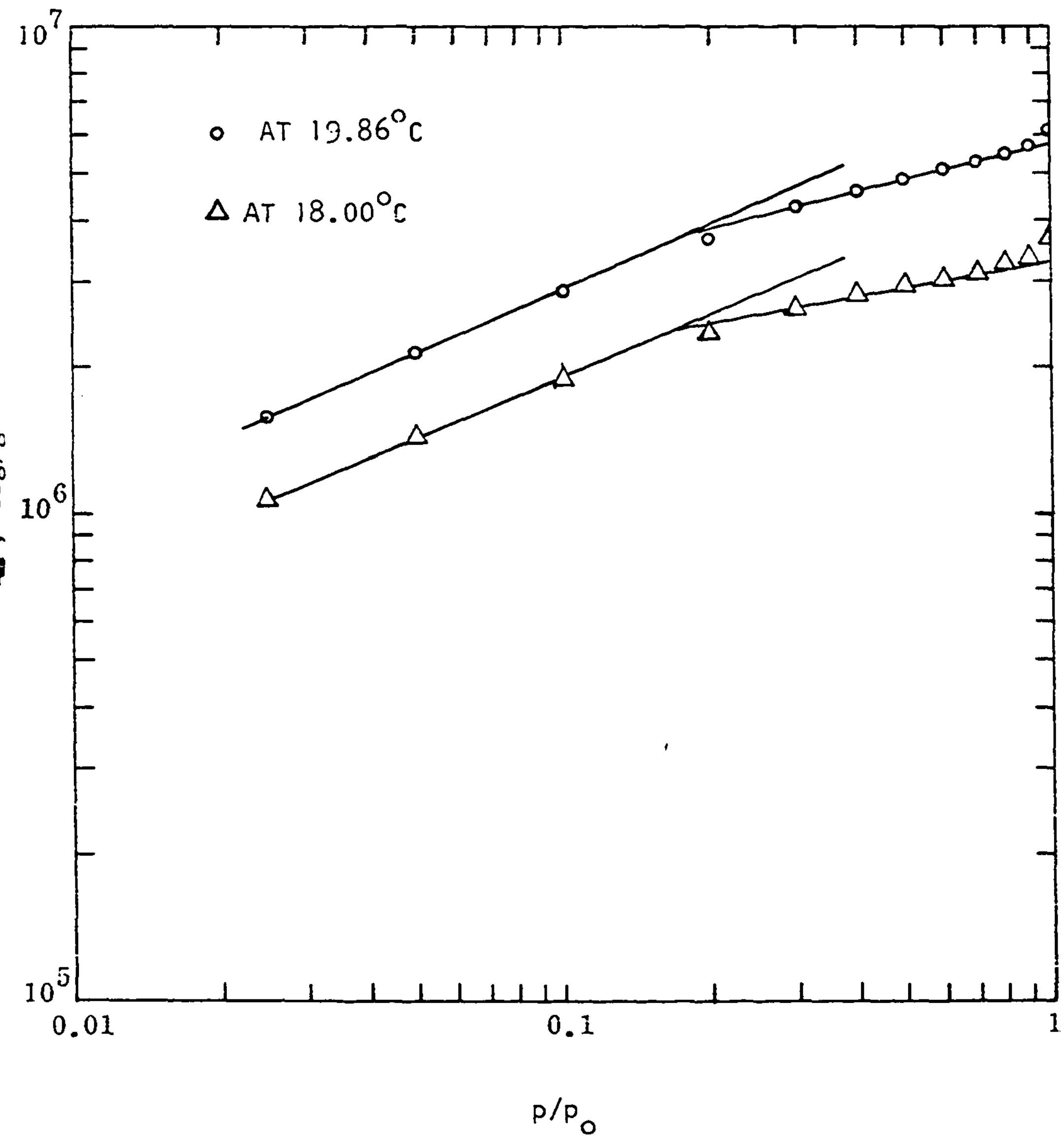

Figure 29. Adsorption energy change of E-glass pellet upon adsorption of benzene vapor

linear but breaks in the slopes of the plots can be observed in the p/p_o range from 0.025 to 0.05. This is in agreement with the observations of Fu and Bartell (47); they reported nonlinearity below p/p_o of 0.05 and attributed it to the decreased accuracy in determining q values at very low pressures. In their development they disregarded this portion of the plots since it was not required for the determination of the surface area of the adsorbents.

Breaks in the slopes of $\log(-\Sigma\Delta F)$ vs. $\log p/p_o$ curves have been reported in various investigations of swelling clays (105, 106). However, E-glass is believed to be non-swelling as discussed earlier. Instead, it was felt that an analysis similar to that of Fu and Bartell may be constructive. The microstructural analysis will now be possible using Fu and Bartell's method (here after it will be called FB method). If we consider that the first straight line is to fill the micropores (or microfissures), then the first intersection, X_{mic}, at about p/p_o of 0.18 to 0.41 is where the micropores are filled up. In the second straight line region where very small amounts of adsorption occur as can be seen from the adsorption isotherm plots, external surfaces dominate the adsorption action until the line reaches a point where capillary condensation takes over. The intersection is then called X_{cap}. Figure 30 represents a typical curve of adsorption energy change for microstructural analysis. Fu and Bartell derived an equation in the form of the following equation for calculation of specific surface:

$$\Sigma = \frac{-\Sigma\Delta F_s + \Sigma\Delta F_m}{\gamma_{lv}} , \qquad (50)$$

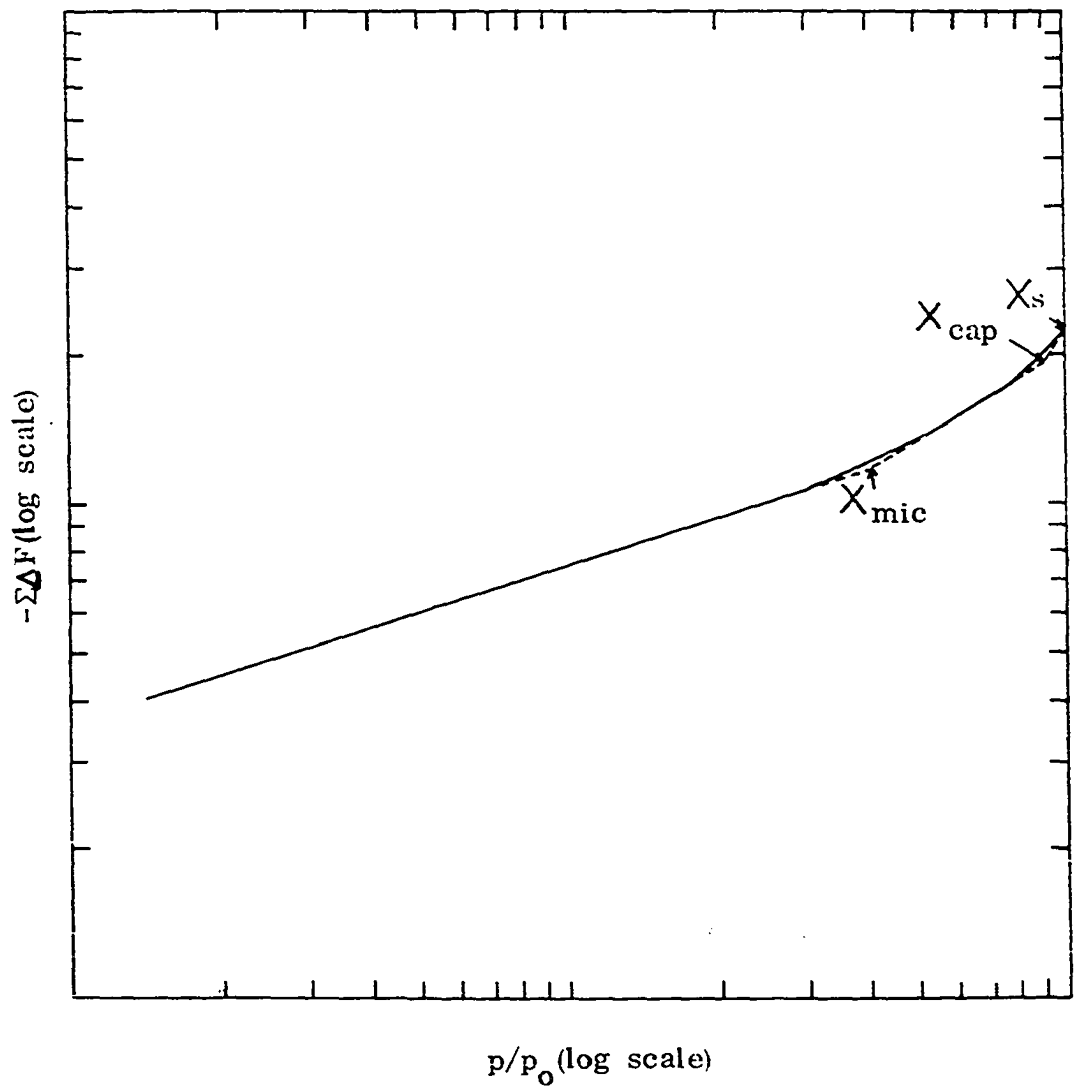

Figure 30. Typical curve of $-\Sigma\Delta F$ versus p/p_o for microstructural analysis

where Σ is the specific surface, $-\Sigma\Delta F_s$ is the ordinate of intercept X_s, and $-\Sigma\Delta F_m$ is the ordinate of intercept X_{mic}, of figure 30 and γ_{LV} is the surface tension of liquid adsorbate. With the same argument we can give the following for inflection point X_{cap}:

$$\Sigma_{cap} = \frac{-\Sigma\Delta F_s + \Sigma\Delta F_c}{\gamma_{lv}} , \tag{51}$$

where Σ_{cap} is the portion of the specific surface beyond micropores in other words the external surface area, then

$$\Sigma_{mic} = \Sigma - \Sigma_{cap} . \tag{52}$$

The analysis can be further developed to obtain the average pore size of the micropores, r_{cap}, by using the Kelvin equation:

$$RT\ln(p/p_o) = -2\gamma V/r, \tag{53}$$

where γ is the surface tension of the adsorbate, V is the molar volume and r is the capillary radius.

The values of specific surfaces and average pore sizes obtained are presented in Table 11. The surface areas obtained from FB method, Σ_{FB}, are found in good agreement with BET areas, Σ_{BET}. However, Σ_{FB} seems to be greater than Σ_{BET} for water as adsorbate, but this trend is reversed when benzene is the adsorbate. It is interesting to note that the external surface area, Σ_{cap}, is in the order of the geometric area calculated in the Appendix. High compression pressure applied to the pellet seems to be sealing off the micropores as reflected in decreasing Σ_{mic}. It appears that subsequent water adsorptions on E-glass increase not only

Table II. Determination of specific surface areas based on FB method

Adsorbate	Sample	Test	Temp.	$-\Sigma\Delta F_s$ erg/gm x 10^6	$-\Sigma\Delta F_m$ erg/gm x 10^6	$-\Sigma\Delta F_c$ erg/gm x 10^6	γ^a_{lv} dyne/cm
Water	Fiber	1	20.05	2.979	2.010	2.800	72.75
	Fiber	2	6.05	2.837	1.835	2.610	74.80
	Powder	3	6.05	3.262	2.090	2.620	74.80
	Pellet	4	10.06	3.482	2.280	3.020	74.22
	Pellet	5	19.99	4.947	3.220	4.310	72.78
Benzene	Pellet	B1	19.86	0.610	0.389	0.559	31.73
	Pellet	B3	18.00	0.372	0.239	0.321	31.74

[a]Date based on CRC Chemistry and Physics Handbook (122).

Table 11. (Continued)

Σ m^2/gm	Σ_{cap} m^2/gm	Σ_{mic} m^2/gm	$(p/p_o)_m$	$(p/p_o)_c$	r_m^b Å	r_c^b Å	Sample form	Adsorbate
1.332	0.246	1.086	0.39	0.90	11.40	99.50	Fiber	Water
1.346	0.164	1.182	0.39	0.90	11.42	101.20	Fiber	
1.492	0.857	0.635	0.44	0.90	11.41	101.20	Powder	
1.621	0.622	0.999	0.44	0.90	11.42	100.05	Pellet	
2.324	0.857	1.467	0.44	0.90	11.45	99.51	Pellet	
0.697	0.161	0.536	0.19	0.88	12.64	227.13	Pellet	Benzene
0.395	0.161	0.232	0.17	0.92	12.71	215.51	Pellet	

$${}^{b}r = \frac{2M\gamma}{2.303RT\rho \log p_o/p}$$

the total surface area, Σ, but also the microarea, Σ_{mic}. The pore sizes of microfissures calculated from equation 53 are found to be 11.40 A° for water as adsorbate and 12.65 A° for benzene as adsorbate, respectively; the capillary pores are found to be around 100 A° and 220 A° for water and benzene as adsorbates, respectively. Micropores so calculated appear increasing in size at each subsequent adsorption run.

The observed breaking strengths of solids are commonly from ten to a thousand times less than the theoretical strengths calculated from heats of vaporization, intermolecular forces, etc. The loss of strength of fiber in the water vapor environment is well recognized (22). This is attributed to the cracks or flaws occurring on the fiber surface which act as a stress multiplier.

Pores can contribute to dislocations by generating stress concentrations. Various adsorbed gases might have an effect upon the dislocations, especially if some chemisorption or stronger interaction should occur at specific sites.

For materials in the glassy state there is evidence (65) that normally produced materials do have microcracks or imperfections, which is confirmed by comparison with the behavior of specially prepared samples. Griffith (51) suggested that all glass specimens are riddled with cracks, and that these cracks act as stress multipliers, the stress at the tip of the crack being greater than the applied stress by a factor depending upon the dimensions and location of the crack. This factor may easily reach a value of 100.

Griffith (52) provided the first plausible theory accounting for the low strength of glass in comparison with the theoretical strength. This theory assumes the presence of the flaws of microcracks (here after defined as microfissures) and defines the strength in terms of the depth of the crack as well as Young's modulus and surface energy. In the Griffith equation:

$$S_t = (2YF/\pi C)^{1/2} \tag{54}$$

where S_t is tensile strength, Y is Young's Modulus, F is surface energy, and C is the depth of the crack or flaw. This equation expresses the critical condition that an increase in the length of the crack sufficiently decreases the strain energy in the material to provide the surface free energy of the newly formed surfaces of the crack.

As we shall see, it seems probably that every square millimeter of a glass surface has many "Griffith" cracks of varying severity. Further, it is possible that the existence of each hackle in a rapidly moving fracture may indicate a "flaw" in the glass structure (113, p. 82), the smallest having radii of only a few mμ and the largest of approximately 5 μ. The micropore sizes calculated in this report for Fiberglas-E supports the Griffith theory which accounts for the rapid reduction of glass fiber tensile strength.

Griffith (52) also found that the strength of freshly drawn fibers falls rapidly with time. The increasing microporous size at subsequent runs presented in this report may well account for the loss of strength of glass fiber with age. However, further work is clearly desirable on the relation between the loss in strength of fibers, their resistance to eathering, and surrounding atmospheric conditions.

Adhesion

As discussed earlier, a thermodynamical approach to adhesion is possible for the E-glass-resin system using water and hydrocarbon adsorptions on E-glass. According to Equation 34 if ΔF_w and ΔF_b are the free energies of wetting of the same solid by water and benzene, respectively, the adhesion tension is given by:

$$\gamma_{sw} - \gamma_{sb} = \Delta F_w - \Delta F_b = \gamma_{adh} \quad . \tag{55}$$

It follows from Equation 55 that the adhesion tension for E-glass is $\gamma_{adh} = -181.33$ erg/cm^2 at 20°C. Water-benzene interfacial tension at this temperature is $\gamma_{wb} = 35.0$ erg/cm^2. The free energy of displacement of benzene by Dupré equation is therefore:

$$\gamma_{sw} - \gamma_{sb} + \gamma_{wb} = \Delta F_d = -146.33 \text{ erg/cm}^2 \ .$$

This implies that an actual contact between E-glass and benzene is unattainable in the presence of bulk water.

Demirel and Enüstün (33) investigated the calcite-water and calcite-benzene systems; they obtained ΔF_d equal to -74 erg/cm^2. They concluded that the tendency of asphalt on calcite to stripping is much smaller than that of quartz based on the comparison of their results with that of Palmer and Clark's (96) investigation on vitreous silica-benzene system and of Boyd and Livingston's (17) investigation on quartz-water system. In Table 12 comparison was made on the free energy of displacement for various materials. As can be seen from the table, hydrocarbon on E-glass is easier to be stripped than calcite but harder than quartz or vitreous-silica. Seventeen percent CaO may have furnished some stripping resistance to

Table 12. Comparison of the free energy of displacement for various materials

Solid	Adsorbate	Iso-temp. °C	ΔF erg/mc^2	S erg/cm^2	γ_{adh} erg/cm^2	ΔF_d erg/cm^2	Investigators
Calcite	Water	25	-264	192			Demirel and Enüstün (33)
	Benzene	25	-155	127	-109	- 74	Demirel and Enüstün (33)
Quartz	Water	25	-316	244			Boyd and Livingston (17)
Vitreous-silica	Benzene	25	- 81	63	-235	-200	Palmer and Clark (96)
E-glass	Water	20	-254	181			Huang et al. (67)
	Benzene	20	- 72	37	-181	-146	Present study

E-glass which consists mainly of silica.

Johannson et al. (69) in their adhesion study on E-glass suggested the coupling agent displacement is due to water attack at the glass surface. It is a fact that a resin like a polyester will show great resistance to moisture absorption when properly bonded to the glass in a fabric laminate, but when equally well cured as a casting it will swell and rupture. The bond of glass fiber to resins is relatively poor, and upon exposure to high atmospheric humidities or actual immersion in water, it is rapidly destroyed by penetration of water into the interstices adjacent to the hydrophilic glass surface.

It has been shown by Eakins (37) that proper preparation of a soda-lime glass fiber surface to remove free alkali increases the resistance to hydrolysis of glass-resin bonds in a remarkable manner.

Heats of Adsorption

The BET parameter C was used to calculate the average heat of adsorption, less the heat of liquefaction, of the first adsorbed monomolecular layer of adsorbate by using Equation 8 which may be expressed as:

$$E_1 - E_L = RT\ln C \ . \qquad (56)$$

The values obtained were corrected according to Clampitt and German (24) by using their correction value:

$$E_1 - E_L = RT\ln C - (\Delta H_s - E_L) \ . \qquad (57)$$

The corrected and uncorrected values are listed in Table 13 for water vapor-E glass and benzene vapor-E glass systems studied.

Table 13. Average heat of adsorption of monomolecular water or benzene adsorbed on E-glass

Adsorbate	Sample form	Test No.	Iso-temp. °C	C	lnC	E_1-E_L[a] cal/mole	E_1-E_L[b] cal/mole
Water	Fiber	1	20.05	370	5.91	3441.9	4596.9
	Fiber	2	6.05	370	5.91	3278.1	4433.1
	Powder	3	6.05	133	4.89	2712.3	3867.3
	Pellet	4	10.06	133	4.89	2751.3	3906.3
	Pellet	5	19.99	93	4.53	2638.7	3793.7
	Pellet	6	19.99	106	4.66	2714.4	3869.4
	Pellet	7	19.99	191	4.61	2685.3	3840.3
Benzene	Pellet	B1	19.86	74	4.30	2498.2	4158.2
	Pellet	B2	18.00	89	4.48	2591.3	4251.3
	Pellet	B3	18.00	98	4.59	2656.0	4316.0

[a]Calculated according to Equation 56.

[b]Calculated according to Equation 57.

Inspection of Table 13 shows that E-glass fibers have higher heats of adsorption than the powdered E-glass. The differences range from 564 cal/mole to 640 cal/mole for water adsorption. Heats of benzene adsorption were slightly lower than those of water adsorption.

As stated earlier, by holding q constant one can make use of the Clausius-Clapeyron equation to determine the isoteric heat of adsorption. But, as pointed out in the discussion of the potential theory, q can be kept constant for a constant potential (ϵ) only when the surface is held constant. When the surface area varies from run to run, or from sample to sample, q can no longer be held constant for a constant potential and therefore the ϵ versus φ plot does not produce a characteristic curve (Figures 31 and 32). As pointed out in the theory, however, the ϵ versus thickness, t plot is not sensitive to surface area changes and does produce a characteristic curve as can be seen from Figures 33 and 34 as opposed to Figures 31 and 32.

Therefore, a new term q_f is introduced to replace q (67):

$$q_f = t \cdot f \cdot \delta_b \tag{58}$$

where t is the thickness of the adsorbed layer:

$$t = \frac{\varphi}{\Sigma} = \frac{q}{f \cdot \delta_b \cdot \Sigma} \ . \tag{59}$$

Substituting Equation 59 into Equation 58:

$$q_f = \frac{q}{\Sigma} \ . \tag{60}$$

Careful examination reveals that q_f is actually the same as surface excess Γ. Hence by solving the Clausius-Clapeyron equation at constant q_f the true isosteric heat of adosorption and isosteric entropy of adsorption can be obtained. Figures 35 and 36 show q_f as a function of relative pressure from which heats of adsorption, ΔH_a and entropies of adsorption, ΔS, were determined as a function of thickness (Figures 37 and 38, and Tables 39, 40, 41, 42, 44 and 45 listed in the Appendix.)

It is seen as a consequence of the heat of adsorption being greater than the heat of liquefaction, the enthalpy change for the transfer of water or benzene from the vapor to the adsorbed phase is positive. The heat of adsorption, however, drops sharply at a film thickness, less than

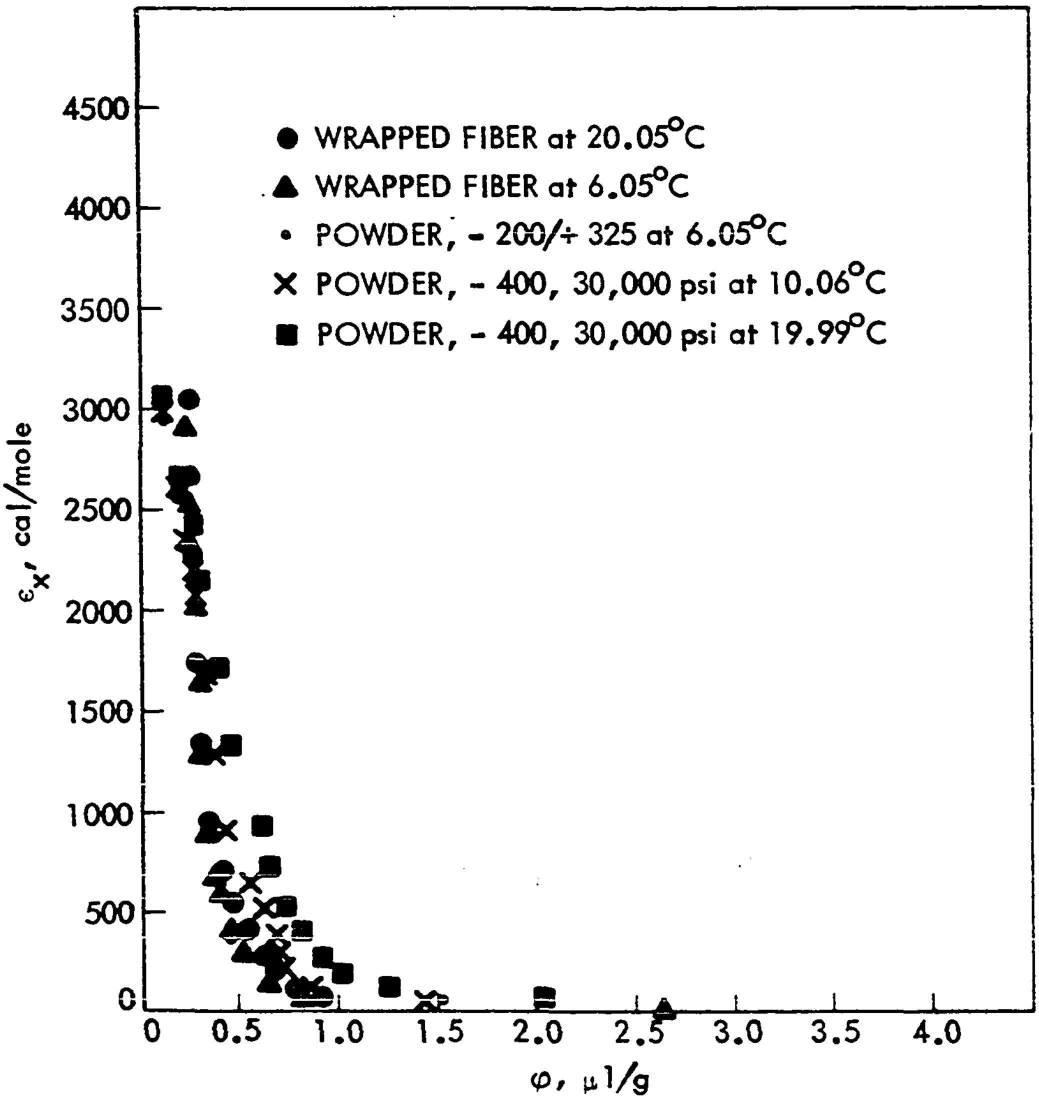

Figure 31. Characteristic curve for the adsorption of water vapor on E-glass (ϵ vs. φ)

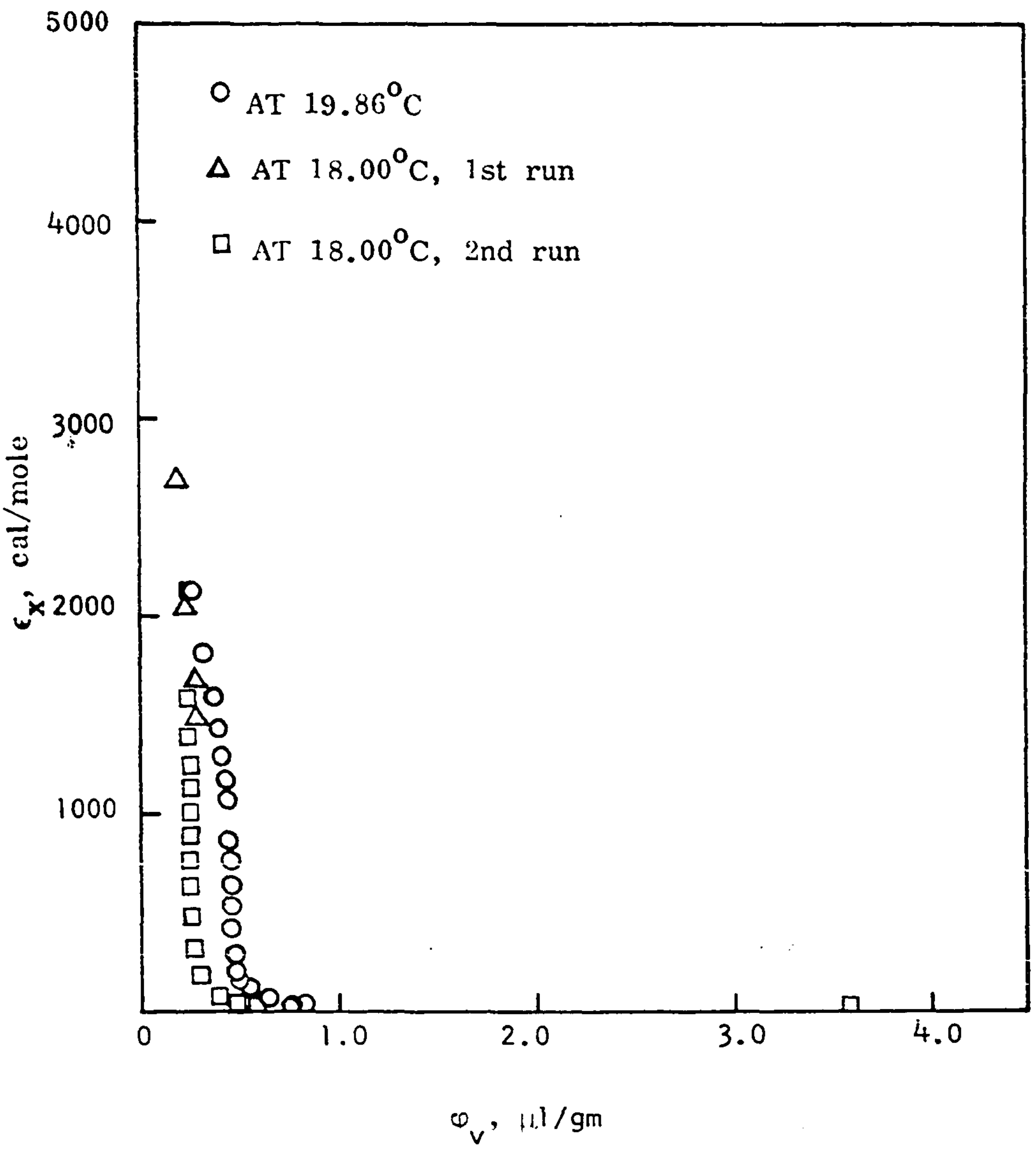

Figure 32. Characteristic curve for the adsorption of benzene vapor on E-glass pellet (ϵ vs. φ)

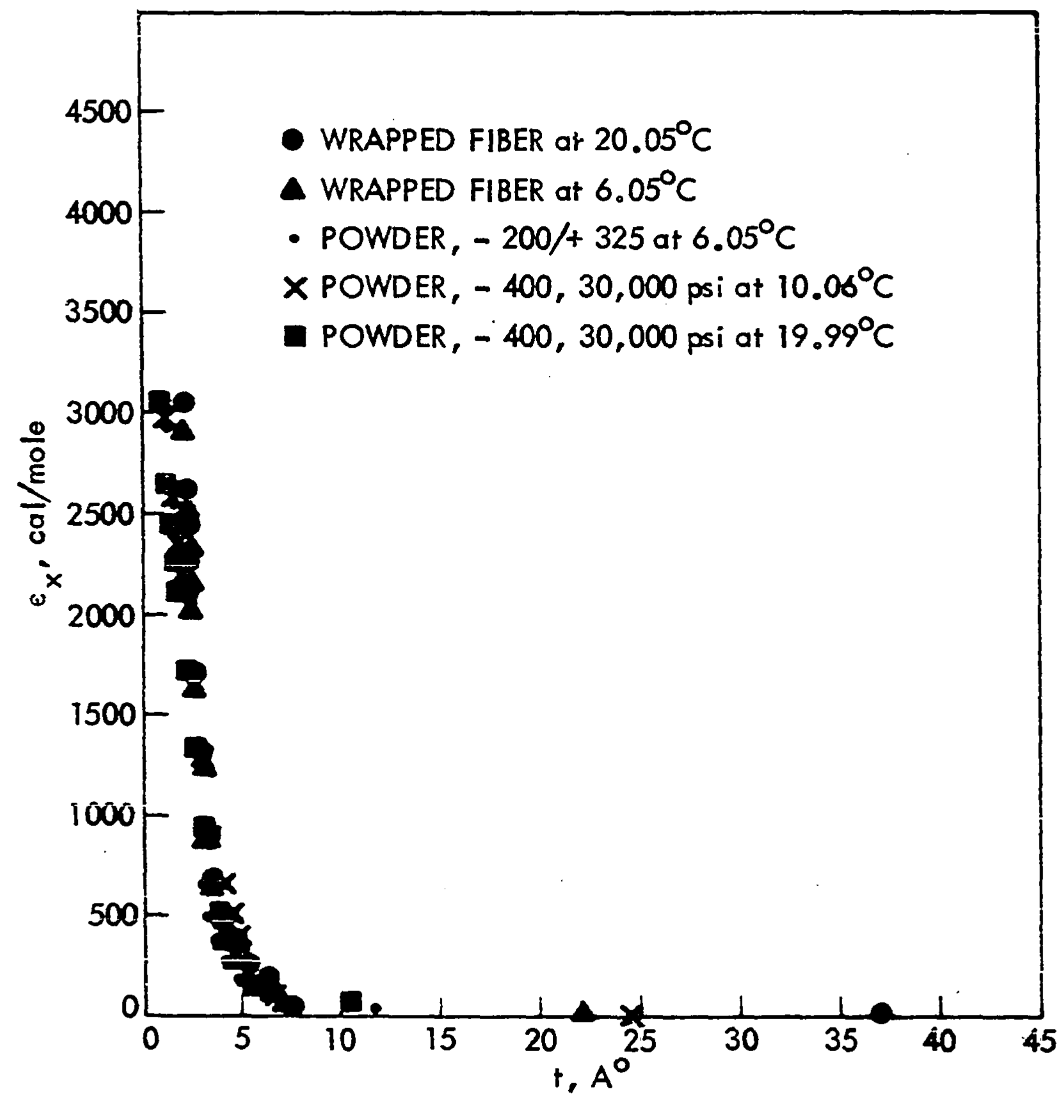

Figure 33. Characteristic curve for the adsorption of water vapor on E-glass (ϵ vs. t)

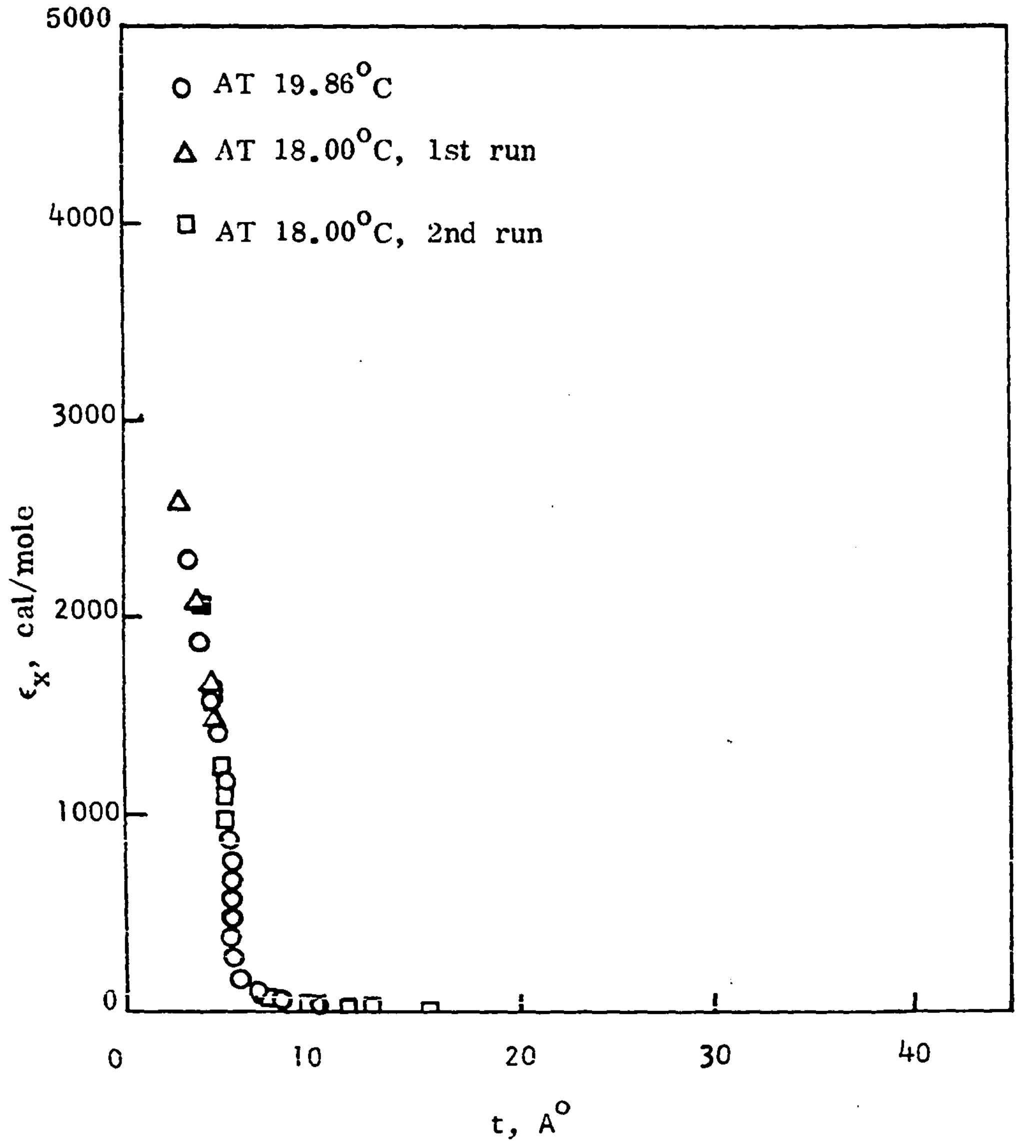

Figure 34. Characteristic curve for the adsorption of benzene vapor on E-glass pellet (ϵ vs. t)

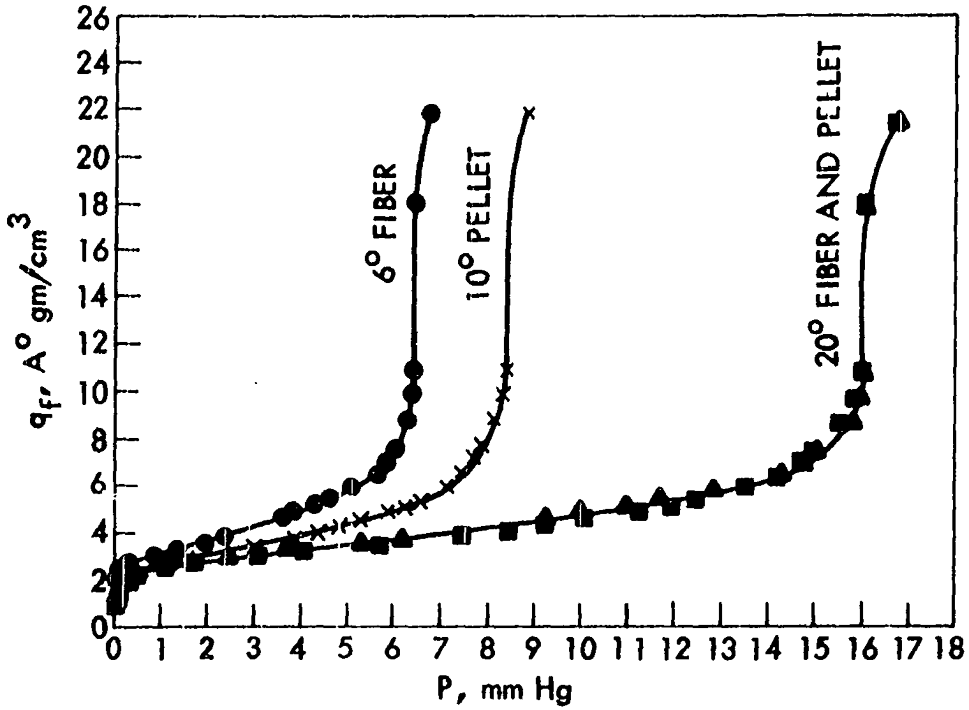

Figure 35. q_f versus p for isosteric heat of adsorption computation (water vapor adsorbed on E-glass)

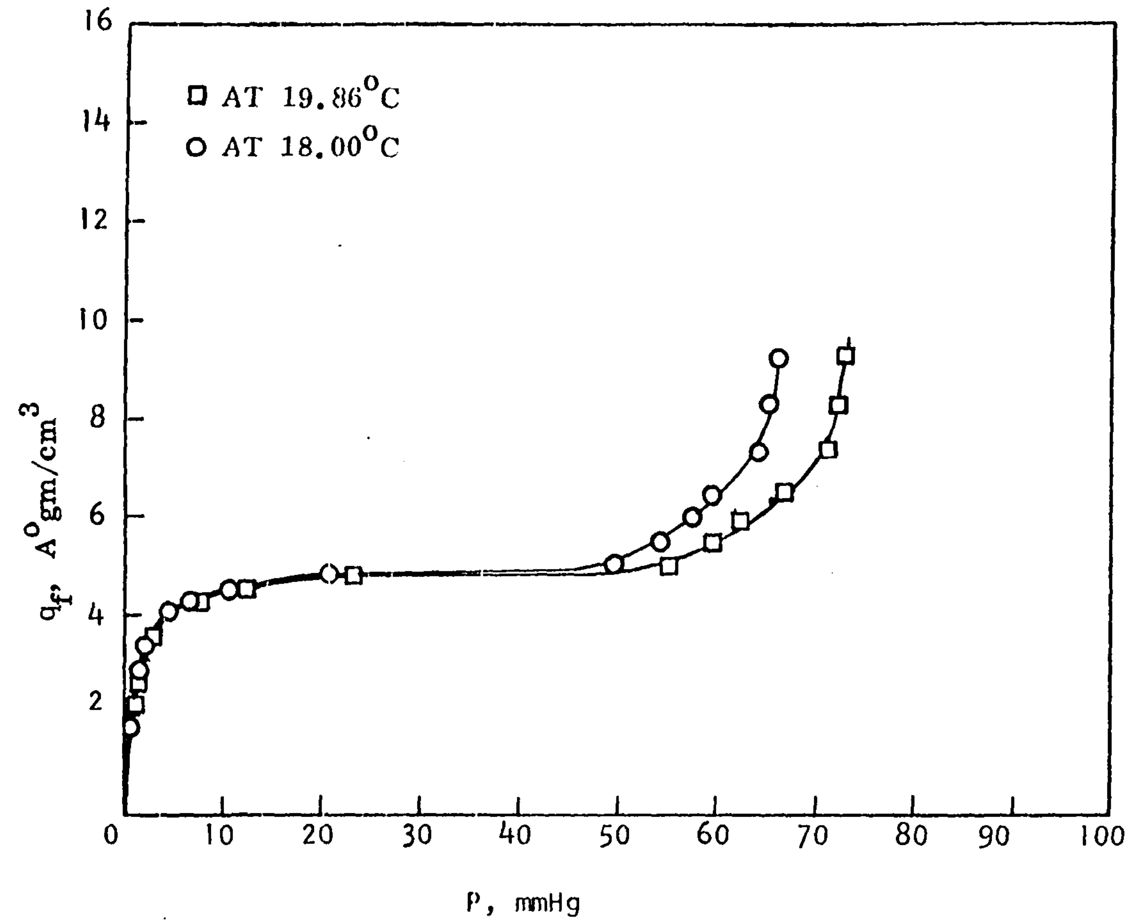

Figure 36. q_f versus p for isosteric heat of adsorption computation (benzene vapor adsorbed on E-glass pellet)

2.7 Å, for water which is about a monolayer thickness. It reaches the heat of liquefaction at about 6 Å film thickness. Comparing Figures 37 and 38 with Table 13, the isosteric heat of adsorption so computed by the modified equation shows good agreement with that computed from the BET parameters for the first layer of adsorbed adsorbate. Again, as discussed earlier, the untreated, water quenched E-glass fiber has higher heats of adsorption than that of powdered or compacted powdered E-glass at low surface coverages. The heats of adsorption for benzene vapor adsorbed on E-glass appear to be lower than that of water vapor. This is acceptable since E-glass has greater affinity towards water vapor (12, 73).

The heat of adsorption of water vapor on E-glass fiber has been reported by Deitz (31). In his investigation, he found that the pristine E-glass fiber appears to have a heat of adsorption value lower than the heat of vaporization, while the water-washed fiber appears to have an even lower value. He explained that the preliminary data were not equilibrium values and the boundary surface of E-glass has great chemical complexity. He said:

> "Contact with liquid water definitely removes calcium and sodium ions, these having great affinity for water vapor. These changes are significant. As a result the above suggested explanation for the difference between the two fibers may not be valid because a comparison of like with like is not being made."

Therefore, the heat of adsorption data reported by Deitz (31) is uncertain because he used the Clausius-Clapeyron equation without specific surface variation corrections.

Water or benzene adsorption on E-glass probably is predominantly a

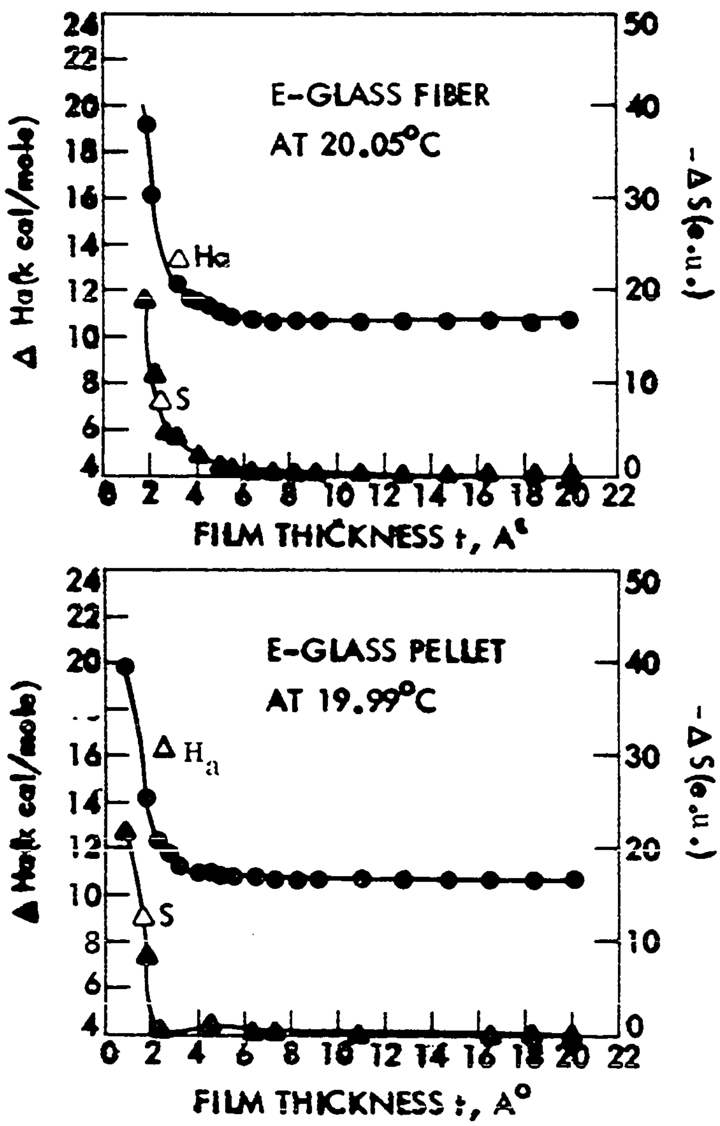

Figure 37. Isosteric heat of adsorption and isosteric entropy of adsorption (water vapor adsorbed on E-glass): (a) E-glass fiber and (b) E-glass pellet

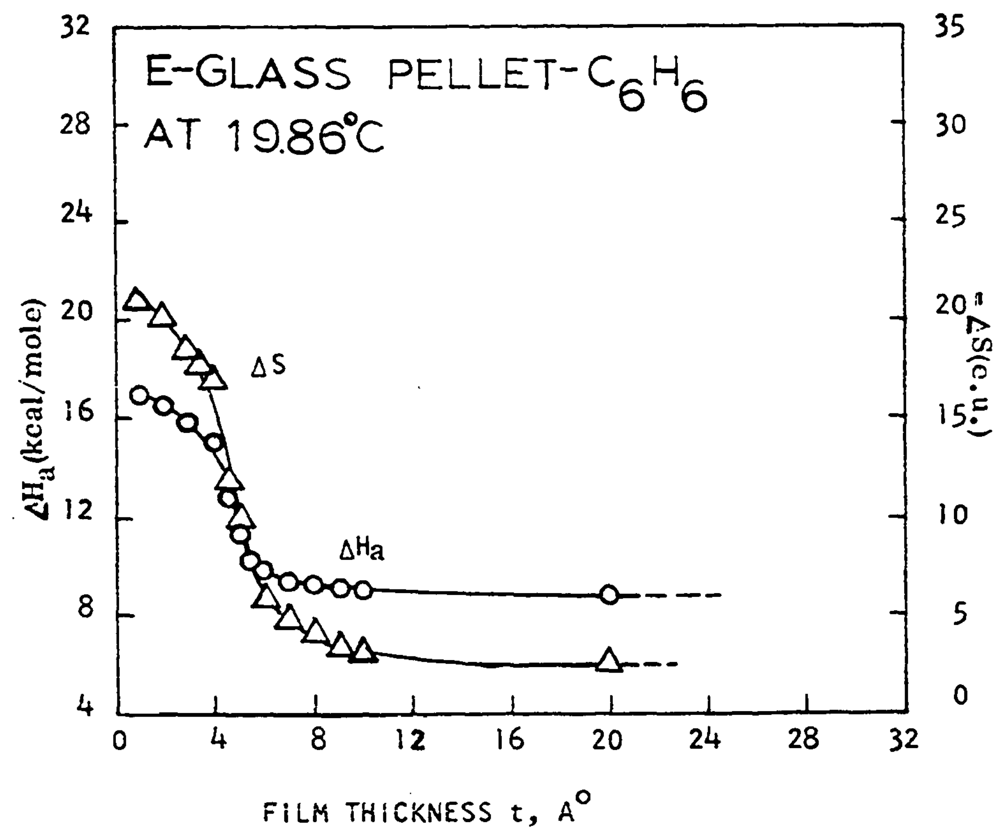

Figure 38. Isosteric heat of adsorption and isosteric entropy of adsorption for benzene vapor adsorbed on E-glass pellet

physical adsorption since in neither case the heat of adsorption exceeds 30 kcal/mole.

A progressive decrease in the heat of adsorption as the surface coverage is increased has been variously ascribed to surface heterogeneity and to interaction between adsorbed molecules (115, 57). If the surface is heterogeneous the more active sites will be covered first and the initial heat of adsorption will be high. Less active sites will be covered later with lower heats of adsorption. An alternative theory assumes that the decreasing value of the heat of adsorption arises because of increasing interaction between adsorbed molecules as the surface sites are filled. Surface heterogeneity and adsorbate interaction on E-glass will be considered later in the discussion of infrared spectroscopy.

Entropies of Adsorption

The entropies of adsorption were calculated from Equation 16, and are presented in Figures 37 and 38, and the Appendix. In case of water adsorption, at the lowest coverage for which a value is available, ΔS is approximately 20 e.u. This in absolute value is about 8 e.u. less than the Trouton constant for water (which may be taken as the entropy change for the transfer of one mole of water from liquid to vapor). The difference of 8 e.u. is equal to that reported by Tompkins (116) for the adsorption of water vapor on sodium chloride (8 e.u.), but is lower than the value reported for adsorption of water vapor on silica or ferric oxide (116).

The adsorption of water vapor on silica or ferric oxide is more ice-like than liquid. The entropy evidence for E-glass indicates a freedom intermediate between liquid and solid. Kemball's supermobile adsorption

(72), where the adsorbed layer behaves as a 'two-dimensional gas' deprived of translational movement at right angle to the surface and some of the vibrational and rotational movement, would be acceptable to explain the entropy loss. A model is appropriate in which the first adsorbed layer is a highly extended liquid layer in which vibrational and rotational freedoms are much reduced.

To interpret entropy of adsorption, two models namely, a perfectly mobile model and a rigidly localized model will be considered. Because of numerous assumptions in both the models, an agreement to perhaps 3-5 e.u. between theory and experiment will be acceptable.

In the gas phase at ordinary temperatures the significant contributions to the entropy are the translational and rotational motions. The three dimensional translational entropy is given by

$$_3S^{tr} = {}_gS_s^{tr} = 11.44 \log T + 6.33 \tag{61}$$

for one mole of ideal water vapor at one atm. The results range from 34.3 to 34.6 e.u. in the range of temperatures used. The three dimensional rotational entropy has been given by Herzberg (61) as follows:

$$_3S^{rot} = \Delta S^{rot} = 3/2R + R\ln \frac{8\pi^2}{\sigma h^3} (8\pi^3 ABC)^{1/2} (KT)^{3/2} \tag{62a}$$

where A, B, C are the moments of inertia and σ the symmetry number. For a water molecule $\sigma = 2$ and A, B, C are 1.024, 1.920 and 2.947 x 10^{-40} gm.cm^2 respectively, which upon substitution give:

$$_3S^{rot} = 6.86 \log T - 6.59 \,. \tag{62b}$$

The results range from 10.1 to 10.3 e.u. in the range of temperatures used.

If the adsorbed molecules is perfectly mobile its rotational freedom remains essentially unrestricted; in place of three dimensional translation there will be a restricted two-dimensional translation plus a weak vibration. Law (78) gives an equation for the two dimensional translation which is expressed by:

$${}_{2}S^{tr} = 4.58\ [1.73T\ \frac{(1-\theta)}{\theta} + 1] \tag{63}$$

giving values ranging from 13.8 to 21.2 e. u..

For ordinary chemical bonds with vibration frequencies in the infrared range, i.e. 1000-5000 cm^{-1}, ${}_{a}S^{vib}$ calculated from Equations 21 and 22 is negligibly small. Unfortunately, this is not true for the weak bond of a mobile film and the entropy can only be estimated roughly. A value of 3 e.u. will be assigned to ${}_{a}S^{vib}$ on the basis of the data reported by Kemball (72).

For a completely localized adsorbate (water on glass) all the entropy associated with the three dimensional translation will disappear. Most of ${}_{3}S^{rot}$ (~10 e.u.) will also disappear, but there will remain the rotation of the hydrogen atoms around the axis passing through the oxygen atom and the center of mass, since the oxygen most likely is bonded to the glass surface. The value of 2-3 e.u., depending on temperatures, has been assigned to ${}_{o}S^{rot}$ (101). For localized adsorption ${}_{o}S^{vib}$ can be neglected. If the bond is like an OH bond (ν ~3475 cm^{-1}), Equation 21 gives ${}_{o}S^{vib} \ll 0.01$ e.u. If attachment is by a Si-O bond (ν ~1100 cm^{-1}), the associated entropy is 0.2 e.u.

Configurational entropy which is related to the number of ways in which adsorbed molecules may be distributed, should also be taken into account in the localized adsorption model. S^{conf} may be readily derived statistically by considering a system composed of n molecules and m sites, so that $n/m = \theta$. The number of ways in which m sites may be arranged into two groups of n occupied and m-n empty sites is $n!/(m-n)!n!$. Then the configurational entropy may be given by $S^{conf} = k\ln m!/(m-n)!n!$. The use of the Stirling approximation, followed by differentiation with respect to n, leads to:

$$S^{conf} = 4.58 \log \frac{(1-\theta)}{\theta} \tag{64}$$

which gives values of 8.1 - 1.4 e.u. over the coverage studied.

Thus for the localized adsorption model,

$$_aS^l = {}_3S^{tr} + {}_3S^{rot} - {}_oS^{rot} - S^{conf} \tag{65}$$

and for mobile adsorption model,

$$_aS^m = {}_3S^{tr} - {}_2S^{tr} - {}_2S^{vib} . \tag{66}$$

For water vapor as adsorbate $_aS^l = 34 \sim 42$ e.u. and $_aS^m = 9 \sim 18$ e.u. The adsorbed water on E-glass is intermediate in nature between the two models. However, there is some indication of greater mobility at greater coverage. The formation of a second layer probably takes place above gaps in the first layer and in such a way as to make hydrogen bonding likely. This is reflected in the decrease in free energy, enthalpy and entropy. A continuation of this process results in the attainment of a liquid water structure above two or three layers.

Law (78) found $\Delta H_a = 14$ kcal/mole for the first layer of water adsorbed on GeO_2 at 300°K, and from entropy considerations he concluded that the adsorption was localized. For the multi-layer region, however, with a ΔH_a of 10 kcal/mole the film, became mobilized.

Kemball (72), studying the adsorption of benzene on mercury, concluded that the benzene molecules lose all rotation except that in the plane of the ring and also lose the translational freedom perpendicular to the surface. The mechanism of this adsorption, therefore, is that the benzene molecules are adsorbed in a flat position on the surface, while they move rather freely over the surface, this motion, of course, being accompanied by a vibration of high frequency, probably of a frequency of about 10^{13} to 10^{14} per sec.

The majority of substances, bound on surfaces by physical adsorption, belong to this class, showing restricted translational and rotational freedom of movement. In many cases the loss of entropy on adsorption, found experimentally, is roughly equal to the entropy change which may be expected theoretically, assuming that the translational degree of freedom perpendicular to the surface is completely lost. This does not imply that no vibration with respect to the surface exists. It only means that the strength of the adsorption is so great that practically all molecules are compelled to vibrate in the ground level of this vibration.

Kinetics of Sorption

The increase in the amount adsorbed with time is shown in Figure 39. IR activated sample (see p. 50) shows greater amount of sorption than non IR-activated sample at any specific time of adsorption. These experimental results on the water vapor E-glass system show that the Bangham equation

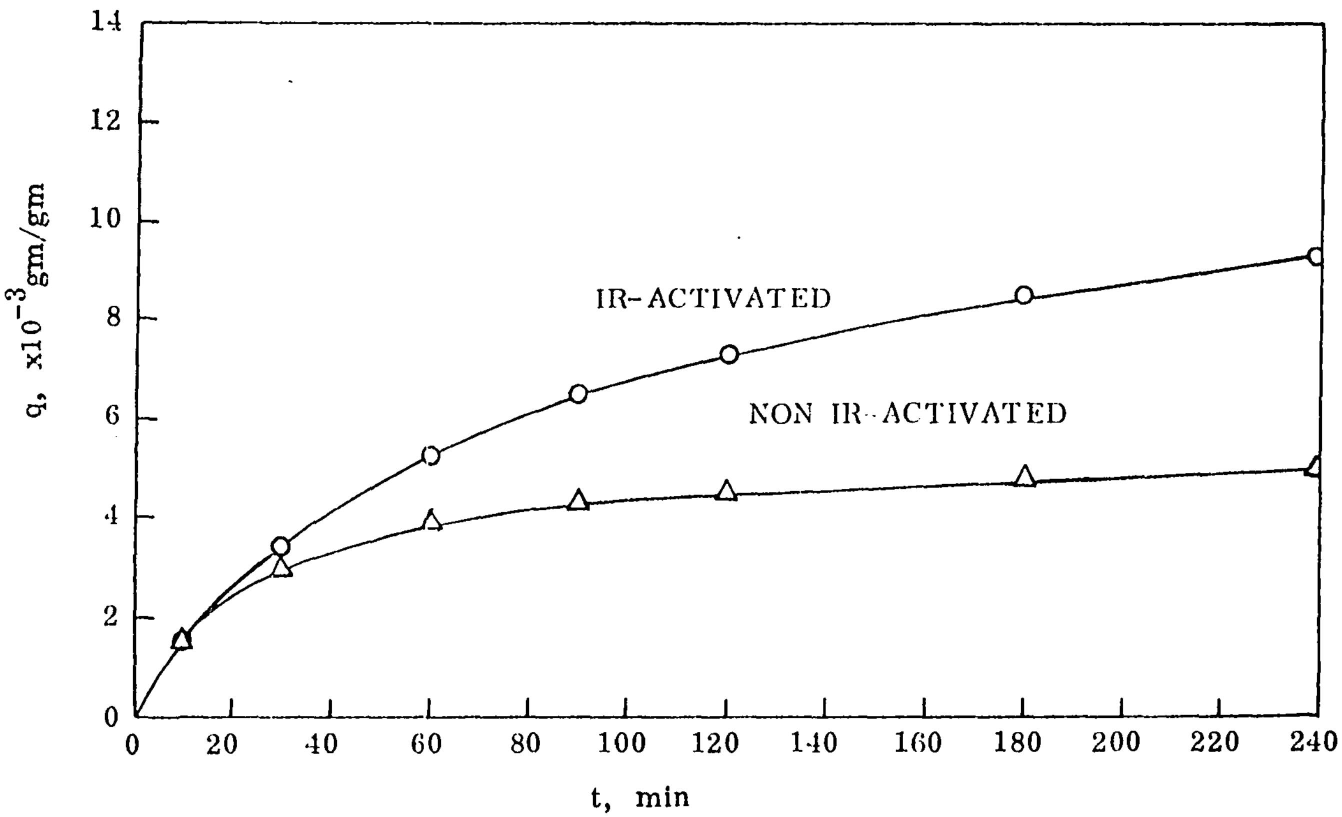

Figure 39. Adsorption isotherm equilibrium curves for water vapor E-glass systems at $p/p_o = 1$, $20^{\circ}C$

(Equation 41) fits the adsorption kinetics of the system (see Figure 40). According to Bangham and Sever (9), the long continued sorption, as in this case, of water vapor by glass is an absorption rather than an adsorption process. As will be seen later, the sorption of water and benzene by E-glass is probably due to a combination of adsorption and absorption.

The rate of adsorption was determined as a function of time for a series of temperatures: 18^o, 18.9^o and 20^oC for saturated water vapor (the data are presented in the Appendix). Figure 41 shows a typical example. IR activated run again shows a greater rate of adsorption than non IR-activated run at any period of time. Figure 42 shows the rate of adsorption as a function of the amount adsorbed. It is found that log (dn/dt) changes linearly with the sorbed amount, n, for the IR activated run in the region of $n = 5 \sim 25 \times 10^{19}$ molec./gm. (i.e. $dn/dt = 3.5 \sim 1 \times 10^{18}$ mole./gm.min.). Non IR-activated run shows rather shorter region of linear relationship ($n = 3 \sim 11 \times 10^{19}$ molec./gm, i.e. $dn/dt = 2 \sim 1.6 \times 10^{18}$ molec./gm.min.) indicating that surface nature differs drastically from IR-activated to non IR-activated run. The latter was found covered with at least one monolayer of water vapor (called hygroscopic surface layer) prior to each experiment. The adsorption process in which this linear relationship holds has been called the "first process" by Tuzi (119) but he does not give an explanation of its mechanism. We shall call this process "chemisorption process" and attempt to give an explanation. Recent studies of the adsorption of water on porous glass by infrared absorption (39, 112) have shown that the absorption centers for water molecules are Si atoms, O atoms and OH groups which appear on the surface. The rate of

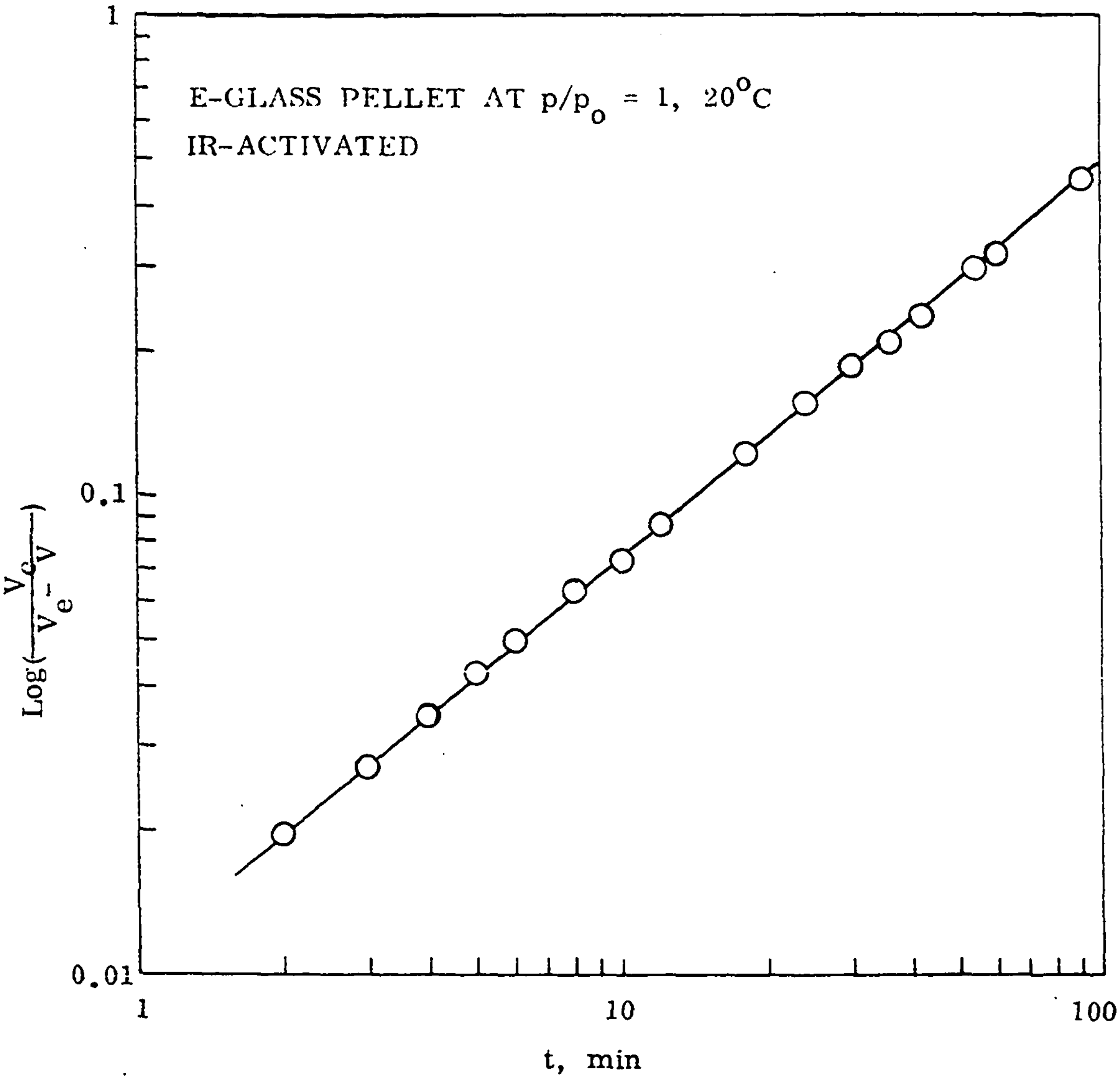

Figure 40. Adsorption rate of water-E-glass system using the modified Bangham equation

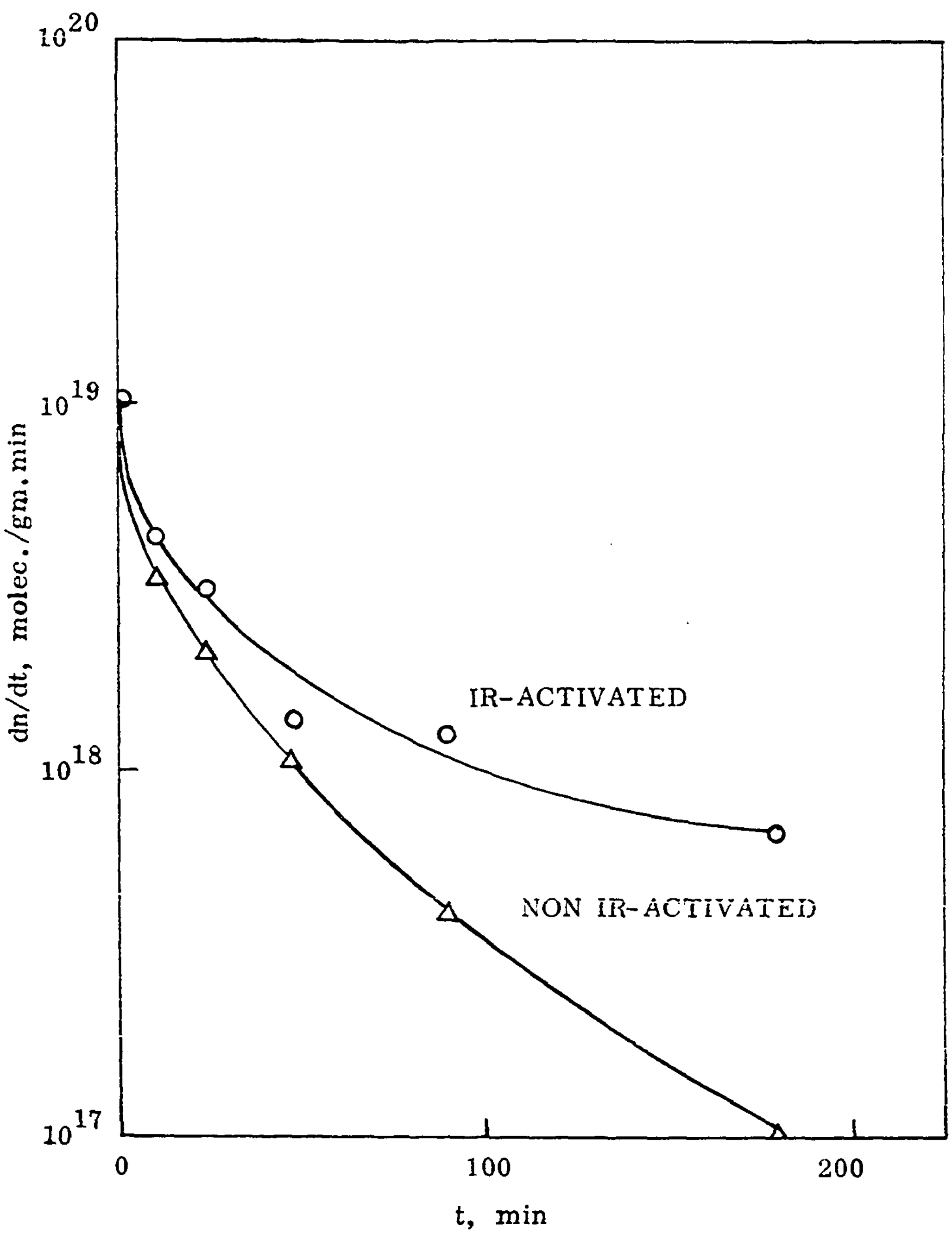

Figure 41. Semi-log plot of adsorption rate of water on E-glass surface versus time

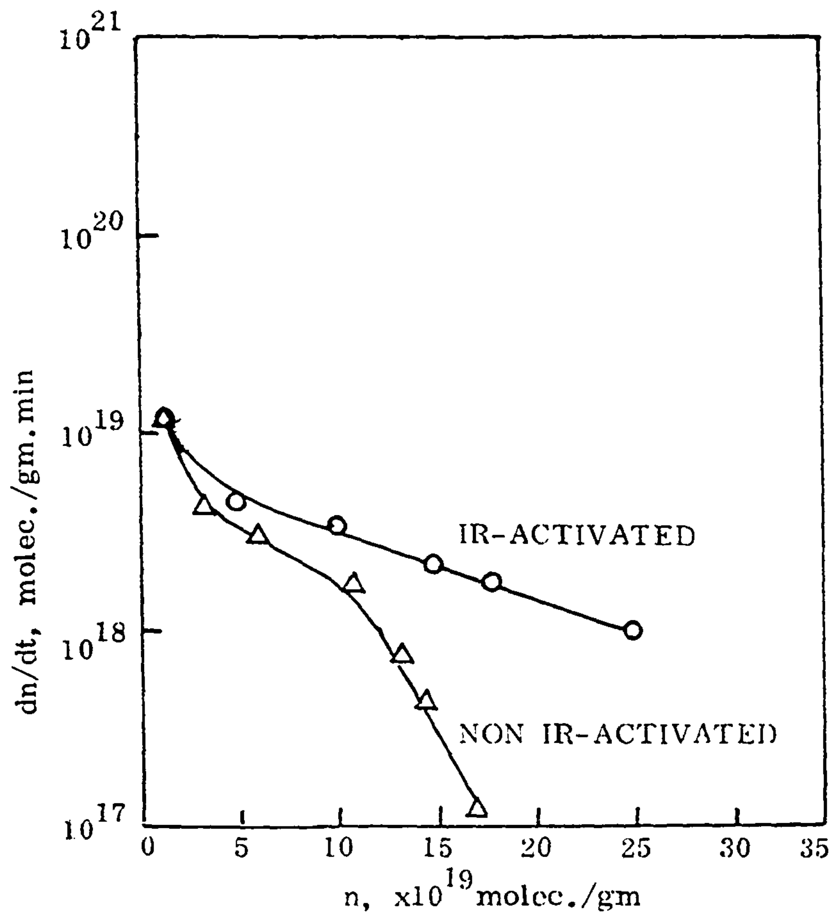

Figure 42. Semi-log plot of sorption rate of water versus amount of adsorption on E-glass

chemisorption depends on the rate of collision of molecules on the surface, the condensation factor, the activation energy and the probability for a molecule to strike an available site (118). The rate of sorption for the chemisorption process is given by:

$$dn/dt = \frac{\sigma p}{2\pi mkT} \quad f(n/n_s)\exp(-E_c/RT) \tag{67}$$

where σ is the condensation factor, $f(n/n_s)$ is the probability for a molecule to strike an available site where n_s represents the number of available sites for chemisorption, and E_c is the activation energy. The sticking probability for sorption is given by:

$$S_p = \sigma f(n/n_s)\exp(-E_c/RT). \tag{68}$$

The sticking probability, S_p can be determined from the rate of adsorption at a given level of coverage using Equation 67.

The activation energy of chemisorption may then be calculated from Equation 68 for the given amount of sorption. From the slope of the sticking probability versus reciprocal temperature plot (see Figure 43), we obtained E_c = 67.8 and 141 kcal/mole for n = 6 x 10^{19} and 12 x 10^{19} molec./gm respectively, for the IR-activated E-glass specimen. The activation energy more than doubled as the adsorbed amount increased twice. The high activation energy of chemisorption is acceptable in view of the nature of hydroxyl hydration on glass surface. In case of non IR-activated E-glass specimen, no definite straight line portion was observed for sorption rate versus amount adsorbed; therefore, no activation energy of chemisorption, which might be rather high, was calculated for non IR-activated specimen.

A close examination revealed another process in which the rate of sorption was proportional to $(\text{time})^{-1/2}$ as shown in Figure 44. This process

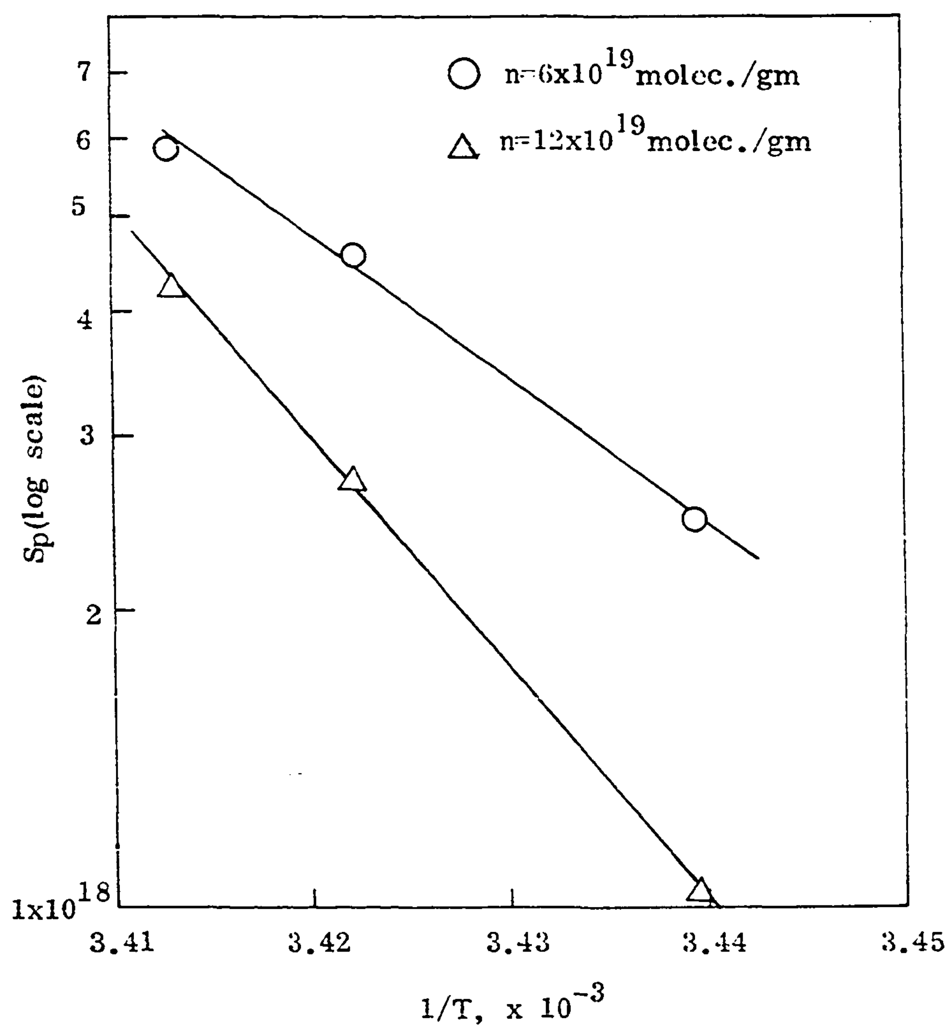

Figure 43. Dependence of the sticking probability of water vapor upon E-glass surface on temperature

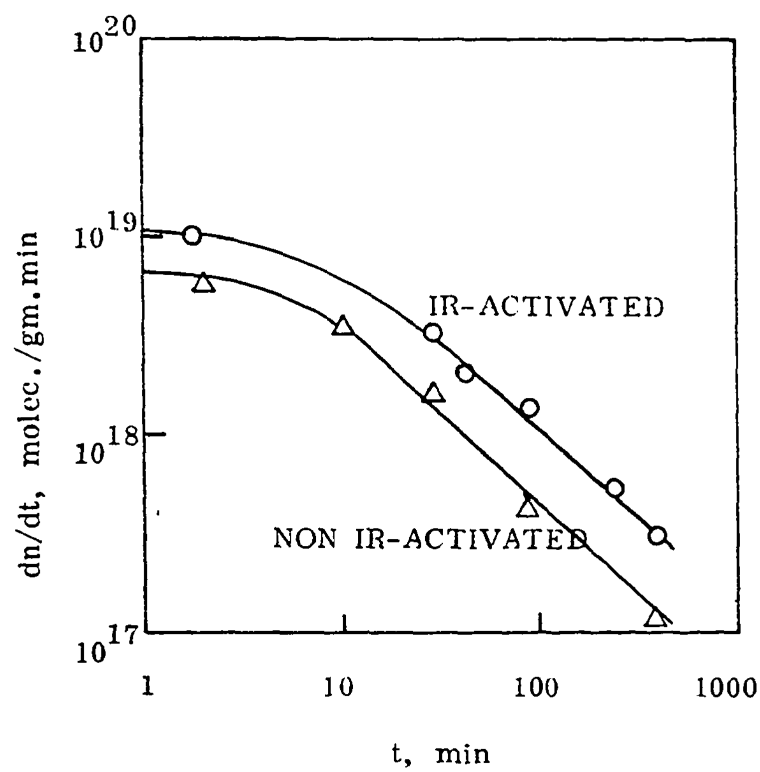

Figure 44. Full log plot of sorption rate of water on E-glass surface versus time

has been called "diffusion process" (119). The non IR-activated run started the diffusion process earlier than the IR-activated run when E-glass was exposed to water vapor.

In general, the diffusion of molecules from a gas phase into a semi-infinite solid trough a boundary at x = 0, obeys Fick's Law:

$$\frac{\partial c}{\partial t} = D \frac{\partial^2 c}{\partial x^2} \tag{69}$$

where c represents the concentration and D the diffusion coefficient through the solid. If it is assumed that $c = 0$ at $x > 0$ for $t = 0$ and $c = c_o$ at $x = 0$ for all t, the rate of sorption and the amount of sorption can be derived from Equation 69 as (119):

$$dn/dt = c_o \sqrt{D/\pi t}\ , \quad \text{and} \tag{70}$$

$$n = 2c_o\sqrt{Dt/\pi}\ . \tag{71}$$

If there is no adsorption in the gas-solid boundary, c_o means the gas phase concentration. However, in the diffusion process, the water diffuses into glass from the adsorbed phase. For this case c_o can be estimated from adsorption data. The activation energy of diffusion, can be calculated according to Arrhenius equation (50, p. 1, 64, p. 205):

$$D = A_D \exp(-E_D/RT) \tag{72}$$

where A_D is a constant and E_D is the activation energy.

As discussed earlier, we could consider capillary condensation as a diffusion process. The rate of capillary condensation was investigated by Washburn (121). For a porous body which behaves like an assemblage of very small cylindrical capillaries he derived the equation:

$$V = k(\gamma t/\eta)^{1/2} \tag{73}$$

where V is the volume of liquid penetrating the capillaries in time t, k is the rate constant, γ is the surface tension and η is the viscosity of the liquid. Since γ and η can be considered as constants at a constant temperature, Equation 73 can be simplified to

$$n = m_D t^{1/2}, \tag{74}$$

since $n = 2c_o \sqrt{Dt/\pi}$, we then get

$$m_D t^{1/2} = 2c_o \sqrt{Dt/\pi} . \tag{75}$$

Therefore,

$$m_D = 1.13\ c_o D^{1/2} \tag{76}$$

where m_D is a function of temperature and is related to the rate constant. Equation 74 was obeyed in the water-E glass systems for IR-activated and non IR-activated runs as was seen in Figure 45 and 46. We may find the activation energy of adsorption of E_a from the relation:

$$m_D = m_o \exp(-E_a/RT) . \tag{77}$$

Equation 77 can further be modified in relation to activation energy of diffusion as follows as given by Johnson Todd (70)

$$m_D = 1.13 c_o D_o^{1/2} \exp(-E_D/2RT) \tag{78}$$

where $E_D = 2\ E_a$, and $1.13\ C_o D_o{}^{1/2} = m_o$.

Equation 77 can be written in the form

$$\log m_D = -B/T + C \tag{79}$$

where $B = E_a/2.303R$ and C is a constant. Figure 47 shows m_D as a function of temperature with and without IR-activated runs respectively. Values

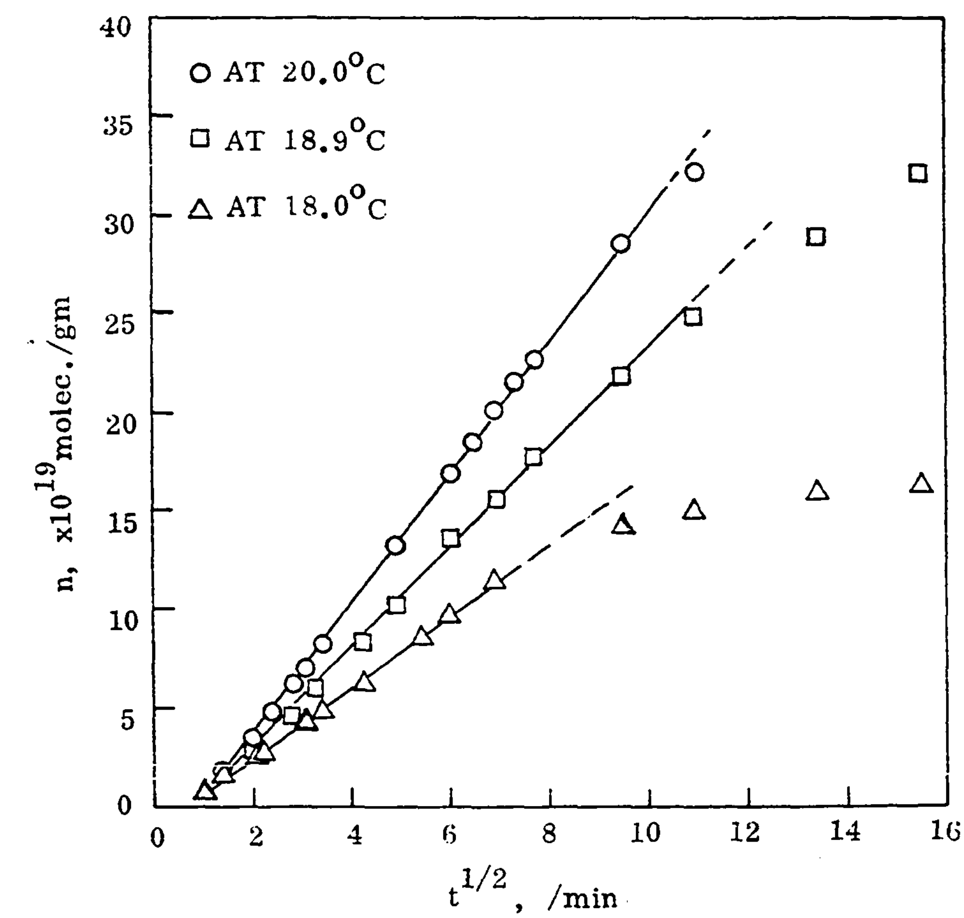

Figure 45. Amount of water sorbed on E-glass versus $t^{1/2}$ at a series of temperatures (IR-activated)

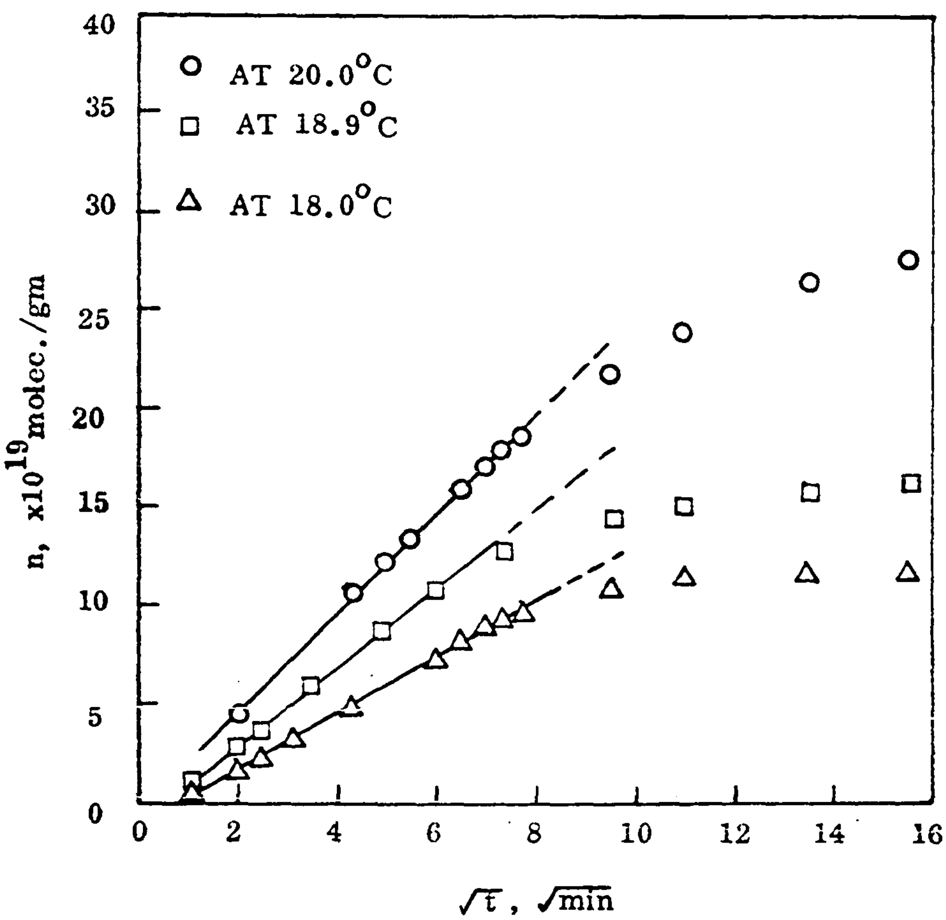

Figure 46. Amount of water sorbed on E-glass versus $t^{1/2}$ at a series of temperatures (non IR-activated)

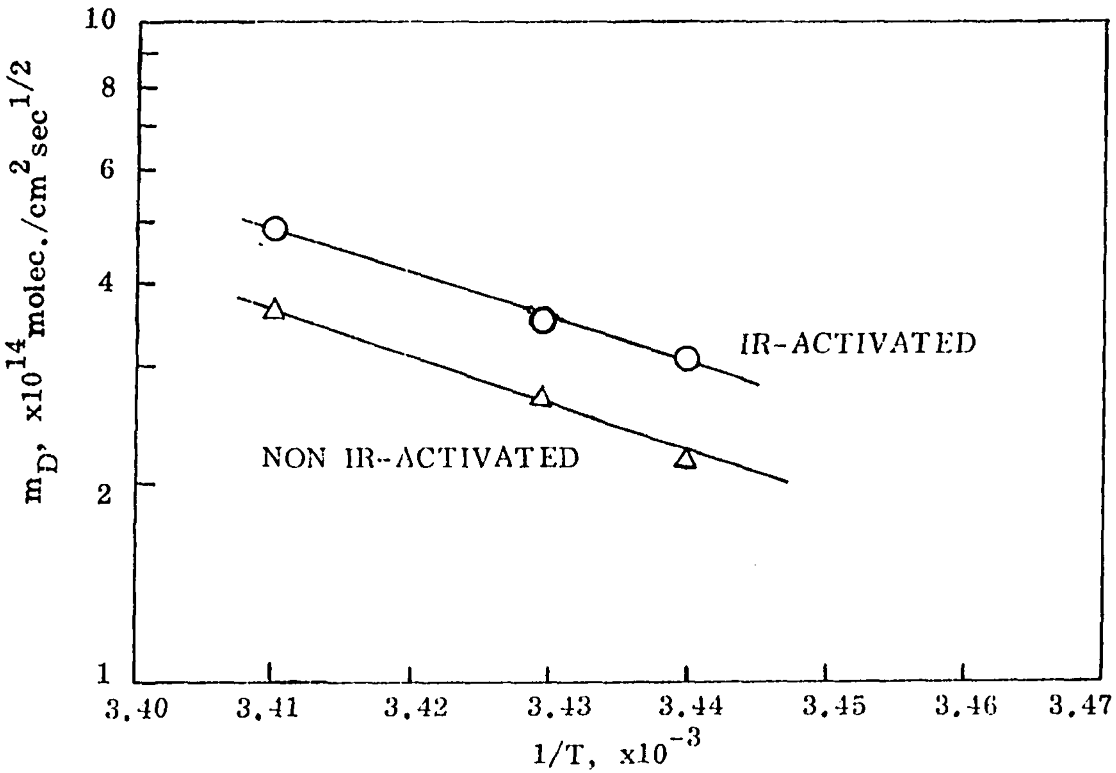

Figure 47. m_D versus reciprocal of temperature for water vapor adsorbed onto E-glass

of m_D, B, C, E_a and E_D for E-glass calculated from Figure 47 are presented in Table 14. The activation energy of adsorption for IR-activated specimen is 2.6 kcal/mole higher than the activation energy of non IR-activated specimens. The energy of activation necessary for the removal of the physically sorbed water is 6.6 ~ 8.2 kcal/mole (76). The high activation energy of diffusion in E-glass implied that evacuation by pumping is insufficient for removing chemisorbed water from E-glass surface. Table 15 gives a comparison of a activation energies of diffusion for various glass water systems. The activation energies of

Table 14. Determination of activation energy of diffusion of water vapor into E-glass

Treatment	Temp. °C	m_D	B, °K	C	E_a[a] Kcal/mole	E_D[b] Kcal/mole
IR-activated	20.0	4.85				
	18.9	3.49				
	18.0	2.58	8570	43.88	39.1	78.2
Non Ir-activated	20.0	3.63				
	18.9	2.69				
	18.0	2.05	7960	41.69	36.5	73.0

[a] $E_a = 2.303RB$

[b] $E_D = 2E_a$

diffusion of water into E-glass was found considerably higher than activation energies of diffusion of water into other glasses (119, 70) except aluminoscilicate. Fifteen per cent of alumina in E-glass must

Table 15. Comparison of activation energy of diffusion of water vapor for various glass

Glass type	E_D,kcal/mole	Reference
Pyrex	41	Johnson Todd (70)
Nonex	38	Tuzi (119)
Terex	57.4	Tuzi (119)
Lime-aluminum	64	Johnson Todd (70)
Vycor	75	Johnson Todd (70)
Aluminosilicate	98	Garbe and Christians (49)
Borosilicate	11	Johnson Todd (70)
Soda-lime-silica	58	Johnson Todd (70)
E-glass	78	Present result

have contributed a great deal of diffusion resistance to E-glass as it is the case with aluminosilicate.

The diffusion coefficient may be calculated from the intercept (n_s) of the n vs. $t^{1/2}$ plot. The values of diffusion coefficient so obtained are presented in Table 16. The results of diffusion coefficient of water into E-glass so obtained agrees well with the extrapolated values from the literature (92). The data from the literature and the results of the present study are plotted in Figure 48.

It is thus shown that we can determine the diffusion coefficients from the adsorption rate data as well as from the usual permeability experiments. The diffusion model proposed thus explains the mechanism of adsorption.

Table 16. Calculation of diffusion coefficient of water vapor into E-glass

Treatment	Temp., °C	dn/dt 36 min. molec./gm$\times 10^{19}$	D^a cm^2/sec.$\times 10^{-17}$
IR-activated	20.0	16.8	8.1
	18.9	13.1	4.7
	18.0	9.8	2.8
Non IR-activated	20.0	14.9	6.4
	18.9	11.9	4.1
	18.0	7.6	1.7

[a] $D = (dn/dt)^2 \pi t / n_s^3$, where $n_s = 22.8 \times 10^{19}$ molec./gm.

The nature of the mechanism by which the water vapor diffuses into E-glass surface is hypothesized. When the water vapor is adsorbed on the glass surface, the force of attraction is so great that it forms hydroxyl groups with the surface active sites, i.e., Si, O or Ca. The hydroxyl groups could move by jumping from one modifier cation to the next if there was sufficient volume to accommodate them, or they could simply move interstitially.

In the absence of any direct evidence, no other mechanism such as the one offered by Steacie (114) will be considered. An experimental work on the relative movements of hydrogen and oxygen of water and on the possible movement of water in an electrical field is obviously desirable.

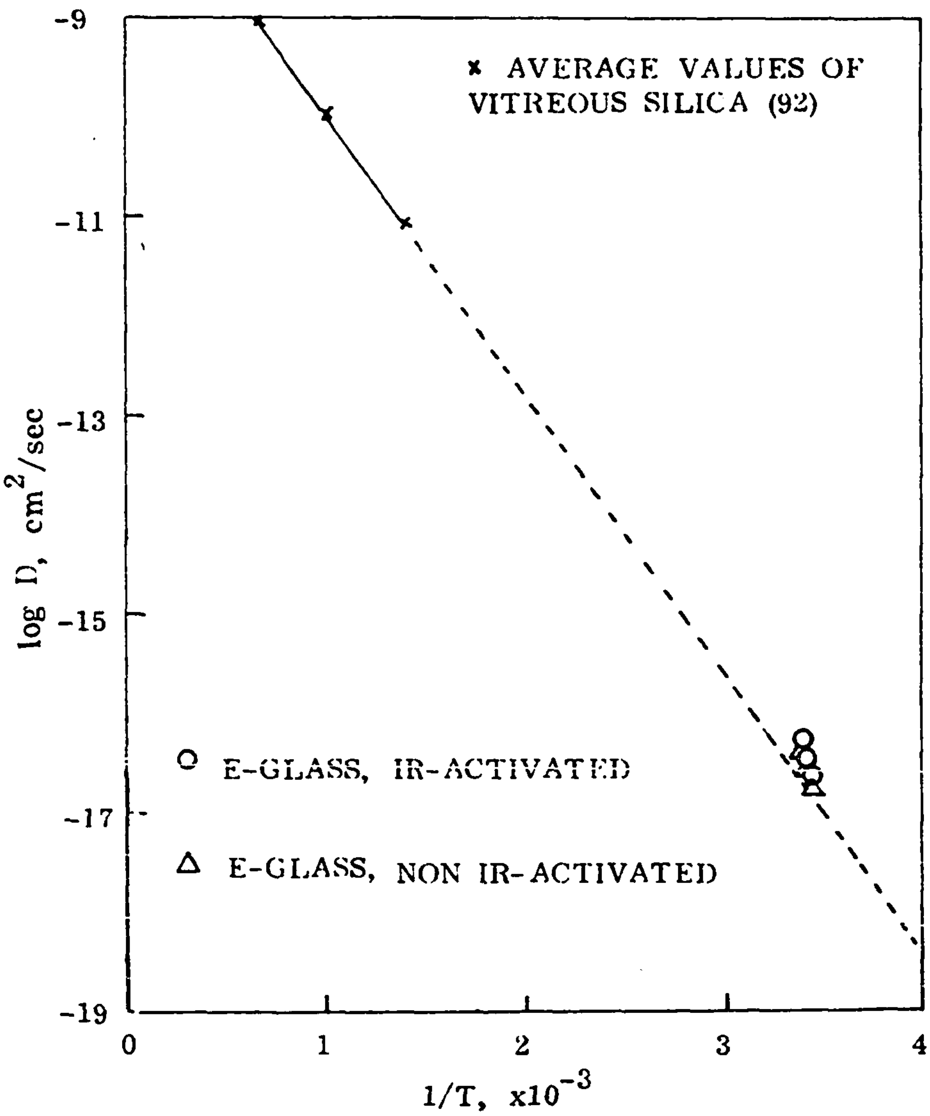

Figure 48. Logarithm of diffusion coefficient of water into glass versus reciprocal of temperature

Infrared Absorption

The main purpose of this phase of the study was to identify the species adsorbed on the surface and to determine the fractional surface coverage by these species. An E-glass spectrum in the infrared region (5000-650 cm^{-1}) was produced using the vacuum frustrated internal reflectance technique described earlier (see Figure 49). All the band frequencies were identified as summarized in Table 17. The frequency of the band at 3750 cm^{-1} is typical of free vibrating OH groups, and its symmetrical appearance indicates that there is no interaction between it and other molecules or surface groups. The presence of hydroxyl groups

Table 17. Infrared spectra of E-glass using the facuum frustrated internal reflectance technique with Beckman IR 4 spectrophotometer

Group	Wave Number, cm^{-1}	Assignment
AlOH	3800-3700	Free OH stretching
SiOH	3750	Free OH stretching
$Mg(OH)_2$	3700-3650	Free OH stretching
$Ca(OH)_2$	3635	Free OH stretching
OH	2800	Hydrogen bonded stretching
HCO_3^-	2375	Stretching
HOH	1750-1650	Crystallized water symmetric bending
CO_3^-	1413	Symmetric stretching
BO_2^-	1410-1340	Stretching vibration
SiO_3^-	1320-770	Stretching vibration

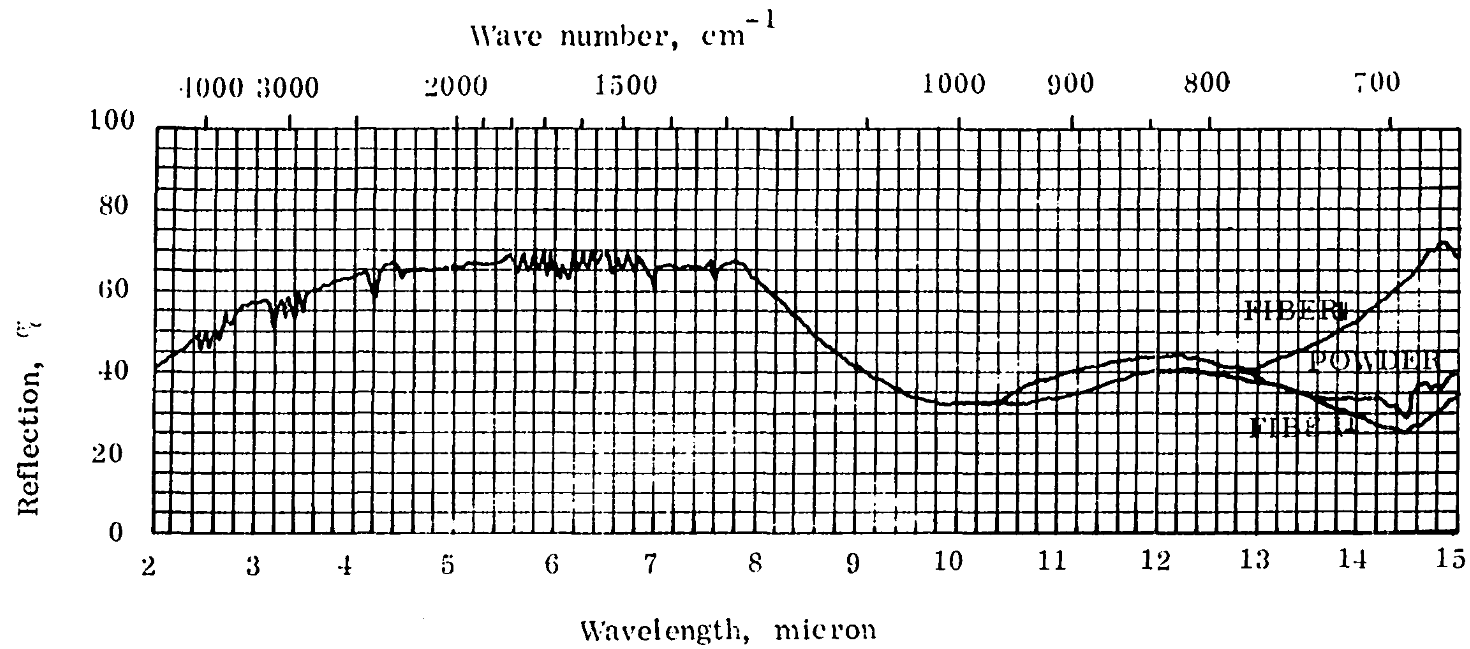

Figure 49. Internal reflection spectrum of Fiberglas-E taken with KRS-5 plate, $\theta = 45^{\circ}$

at the region of 3800-3700 cm^{-1} can be explained on the basis of a computer model of the alumina surface postulated by Peri (97). He predicted, according to his computer model, a surface containing five different types of hydroxyl groups. These groups are variously referred to as 'free hydroxyl groups' or 'isolated silanol-aluminol groups' (86). The assigned vibrational frequencies are shown in Table 18. It was found that the OH bonds (including hydroxyls associated with magnesium and calcium ions) existed on the surface in all cases as the E-glass was evacuated and heated to a moderate temperature of 85°C by an infrated lamp. These hydroxyls existing on alumino-silicate glass were also found unevacuable by many investigators (1, 2). Some fringes around 1750-1650 cm^{-1} which were identified as rotational frequencies of crystalline water showed a rather interesting behavior. It indicated, from

Table 18. Hydroxyl groups associated with alumina[a]

Band	Wave Number, cm^{-1}	No. of Nearest Oxide Neighbors
A	3800	4
B	3780	3
C	3744	2
D	3733	1
E	3700	0

[a]Assignment of frequencies based on Peri's data (97).

the band shape, restricted rotation as well as defect (as a result of flaws) on the E-glass surface which had been treated with deionized water when manufactured. There is one very sharp and intense band appearing at 2375 cm^{-1}. It was identified as HCO_3^- stretching frequency. Also the absorption at 1413 cm^{-1} was credited to CO_4 vibrations due to the presence of CO_2 in the glasses. It was surprising to find CO_2 existing in E-glass. And yet, many investigators (100, 82) have found the CO_2 absorption in sodium silicate glasses. However, the band appearing at 2375 cm^{-1} could be a BOH stretching vibration band. The large valley from 1320 to 770 cm^{-1} is characteristic of silicate glasses and is due to the SiO_2 network. The magnesium hydroxide exhibited a broad absorption band between 3700 and 3650 cm^{-1} that is due to the antisymmetrical OH stretching vibration of the lattice hydroxide and a small band at 3770 cm^{-1} that is a combination band also characteristic of the bulk material.

As discussed earlier, the spectral shifts of hydroxyl stretching frequency to lower wave numbers is evidence of interaction with the adsorbed gas molecules. The strong, broad absorption band that appeared at about 3500 cm^{-1} was attributed to molecular water that is physically adsorbed upon the surface. Confirmatory evidence is provided by a study of the spectrum of adsorbed water in the bending region of the spectrum (14). Addition of water vapor to dehydrated E-glass caused the appearance of bands at 3400 and 1635 cm^{-1}. Both bands increase concomitantly in intensity with the addition of water (see Figure 50).

The spectrum of the adsorbed benzene was little different from that of the liquid, the band frequency deviations being less than 10 cm^{-1}

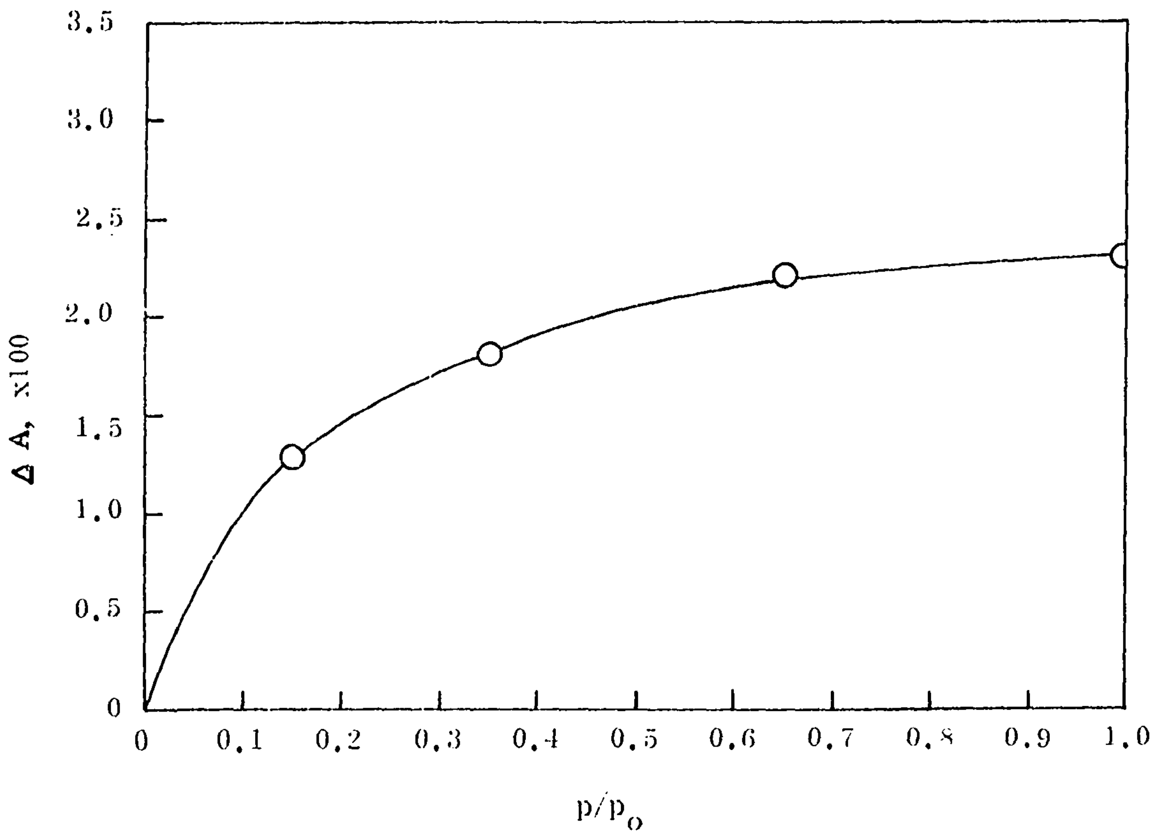

Figure 50. Appearance of peak at 3400 cm^{-1} due to adsorption of water on E-glass

indicating physically adsorbed species. A very clearly sharp band appeared at 673 cm^{-1}. This is 2 cm^{-1} greater than that of benzene vapor but 2 cm^{-1} lower than that of liquid benzene. Thus, it appeared that the adsorbed state was somewhat in between a gas and a liquid as discussed earlier. This probably being a specific interaction occurred between a surface hydroxyl group and the π-electron system of an aromatic molecule which led to changes in the infrared spectrum of the adsorbed molecule. A second point of interest was that the intensity of this band was linearly related to the amount of benzene present on the surface. Figure 51 presented a plot of relative changes in the intensity of the bands at 673 cm^{-3} as a function of benzene vapor pressure. In view of the figure, the greatest perturbations were observed at low coverage. This also can be seen from Figure 52, where band shift is plotted against relative pressure. The intensity ratios initially were about twice those observed for liquid benzene and indicated major changes in the electron distribution in the neighborhood of the atoms giving rise to these vibrations. Similar perturbations have been noted for benzene adsorbed on molecular sieves and alkali halides (1).

It has been observed that the infrared absorption band due to the stretching vibration of surface hydroxyl groups at 3750 cm^{-1} shifts to a lower frequency when gas molecules are adsorbed on the surface. The magnitude of this shift, $\Delta\nu_{OH}$, is considered to be a measure of the strength of the interaction between hydroxyl groups and adsorbed molecules. Galkin et al. (48) pointed out that a difference, ΔQ_a, between the heat of adsorption of a gas on a silica surface covered with

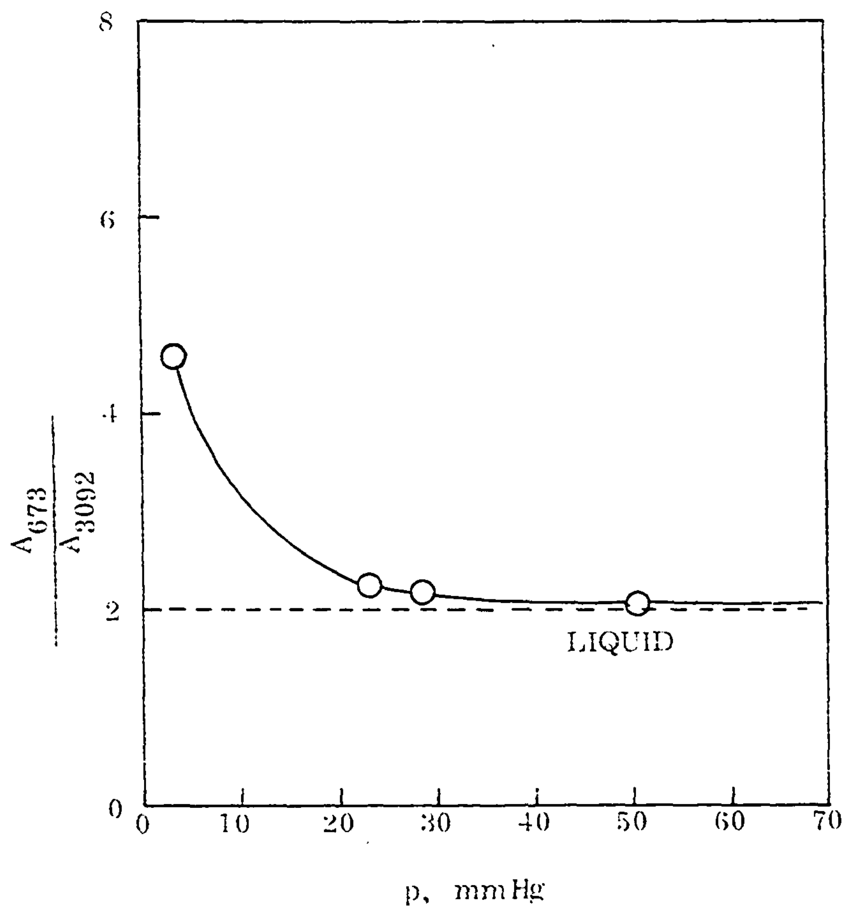

Figure 51. Effect of surface hydroxyl groups on adsorbed benzene

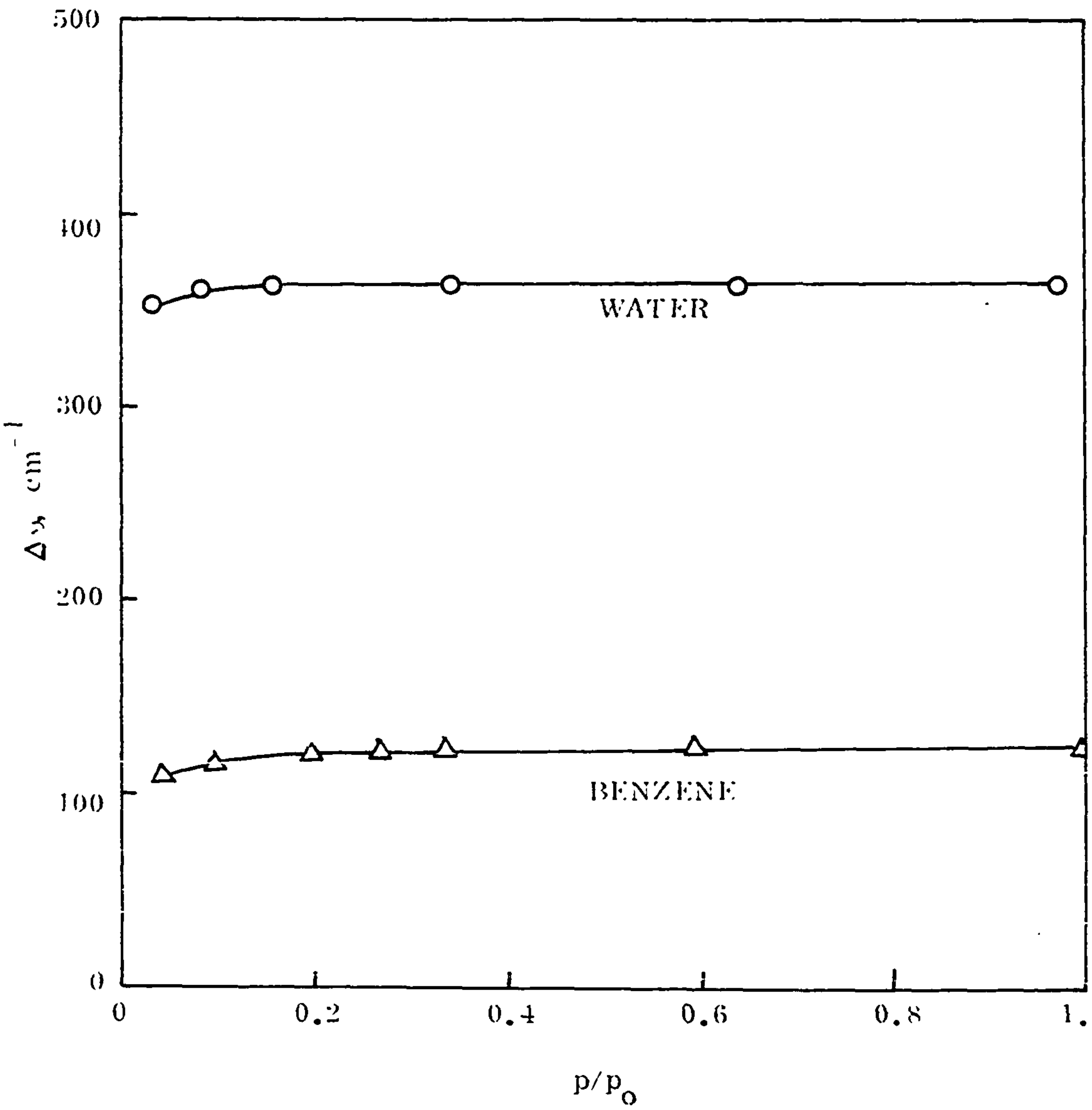

Figure 52. Relationship between shift of the absorption band of surface free hydroxyl groups, $\Delta\nu$, and surface coverage on adsorption of water and benzene

hydroxyl groups and the heat of adsorption of the same gas on a dehydroxylated surface, should also be a measure of the strength of the interaction between surface hydroxyl groups and adsorbed molecules. The relation between ΔQ_a and $\Delta\nu_{OH}$ has been proved to be roughly linear (5, 54, p. 96).

Table 19 shows the calculated values of the surface hydroxyl groups perturbations and ΔQ_a's due to adsorption of water vapor and benzene. Overlapping of the fundamental OH-stretching bands of water molecules and hydroxyl groups makes it impossible to measure $\Delta\nu_{OH}$ directly. However, $\Delta\nu_{OH}$ can be obtained from the difference between the frequency shifts of the OH-stretching plus OH-bending combination band and the

Table 19. Values of $\Delta\nu_{OH}$ and ΔQ_a for adsorbed water and adsorbed benzene on E-glass

Adsorbate	OH frequency[a] cm^{-1}	$\Delta\nu_{OH}$ cm^{-1}	ΔQ_a Kcal/mole
none	3690[b]	60	
water	3400	350	2.7
Benzene	3645	105	1.8

[a] $\nu_{Si-OH} = 3750\ cm^{-1}$ for IR activated and evacuated E-glass surface.

[b] Evacuated E-glass surface.

OH-bending fundamental band as suggested by Anderson (5). The $\Delta\nu_{OH}$ so calculated for water is about 200 cm^{-1}. $\Delta\nu_{OH}$ for benzene is 105 cm^{-1}

about half of that of water. Figure 53 shows the dependence of the value $\Delta\nu$ on the heat of adsorption for a surface coverage of 0.5 constructed using the data reported in the literature. We believed that this study should yield important information on the nature and energy of short-range molecular interaction upon adsorption.

The heat of adsorption of water and benzene vapors on E-glass decreased with surface coverage. The heat of specific adsorption of benzene on the surface hydroxyly groups is higher than the heat of non-specific adsorption; as the coverage is increased, nonspecific adsorption will start to take place, and the heat of adsorption in the later stages of the process will approach that of the saturated molecule. From the analysis of the entropy of adsorption, it indicated, as discussed earlier, that the adsorbed benzene undergoes either two-dimensional translation and rotation in the plane of the ring or a motion in which it can also rotate around one of the axes lying in the plane of the ring. The shift of the band due to surface hydroxyl groups from 3750 cm^{-1} to values reported in Table 19 on the one hand and higher intensities (Figure 50) of shifted band on the others indicate that water adsorption occured on OH cites. Recently, Basila (13) in the investigation of the interaction of water with the surface of highly dehydrated silica-alumina glass pointed out that the adsorbed water is fixed and is held on acidic sites far removed from surface hydroxyl groups that hydrogen-bonding to these groups does not occur.

Roev et al. (107), on the basis of infrared studies, concluded that the the silica-alumina surface contained only one type of hydroxyl group.

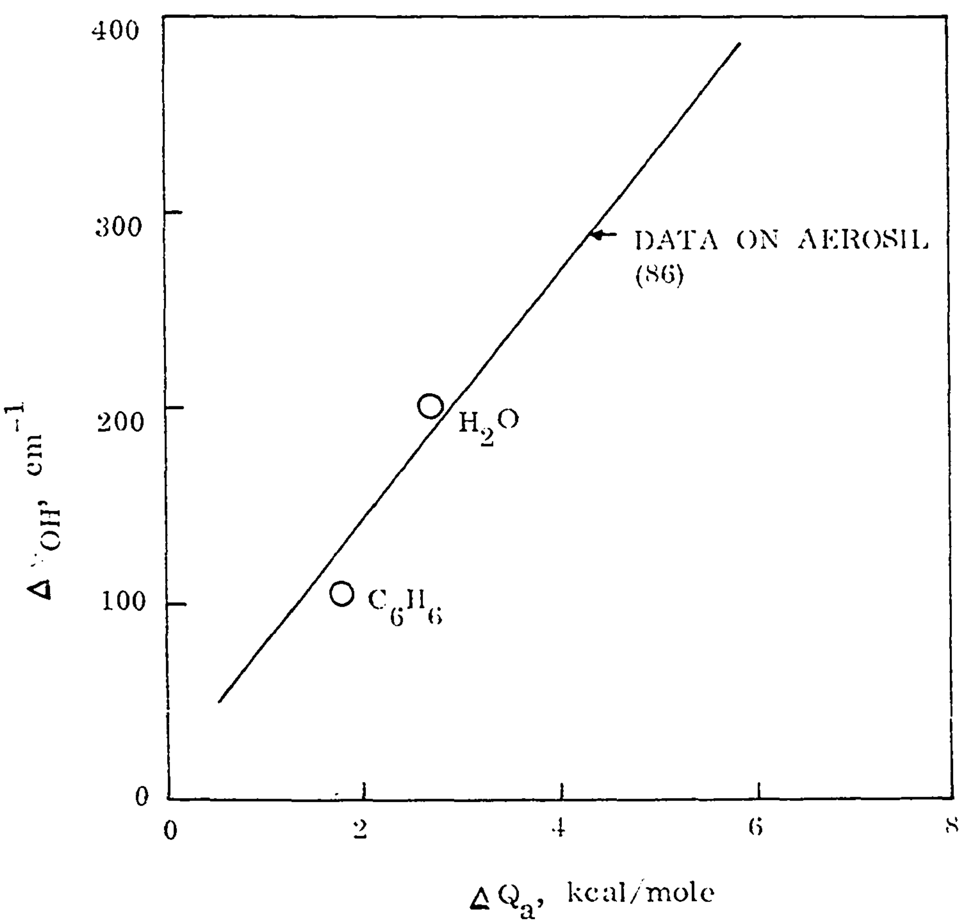

Figure 53. Plot of $\Delta\nu_{OH}$ against ΔQ_a

The corresponding band, which is observed at 3745 cm^{-1}, is easily deuterated and shifted to 2762 cm^{-1}. Although it is possible that accidental degeneracy could give rise to a single hydroxyl stretching frequency in place of the three vibrations observed on alumina, the close similarity in both frequency and band half-widths for the OH group on silica-alumina (12 cm^{-1}) and silica (10 cm^{-1}) favors the assumption that the hydroxyl groups are attached to silicon atoms in the surface rather than aluminum atoms (54, p. 171). Sewell and Morgan (111) in their study of methanol vapor adsorption on soda-lime-silica glass stated that the surfaces of the glasses were hydroxylated in the cleavage process as indicated below:

$$\equiv Si-O-Si\equiv \xrightarrow[\text{humid atmosphere}]{\text{cleavage in}} 2 \equiv Si-O-H.$$

The slow and irreversible adsorption observed in this investigation suggests that these surface hydroxyl groups may diffuse into the glass supporting the assumption of diffusion process for solubility of gases in solids (114). The fundamental characteristic of the usual adsorption isotherm is the large amount of gas which is taken up at low pressures. A small amount of solubility, where Henry's law usually holds, will exert little influence on the total sorption at low pressures, but will have a larger effect at high pressures. Since the low pressure range of the isotherm is the essential part for computations disolved adsorbate does not influence the results of single experiments appreciably. Subsequent experiments, however, as found out in this study will show appreciable differences especially if the sample is not activated by IR irradiation and evacuation.

CONCLUSIONS

The following conclusions have been reached on the basis of the results obtained.

1. Permanent hysteresis was observed in each sorption experiment with the E-glass-water system. The first layer of adsorbed water could not be degassed by pumping. To close the hysteresis loop it was necessary to heat the sample with an infrared lamp. The permanent hysteresis is believed to be caused by diffused hydroxyls on the surface. Heating by infrared radiation, reverses the hydrolysis possibly causing a change of the surface structure. This change results in a variation of the specific surfaces.

2. The adsorption isotherms obtained were of Brunauer type IV adsorption isotherms, indicating capillary condensation dominated the adsorption process at high relative pressures.

3. Specific surface was determined by three independent methods, namely, light microscopy, BET, and Fu and Bartell (FB) methods. Very good agreements were found between the results. The BET specific surface (1.2-1.9 m^2/gm) agreed very closely with the FB total specific surface (1.3-2.3 m^2/gm). On the other hand the FB external (0.16-0.85 m^2/gm) surface area agreed very closely with geometric areas calculated from light microscope observation (0.16 m^2/gm).

4. Good correlations were obtained between the mean pore diameter calculated from the specific surface and the mean pore diameter calculated according to capillary condensation theory (110 - 220 Å).

5. The existence of micropores constituting 85% of the total surface was hypothesized to be responsible for a ten-fold difference between the surface area determined by BET method and light microscopy.

6. The specific surface of E-glass determined by the BET method using water vapor ranged from 1.2 m^2/gm for the E-glass fiber to 1.9 m^2/gm for the E-glass pellet. The specific surface of the E-glass pellet determined by the BET method using benzene ranged from 0.84 m^2/gm to 0.52 m^2/gm. If the molecular area is assumed to be 32.2 $Å^2$. If 42 $Å^2$ is used for the molecular area (91) specific surfaces are found ranging from 0.68 m^2/gm to 1.10 m^2/gm. The molecular area of benzene in micropores may be larger than either area assumed (91); if this is the case BET areas obtained from benzene adsorption are not too far from those obtained from water adsorption.

7. The well-known loss of strength of fiber in the water vapor environment was hypothesized to be due to the cracks or flaws occurring due to water adsorption on the fiber surface. These cracks act as stress multipliers. The micropore sizes calculated in this report for Fiberglas-E supports the Griffith rupture theory which accounts for the rapid reduction of glass fiber tensile strength.

8. The increasing microspore size as well as increasing surface area with subsequent runs presented in this report may account for the loss of strength of glass fiber with age.

9. A ϵ versus t plot is proposed to replace the usual ϵ versus φ plot of the potential theory. Where ϵ surface potential, t thickness of the adsorbate on the surface and φ is the volume of the adsorbate on the

surface. The proposed plot was found to be independent of the specific surface whereas the usual plot was found to depend on the specific surface. This supports the accuracy of the surface area determinations.

10. The free energy of wetting for the water-E-glass system at 20°C was -253.69 erg/cm^2; the free energy of wetting for the benzene-E-glass system at 20°C was -72.36 erg/cm^2.

11. The free energy of displacement of benzene by water was -146.33 erg/cm^2. This implies that an actual contact between E-glass and benzene is unattainable in the presence of bulk water. Therefore benzene has less affinity for an E-glass surface than water has.

12. A modified Clausius-Clapeyron equation, $\ln(p_1/p_2)q_f = H_a/R(1/T_2 - 1/T_1)$, where $q_f = tf\ \delta_b$ is proposed to compute the isosteric heat of adsorption (q_f is in a sense equal to Γ the surface excess, f is a correction factor and δ_b is the density of the adsorbate).

13. The isosteric heat of adsorption computed by the modified equation gave good agreement with that computed from the BET parameters for the first layer of adsorbate. See Table 13. The average value is about 3Kcal/mole.

14. The heat of adsorption reaches the heat of liquefaction beyond two to three layers of adsorbate on E-glass.

15. Water-treated E-glass fiber has a higher heat of adsorption than that of powdered E-glass or compacted E-glass. The differences range from 564 cal/mole to 640 cal/mole.

16. The isosteric heat of adsorption for benzene vapor is lower than that for water vapor at same coverage (see Figures 37 and 38).

17. The computed isosteric entropies of adsorption indicate that the state of adsorbed phase is between the solid and the liquid state at low coverage. The liquid state is reached at high coverage.

18. The fact that the entropy in the adsorbed state is lower than in a liquid state indicates that the adsorbed molecules have a lower degree of freedom than the molecules in the liquid.

19. Adsorption of water or benzene by E-glass is a spontaneous process because of decreasing free energy or increasing entropy.

20. The diffusion coefficient can be calculated from the adsorption rate data.

21. Adsorption rate studies indicated that water vapor diffuses into E-glass at a rate of 10^{-17} cm^2/sec at ordinary temperature.

22. The experimental adsorption rate results on the water-E-glass system fits the Bangham equation indicating the adsorption process is a combination of adsorption and absorption.

23. Slow and irreversible effects due to high activation energy of adsorption in the water-E-glass system may be explained on the basis of a combination of adsorption and diffusion. This also explains the solubility of gases in E-glass.

24. A mechanism by which the water vapor diffuses into E-glass is hypothesized. When the water vapor is adsorbed on the glass surface, the force of attraction is so great that it forms hydroxyl groups with

the surface active sites. The hydroxyl groups could move by jumping from one modifier cation to the next if there was sufficient volume to accommodate them, or they could simply move interstitially.

25. From the heat of adsorption decrease and infrared band frequencies and intensities variations with adsorption, it was concluded that both water and benzene were adsorbed on hydroxyl groups at low coverage. After the saturation of hydroxyl sites, however, they were adsorbed on remaining sites of the heterogeneous surface.

26. The infrared band due to the stretching vibration of surface hydroxyl groups at 3750 cm^{-1} shifts to a lower frequency when gas molecules are adsorbed on the glass surface. The magnitude of this shift is a measure of the strength of the interaction between hydroxyl groups and adsorbing molecules. It was found that this shift is roughly linearly related to the difference between the heat of adsorption of a gas on a surface, i.e., silica, covered with hydroxyl groups and the heat of adsorption of the same gas on a dehydroxylated surface.

BIBLIOGRAPHY

1. Abramov, V. N., Kiselev, A. V. and Lygin, V. I. Nature of adsorption by zeolites. Infrared spectrum of benzene adsorbed by zeolites of types 13 Kh and 10 Kh. Russian Journal of Physical Chemistry 37(5): 613-616. 1963.

2. Adams, R. V. Some experiments on the removal of water from glasses. Physics and Chemistry of Glasses 2: 50-54. 1961.

3. Adamson, A. W. Physical chemistry of surfaces. 2nd ed. Interscience Publishers, New York. 1967.

4. Allen, P. W., Everett, D. H. and Penney, M. F. The thermodynamics of hydrocarbon solutions. I. Technique of vapour-pressure measurements; the vapour pressure of benzene. Royal Society of London, Proceedings, Series A, 212: 149-163. 1952.

5. Anderson, J. H., Jr. Calorimetric vs. infrared measures of adsorption bond strengths on silica. Surface Science 3: 290-291. 1965.

6. Bacon, F. R. The chemical durability of silicate glass. The Glass Industry 49: 1-19. 1968.

7. Bangham, D. H. The Gibbs adsorption equation and adsorption on solids. Faraday Society Transactions 33: 805-811. 1937.

8. Bangham, D. H. and Razouk, R. I. Adsorption and wettability of solid surfaces. Faraday Society Transactions 33: 1459-1463. 1937.

9. Bangham, D. H. and Sever, W. An experimental investigation of the dynamical equation of the process of gas-sorption. Philosophical Magazine, Series 6, 49: 935-944. 1925.

10. Barrer, R. M. Diffusion in and through solids. Cambridge University Press, London. 1941.

11. Barrer, R. M. Specificity in physical sorption. Journal of Colloid and Interface Science 21: 415-434. 1966.

12. Bartell, F. E. and Fu, Y. The specific surface area of activated carbon and silica. Journal of Physics and Colloid Chemistry 55: 662-675. 1951.

13. Basila, M. R. An infrared study of a silica-alumina surface. Journal of Physical Chemistry 66: 2223-2228. 1962.

14. Benesi, H. A. and Jones, A. C. An infrared study of the water-silica gel system. Journal of Physical Chemistry 63: 179-182. 1959.

15. Berenyi, L. Prüfung der Polânyischen theorie der adsorption. Zeitschrift für Physikalische Chemie 94: 628-662. 1920.

16. Berenyi, L. Neuere adsorptionsberechnungen. Zeitschrift für Physikalische Chemie 105: 55-72. 1923.

17. Boyd, G. E. and Livingston, H. K. Adsorption and energy changes at crystalline solid surfaces. American Chemical Society Journal 64: 2383-2388. 1942.

18. Brunauer, S. The adsorption of gases and vapors. Physical adsorption. Princeton University Press, Princeton, N.J. 1943.

19. Brunauer, S. Solid surfaces and solid-gas interface. Advances in Chemistry Series 33: 5-17. 1961.

20. Brunauer, S., Deming, L. S., Deming, W. E. and Teller, E. On a theory of the van der Waals adsorption of gases. American Chemical Society Journal 62: 1723-1732. 1940.

21. Brunauer, S., Emmett, P. H. and Teller, E. Adsorption of gases in multimolecular layers. American Chemical Society Journal 60: 309-319. 1938.

22. Burgman, J. A. and Hunia, E. M. The effect of fiber diameter, environmental moisture, and cooling time during fiber formation on the strength of E-glass fibers. Unpublished paper presented at Rolla Conference on Glass Fibers, Rolla, Missouri, March, 1971.

23. Carmen, P. C. and Raal, F. A. Role of capillary condensation in physical adsorption. Nature 167: 112-113. 1951.

24. Clampitt, B. H. and German, D. E. Heat of vaporization of molecules at liquid-vapor interfaces. Journal of physical chemistry 62: 438-440. 1958.

25. Cockram, D. R., Haider, Z. and Roberts, G. J. The diffusion of 'water' in soda-lime glass within and near the transformation range. Physics and Chemistry of Glasses 10(1): 18-22. 1969.

26. Corning Glass. Properties of selected commercial glasses. Corning Glass Works Bulletin 83. 1965.

27. Craig, R. G., Van Voorhis, J. J. and Bartell, F. E. Free energy of immersion of compressed powders with different liquids. I. Graphite powders. Journal of Physical Chemistry 60: 1225-1230. 1956.

28. Damköhler, G. Über die adsorptiosgeschwindigkeit von gasen an porösen adsorbentien. Zeitschrift für Physikalische Chemie 174: 222-238. 1935.

29. De Boer, J. H. Atomic forces and adsorption. Advances in Colloid Science 3: 1-60. 1950.

30. De Boer, J. H. The dynamical character of adsorption. 2nd ed. Oxford at the Clarendon Press. London. 1968.

31. Deitz, V. R. Interaction of water vapor with pristine E-glass fiber. Naval Research Laboratory Report 6812. 1968.

32. Demirel, T. Adsorption of water vapor by sodium and calcium montmorillonites. Unpublished Ph.D. thesis. Ames, Iowa, Library, Iowa State University of Science and Technology. 1962.

33. Demirel, T. and Enüstün, B. V. Free energies of wetting of minerals. I. Communications de la Faculte des Sciences de L'universite D'Ankara, Series B, 6: 1-19. 1957.

34. Dobay, D. G., Fu, Y. and Bartell, F. E. Energetics of the adsorption of aliphatic amines by silica gel. American Chemical Society Journal 73: 308-314. 1951.

35. Donnet, J. B., Battistella, R. and Chatenet, B. Study of glass fiber surfaces by electron microscopy and gas adsorption. Unpublished paper presented at Rolla Conference on Glass Fibers, Rolla, Missouri, March, 1971.

36. Dupré, A. Theorie machanique de la chaleur Gauthier. Villars, Paris, 1869.

37. Eakins, W. J. Effect of water on glass fiber-resin bonds. ASTM Special Technical Publication 452: 137-148. 1968.

38. Egorov, M. M., Egorova, T. S., Kiselev, V. F. and Krasilnikov, K. G. Adsorption of water vapor on silica gels of different degree of hydration. Soviet Research and Ceramics 2: 397-401. 1957.

39. Eischens, R. P. and Pliskin, W. A. The infrared spectra of adsorbed molecules. Advances in Catalysis 10: 1-56. 1958.

40. Emmett, P. H. The measurement of the surface areas of finely divided or porous solids by low temperature adsorption isotherms. Advances in Colloid Science 1: 1-36. 1942.

41. Everett, D. H. Thermodynamics of adsorption. Faraday Society Transactions 46: 453-459. 1950.

42. Fahrenfort, J. Attenuated total reflection. A new principle for the production of useful infrared spectra of organic compounds. Spectrochimica Acta 17: 698-709. 1961.

43. Folman, M. and Yates, D. J. C. Perturbation effects due to hydrogen bonding in physical adsorption studied by length-change and infrared techniques. Royal Society of London, Proceedings, Series A, 246: 32-51. 1958.

44. Folman, M. and Yates, D. J. C. Expansion-contraction effects in rigid adsorbents at low coverages. Faraday Society Transactions 54: 429-440. 1958.

45. Folman, M. and Yates, D. J. C. Infra-red and length-change studies in adsorption of H_2O and CH_3OH on porour silica glass. Faraday Society Transactions 54: 1684-1691. 1958.

46. Foster, A. G. The sorption of condensible vapors by porous solids. I. The applicability of the capillary theory. Faraday Society Transactions 28: 645-657. 1932.

47. Fu, Y. and Bartell, F. E. Surface area of porous adsorbents. Journal of Physics and Colloid Chemistry 55: 662-675. 1951.

48. Galkin, G. A., Kiselev, A. V. and Lygin, V. I. Infrared spectra and energy of adsorption of aromatic compounds on silica. Faraday Society Transactions 60: 431-439. 1964.

49. Garbe, S. and Christians, K. Vakuum-Technik 11: 9. 1962. Original not available; cited in Holland, L. The properties of glass surfaces. p. 205. John Wiley and Sons Inc., New York. 1964.

50. Glasstone, S., Laidler, K. J. and Eyring, H. The theory of rate processes. 1st ed. McGraw-Hill Book Company, Inc., New York. 1941.

51. Griffith, A. A. The phenomena of rupture and flow in solids. Royal Society of London, Philosophical Transactions, Series A, 221: 163-198. 1921.

52. Griffith, A. A. The theory of rupture. International Congress for Applied Mechanics, Proceedings, Delft, 1: 55-63. 1924.

53. Hagymassy, J., Jr., Brunauer, S. and Mikail, R. S. Pore structure analysis by water vapor adsorption. I. t-curves for water vapors. Journal of Colloid and Interface Science 29(3): 485-491. 1969.

54. Hair, M. L. Infrared spectroscopy in surface chemistry. Marcel Dekker Inc., New York. 1967.

55. Hallberg, S. The adhesion of bituminous binders and aggregates in the presence of water. Vol. 78. Statens Vaginstitut, Stockholm. 1950.

56. Halsey, G. D., Jr. Physical adsorption on non-uniform surface. Journal of Chemical Physics 16: 931-937. 1948.

57. Halsey, G. D., Jr. The role of surface heterogeneity in adsorption. Advances in Catalysis 4: 259-269. 1952.

58. Harkins, W. D. and Boyd, A. R. The binding energy between a crystalline solid and a liquid: The energy of adhesion and emersion. Energy of emersion of crystalline powders. II. American Chemical Society Journal 64: 1195-1204. 1942.

59. Harkins, W. D. and Jura, G. Surface of solids. X. Extension of the attractive energy of a solid into an adjacent liquid or film, the decrease of energy with distance, and the thickness of films. American Chemical Society Journal 66: 919-927. 1944.

60. Harrick, N. J. Internal reflection spectroscopy. Interscience Publishers, New York. 1967.

61. Herzberg, G. Molecular spectra and molecular structure. D. Van Nostrand Company, Inc., New York. 1945.

62. Hill, T. L. Statistical mechanics of adsorption. V. Thermodynamics and heat of adsorption. Journal of Chemical Physics 17: 520-535. 1949.

63. Hill, T. L. Theory of Physical adsorption. Advances in Catalysis 4: 211-258. 1952.

64. Holland, L. The properties of glass surfaces. John Wiley and Sons Inc., New York. 1964.

65. Holloway, D. G. The strength of glass. Contemporary Physics 1: 230-235. 1960.

66. Howard, H. C. and Culbertson, J. L. Some heats of wetting of unit surfaces. American Chemical Society Journal 72: 1185-1187. 1950.

67. Huang, R. J., Demirel, T. and McGee, T. D. The adsorption of water vapor on Fiberglas-E. Unpublished mimeographed paper presented at Rolla Conference on Glass Fibers, Rolla, Missouri, March, 1971. Ames, Iowa, Iowa State University of Science and Technology, Department of Civil Engineering. 1971.

68. Huang, R. J., Demirel, T. and McGee, T. D. An empirical expression for capillary depression of mercury. Unpublished mimeographed paper presented at Iowa Academy of Science annual meeting, Dubuque, Iowa, April, 1971. Ames, Iowa, Iowa State University of Science and Technology, Departmentof Civil Engineering. 1971.

69. Johannson, O. K., Stark, F. O., Vogel, G. E. and Fleschmann, R. M. Evidence of chemical bond formation at silane coupling agent interfaces. Journal of Composite Materials 1: 278-292. 1967.

70. Johnson Todd, B. Outgassing of glass. Journal of Applied Physics 26: 1238-1243. 1955.

71. Jura, G. and Harkins, W. E. Determination of the decrease of free surface energy of a solid by an adsorbed film. American Chemical Society Journal 66: 1356-1362. 1944.

72. Kemball, C. Entropy of adsorption. Advances in Catalysis 2: 239-250. 1950.

73. Kiselev, A. V. Adsorption properties of hydrophobic surfaces. Journal of Colloid and Interface Science 28(3): 430-441. 1968.

74. Kline, G. M. and Reinhart, F. W. Fundamentals of adhesion. Mechanical Engineering 72(9): 717-722. 1950.

75. Kozirowski, Y. and Folman, M. Infrared spectrum and surface polymerization of adsorbed HCN. Faraday Society Transactions 60: 1532-1538. 1964.

76. Lange, K. R. The characterization of molecular water on silica surfaces. Journal of Colloid Science 20: 231-240. 1965.

77. Langmuir, J. The adsorption of gases on plane surfaces of glass, mica and platinum. American Chemical Society Journal 40: 1361-1403. 1918.

78. Law, J. T. The adsorption of water vapor on germanium and germanium dioxide. Journal of Physical Chemistry 59: 67-71. 1955.

79. Little, L. H. Infrared spectra of adsorbed species. Academic Press, New York. 1966.

80. Livingston, H. K. The corss-sectional areas of molecules adsorbed on solid surfaces. Journal of Colloid Science 4: 447-457. 1949.

81. Loesser, E. H., Harkins, W. D. and Twiss, S. B. Adhesion of liquids to solids. Molecular interaction between metal and adsorbed vapors. Journal of Physical Chemistry 57: 251-254. 1953.

82. Martinsen, W. E. Selected properties of sodium silicate glasses and their structural significance. Unpublished Ph.D. thesis. Ames, Iowa, Library, Iowa State University of Science and Technology. 1969.

83. McBain, J. W. Der mechanismus der adsorption von wassertoff durch kohlenstoff. Zeitschrift für Physikalische Chemie 68: 471-497. 1909.

84. McBain, J. W. Theories of occlusion; and the sorption of iodine by carbon. Faraday Society Transactions 14: 202-212. 1919.

85. McBain, J. W. An explanation of hysteresis on the hydration and dehydration of gels. American Chemical Society Journal 57: 699-700. 1935.

86. McDonald, R. S. Study of the interaction between hydroxyl groups of aerosil silica and adsorbed non-polar molecules by infrared spectrometry. American Chemical Society Journal 79: 850-855. 1957.

87. McGavack, W. D. and Patrick, W. A. The adsorption of sulfur dioxide by the gel of silicic acid. American Chemical Society Journal 42: 946-978. 1920.

88. McMillan, W. G. and Teller, E. The role of surface tension in multilayer gas adsorption. Journal of Chemical Physics 19: 25-32. 1951.

89. Menzies, A. W. C. Contamination by dust particles and intensive desiccation. Nature 125: 445-446. 1930.

90. Mikhail, R. SH. and Shebl, F. A. Adsorption in relation to pore structures of silicas. I. Organic vapor adsorption on micropores silica gel. Journal of Colloid and Interface Science 32(3): 505-517. 1970.

91. Mikhail, R. SH. and Shebl, F. A. Adsorption in relation to pore structures of silicas. II. Water vapor adsorption on wide-pore and microporous silica gels. Journal of Colloid and Interface Science 34(1): 65-75. 1970.

92. Moulson, A. J. and Roberts, J. P. Water in silica glass. Faraday Society Transactions 57: 1208-1216. 1961.

93. National Research Council of the United States of America. International critical tables. Vol. I. McGraw-Hill Book Company, Inc., New York. 1926.

94. Orchistron, H. D. Adsorption of water vapor. II. Clays at 25°C. Soil Science 78: 463-479. 1954.

95. Orchistron, H. D. Adsorption of water vapors. III. Homoionic montmorillonites at 25°C. Soil Science 79: 71-78. 1955.

96. Palmer, W. G. and Clark, R. E. D. Adsorption on measured surfaces of vitreous silica. Royal Society of London, Proceedings, Series A, 149: 360-384. 1935.

97. Peri, J. B. Infrared study of OH and NH_2 groups on the surface of a dry silica aerogel. Journal of Physical Chemistry 70: 2937-2945. 1966.

98. Pliskin, W. A. The stability of glazed silicon surfaces to water attack. Institute of Electronic and Electrical Engineering Proceedings 52: 1468-1471. 1964.

99. Polanyi, M. Über die adsorption von standpunkt des dritten wärmesatzes. Verhandlungen Deutsche Physikalische Gesellschaft 16: 1012-1016. 1914.

100. Pozubenkov, A. F. and Florinskaya, V. A. Relation between the structure and properties of sodium silicate glasses. In Poraikoshites, E. A., ed. The structure of glass. Vol. 7. Pp. 6-13. New York, New York, Consultants Bureau, Inc. 1966.

101. Rand, M. J. The adsorption of water vapor by porous glass. Electrochemical Society Journal 109(5): 402-408. 1962.

102. Rawson, H. Inorganic glass-forming systems. Academic Press, New York. 1967.

103. Razouk, R. I. and Salem, A. S. The adsorption of water vapor on glass surfaces. Journal of Physics and Colloid Chemistry 52: 1208-1227. 1948.

104. Roderick, G. L. Water vapor-sodium montmorillonite interaction. Unpublished Ph.D. thesis. Ames, Iowa, Library, Iowa State University of Science and Technology. 1965.

105. Roderick, G. L. and Demirel, T. Water vapor-sodium montmorillonite interaction. Highway Research Record 128: 45-67. 1966.

106. Roderick, G. L., Senich, D. and Demirel, T. X-ray diffraction and adsorption isotherm studies of the montmorillonite-water system. International Clay Conference, Tokyo, Japan, Proceedings 1: 659-668. 1969.

107. Roev, L. M., Filimonov, V. N. and Terenin, A. N. Infrared spectra of molecules during their interaction with adsorption centers on an alumino-silicate catalyst. Optika I Spectroskopiia 4: 328-334. 1958.

108. Ross, S. and Olivier, J. P. On physical adsorption. Interscience Publishers, New York. 1964.

109. Scholes, S. R. Modern glass practice. Rev. ed., Industrial Publications, Inc., Chicago. 1952.

110. Senich, D. X-ray diffraction and adsorption isotherm studies of the calcium montmorillonite-H_2O system. Unpublished Ph.D. thesis. Ames, Iowa, Library, Iowa State University of Science and Technology. 1966.

111. Sewell, P. A. and Morgan, A. M. Methanol vapor adsorption on silica and soda-lime-silica glass. American Ceramic Society Journal 52(3): 136-138. 1968.

112. Sidov, A. N. Spectral investigation of the adsorption of water on porous glass as a function of the degree of hydration on its surface. Optics and Spectroscopy 8: 424-426. 1960.

113. Stanworth, J. E. Physical properties of glass. Oxford at the Clarendon Press, London. 1950.

114. Steacie, E. W. R. Solubility as a complicating factor in adsorption measurements at gas-solid interfaces. Journal Physical Chemistry 35: 2112-2117. 1931.

115. Taylor, H. S. The heterogeneity of catalyst surfaces for chemisorption. Advances in Catalysis 1: 1-26. 1948.

116. Tompkins, D. The study of multilayer formation on ionic adsorbents. U.S. Department of Commerce Clearinghouse AD 662 024. March, 1958.

117. Topping, J. Errors of observation and their treatment. The Institute of Physics, London. 1957.

118. Trapnell, B. M. W. Chemisorption. 2nd ed. Butterworths Scientific Publishers, Washington, D. C. 1964.

119. Tuzi, Y. Sorption of water vapor on glass surface in vacuum apparatus. Journal of Physics Society of Japan 17: 218-227. 1962.

120. Volf, M. B. Technical glass. Sir Isaac Pitman and Sons, Ltd., London. 1961.

121. Washburn, E. W. The dynamics of capillary flow. Physical Review Series 2, 17: 374-375. 1921.

122. Weast, R. C. and Selby, S. M. Handbook of chemistry and physics. 48 ed. The Chemical Rubber Company, Cleveland, Ohio. 1967.

123. Wicke, E. Empirische und theoretische untesuchungen der sorptionsgeschwindigekeit von gasen an porosen stoffen. I. Kolloid Zeitschrift 86: 167-186. 1939.

124. Young, T. An essay on the cohesion of fluids. Royal Society of London, Philosophical Transactions 95: 65-87. 1805.

125. Zisman, W. A. Influence of constitution on adhesion. Industrial and Engineering Chemistry 55(1): 18-38. 1963.

ACKNOWLEDGMENTS

This investigation was done as part of the study of composite materials conducted at the Engineering Research Institute, Iowa State University under the sponsorship of the Aerospace Research Laboratories Office of Aerospace Research, United States Air Force, Contract F 33615-68-c-1034. This support is gratefully acknowledged.

I wish to express my sincere appreciation to Dr. T. Demirel, Professor of Civil Engineering, for guidance, advice and assistance given throughout the investigation. The author is also indebted to Dr. T. D. McGee--Project Manager, Professor of Ceramic Engineering, Iowa State University, for his encouragement and guidance on glass surface structure problems. Thanks are also due to Dr. V. A. Fassel, Deputy Director of the Ames Laboratory, Iowa State University, and Dr. R. N. Kniseley, Chemistry Department, Iowa State University, for their advice and encouragement on infrared absorption problems. My thanks to Dr. H. F. Franzen, Associate Professor of Chemistry, Iowa State University, and Dr. H. Y. Chen, Department of Chemistry, Iowa State University, for their valuable advice on thermodynamical problems.

APPENDIX

Mathematical Formulation of Multimolecular Adsorption Isotherm

The following is an independent derivation of Brunauer, Emmett and Teller's (21) multimolecular adsorption isotherm equation. The approach followed in the derivation is that formulated by de Boer and his co-workers (29, 20).

To start, let us assume that the total number of molecules which is adsorbed per cm^2 is the sum of molecules covering a fraction of each layer, i.e.,

$$\sigma = \sigma_o \theta_1 + 2\sigma_o\theta_2 + 3\sigma_o\theta_3 + \ldots = \sigma_o \sum_{i=1}^{i=\infty} i\,\theta_i \qquad \text{(A1)}$$

where σ_o is the number of molecules which would form one complete monolayer on one cm^2 surface, and θ_i is the fraction of the surface actually covered by the ith layer.

The number of molecules striking and sticking to the bare surface must, at equilibrium, be equal to the number of molecules evaporating from the surface, hence for the first layer:

$$n\theta_o = \nu_o\sigma_o\theta_1 \qquad \text{(A2)}$$

where n is the number of molecules striking one cm^2 of the surface per second, θ_o the fraction of the total surface remaining bare and ν_o is the fraction of the adsorbed molecules of the first layer evaporating per second.

For dynamic equilibrium:

$$n\theta_o - n\theta_1 + \nu_1\sigma_o\theta_2 - \nu_o\sigma_o\theta_1 = 0 \qquad \text{(A3)}$$

the first term $n\theta_o$ corresponds to an increase in the first layer capacity due to adsorption on bare surface, the second term corresponds to a decrease in the first layer capacity due to adsorption on the first layer, the third term corresponds to an increase in the first layer capacity due to evaporation from the second layer, and the fourth term corresponds to a decrease in the first layer capacity due to evaporation from the first layer. For equilibrium the net result should be zero leading to Equation A3. Substituting Equation A2 into Equation A3, we obtain

$$n\theta_1 = \nu_1\sigma_o\theta_2 \ .$$

Continuing the same argument, we get for the ith layer:

$$n\theta_{i-1} = \nu_{i-1}\ \sigma_o\theta_i \ . \qquad \text{(A4)}$$

If we replace $\nu_i = 1/t_i$, where t_i is time of adsorption, the time during which a molecule remains adsorbed, we obtain the following expressions:

$$\sigma_o\theta_1 = n\ \theta_o\ t$$

$$\sigma_o\theta_2 = n\ \theta_1 t_1$$

$$\sigma_o\theta_i = n\ \theta_{i-1}\ \ t_{i-1} \ . \qquad \text{(A5)}$$

Furthermore, we will assume that the time of adsorption for a molecule bound on top of another adsorbed molecule of its own kind will be the same, i.e.,

$$t_1 = t_2 = \cdots = t_{i-1} = t_1 \tag{A6}$$

Therefore, Equation A5 can be simplified to

$$\theta_2 = X\,\theta_1$$

$$\theta_3 = X\,\theta_2 = X^2\theta_1$$

$$\theta_i = X^{i-1}\,\theta_1 \tag{A7}$$

where $X = nt_1/\sigma_o$. (A8)

Since $\theta_1 = nt\,\theta_o/\sigma_o$, by substituting this into Equation A7 we get:

$$\theta_i = X^i t\,\theta_o/t_1 \tag{A9}$$

The total number of molecules which are adsorbed is obtained by substituting the above expression into Equation A1:

$$\sigma = \sigma_o \sum_{i=1}^{i=\infty} i\theta_i = \sigma_o \frac{t}{t_1}\,\theta_o \sum_{i=1}^{i=\infty} i\,X^i \tag{A10}$$

where $\theta_o = 1 - \theta_1 - \theta_2 \cdots - \theta_i \cdots$

$$= 1 - \sum_{i=1}^{i=\infty} \theta_i$$

$$= 1 - \frac{t}{t_1}\,\theta_o \sum_{i=1}^{i=\infty} X^i\ . \tag{A11}$$

Rearranging:

$$\theta_o = \frac{1}{1 + \frac{t}{t_1} \sum_{i=1}^{i=\infty} X^i} \tag{A12}$$

Substituting Equation A12 into Equation A10 and putting $t/t_1 = C$, we obtain

$$\sigma = \frac{\sigma_o C \sum_{i=1}^{i=\infty} i\, X^i}{1 + C \sum_{i=1}^{i=\infty} X^i} \quad . \tag{A13}$$

Using the following mathematical expressions:

$$\sum_{i=1}^{i=\infty} i\, X^i = \frac{X}{(1-X)^2} \text{, and}$$

$$\sum_{i=1}^{i=\infty} X^i = \frac{X}{1-X} \text{, we get}$$

$$\sigma = \frac{C\, \sigma_o\, X}{(1-X)\ (1-X + CX)} \quad . \tag{A14}$$

Substituting the expression $X = nt_1/\sigma_o$ into the following well-known relationship

$$n = \frac{NP}{\sqrt{2\pi MRT}} = \beta P \tag{A15}$$

where N is Avogadro's constant, M is molecular weight of the adsorbate, we obtain

$$X = \frac{\beta t_1 P}{\sigma_o} \quad . \tag{A16}$$

Substituting $P_o = \sigma_o/\beta t_1$ into Equation A16,

$$X = P/P_o.$$

Inserting this into Equation A14, we get

$$\sigma = \frac{CP\sigma_o}{(P_o-P)[1 + (C-1)\ P/P_o]} \quad . \tag{A17}$$

Converting number of molecules of the adsorbate σ per cm^2 to volume of adsorbate V per gm of adsorbent using the following relationships:

$$\sigma = \frac{VPN}{M\ \Sigma} \quad \text{and} \quad \sigma_o = \frac{V_m PN}{M\ \Sigma} \tag{A18}$$

where P is the density, and V_m is the volume of the adsorbed gas when the entire surface is covered with a complete unimolecular layer, we get:

$$V = \frac{CP\ V_m}{(P_o-P)[1 + (C-1)\ P/P_o]}, \text{ or} \tag{A19}$$

$$\frac{P}{V(P_o-P)} = \frac{1}{V_m C} + \frac{C-1}{V_m C}\ \frac{P}{P_o} \ . \tag{A20}$$

This is the equation for the adsorption isotherm with three constant, e.g., C, P_o and V_m. If these three constants are evaluated from experimental data, the value for V_m gives a direct measure of the surface area Σ of the adsorbent, and the value C gives the heat of adsorption, i.e.,

$$C = t/t_1 = \frac{t_o\, e^{E_1/RT}}{t_{o1} e^{E_L/RT}} = e^{(E_1-E_L)/RT} \quad \text{(A21)}$$

since $t_o = t_{o1}$.

Definition of Adsorptive Enthalpy

In Figure 54, the adsorption of a gas at pressure p onto a solid surface S consists of a nonspontaneous liquefaction process with a free energy change of $dn\Delta G_1$ and a corresponding enthalpy change of $dn\Delta H_1$, and a spontaneous adsorptional spreading process with an adsorptive free energy change of $dn\Delta G$ and a corresponding adsorptive enthalpy change of $dn\Delta H$.* At equilibrium the free energy change of the whole process is zero, i.e.,

$$dn\Delta G_a = dn\Delta G_1 + dn\Delta G = 0. \quad \text{(A22)}$$

or
$$\Delta G = -\Delta G_1 \quad \text{(A23)}$$

Since
$$\Delta G_1 = RT \ln p_o/p \quad \text{(A24)}$$

$$\Delta G = -\Delta G_1 = -RT \ln p_o/p. \quad \text{(A25)}$$

However the enthalpy change, ΔH_a, for the whole process is not zero:

$$dn\Delta H_a = dn\Delta H_1 + dn\Delta H \quad \text{(A26)}$$

or adsorptive enthalpy, $\Delta H = \Delta H_a - \Delta H_1$ (A27)

corresponding to the free energy change ΔG.

---

*Free energy and enthalpy changes considered here are actually partial molar quantities namely chemical potential and partial molar enthalpy.

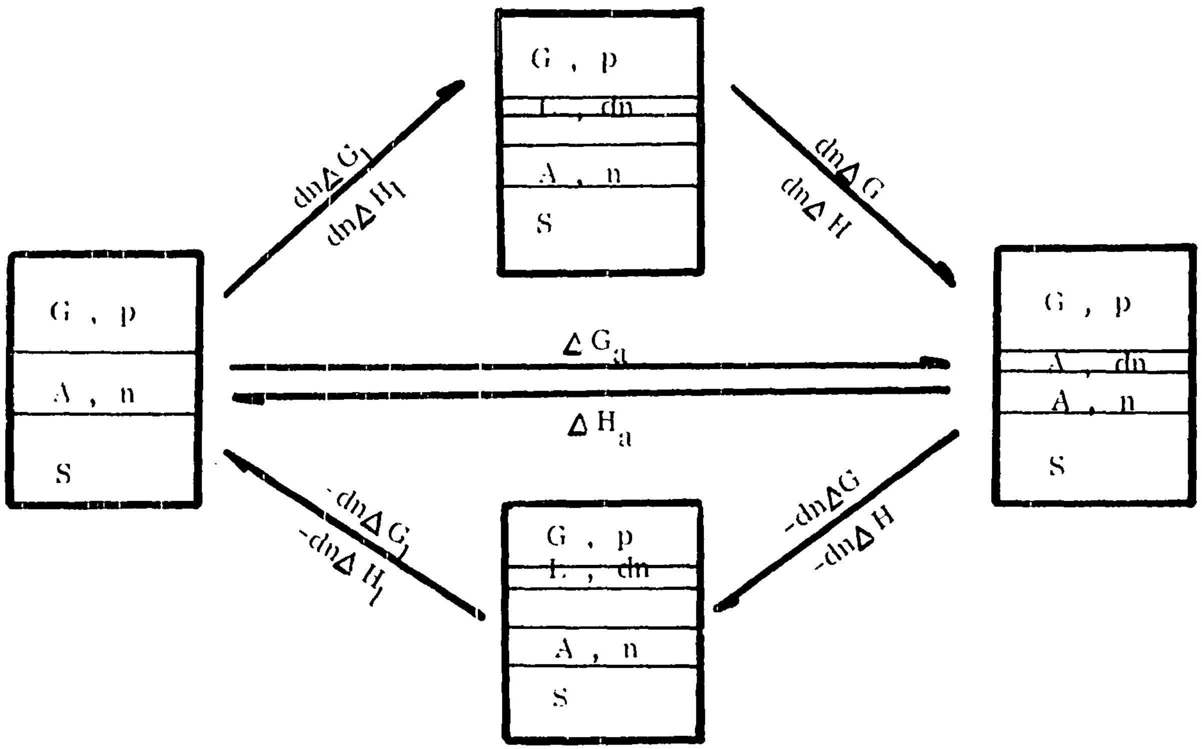

Figure 54. Thermodynamical sorption model at equilibrium

The same relations may be represented by the following steps:

$$A(g) \rightarrow A(l);\ \Delta G_l,\ \Delta H_l$$

$$+)\ A(l) \rightarrow A(a);\ \Delta G,\ \Delta H$$

$$\overline{}$$

$$A(g) \rightarrow A(a);\ \Delta G_a,\ \Delta H_a\ .$$

Adsorption Isotherm Data

<u>E-glass-water vapor system</u>

Table 20. Adsorption isotherm data for water on E-glass fiber, first run[a]

P, mmHg	$P/P_o, \times 10^{-2}$	$q, \times 10^{-3}$	$\frac{P/P_o}{q}$	$\frac{P/P_o}{q(1-P/P_o)}$	$\frac{q}{P/P_o}$
0.145	0.827	0.300	27.553	27.782	0.0363
0.443	2.468	0.329	75.033	76.931	0.0133
3.189	18.181	0.386	471.01	575.68	0.00214
5.882	33.535	0.457	733.80	1104.04	0.00136
8.605	49.059	0.600	817.65	1605.10	0.00122
11.091	63.233	0.701	902.03	2453.38	0.00111
12.936	73.751	0.801	920.74	3507.72	0.00109
14.038	80.034	0.872	917.82	4596.93	0.00109
15.035	85.718	0.952	900.21	6303.13	0.00111
15.651	89.230	1.000	892.30	8285.08	0.00112
16.192	92.315	1.072	860.51	11197.27	0.00116
16.558	94.401	1.258	750.41	13402.50	0.00133
17.062	97.275	1.544	630.02	23077.50	0.00159
17.393	99.162	3.288	301.58	30412.00	0.00332

[a] Note: P_o = 17.540 mmHg at 20.05°C

Table 21. Desorption isotherm data for water vapor on E-glass fiber, first run[a]

P, mmHg	p/p_o, $\times 10^{-2}$	q, $\times 10^{-3}$	$\frac{p/p_o}{q}$	$\frac{p/p_o}{q(1-p/p_o)}$	$\frac{q}{p/p_o}$
17.113	97.61	3.774	258.64	10821.67	0.00387
14.927	85.14	1.314	647.94	4360.33	0.00154
13.523	77.13	1.230	627.09	2742.37	0.00159
11.474	65.44	1.178	555.57	1607.83	0.00180
9.671	55.16	1.000	551.62	1230.25	0.00181
7.527	42.936	0.856	501.59	878.99	0.00199
6.209	35.420	0.914	387.53	600.07	0.00258
2.942	16.780	0.714	235.01	282.40	0.00425
0.945	5.389	0.744	72.43	76.56	0.01380
0.736	4.200	0.772	54.40	56.79	0.01840
0.561	3.200	0.744	43.01	44.43	0.02325

[a]Note: p_o = 17.54 mmHg at 20.05°C

Table 22. Adsorption isotherm data for water vapor on E-glass fiber, second run[a]

P, mmHg	$P/P_o, \times 10^{-2}$	$q, \times 10^{-3}$	$\frac{P/P_o}{q}$	$\frac{P/P_o}{q(1-P/P_o)}$	$\frac{q}{P/P_o}$
0.301	4.294	0.357	120.28	125.68	0.00831
1.514	21.59	0.415	520.24	663.49	0.00192
2.454	35.00	0.486	720.16	1107.94	0.00139
3.682	52.50	0.529	992.44	2089.34	0.00101
5.334	76.06	0.715	1063.77	4443.51	0.00094
6.085	86.77	0.815	1064.66	8047.34	0.00094
6.522	93.00	1.030	902.91	12898.75	0.00111
6.825	97.32	1.400	695.14	25938.17	0.00144

[a] Note: p_o = 7.913 mmHg at 6.00°C

Table 23. Desorption isotherm data for water vapor on E-glass fiber, second run[a]

P, mmHg	p/p_o, $\times 10^{-2}$	q, $\times 10^{-3}$	$\frac{p/p_o}{q}$	$\frac{p/p_o}{q(1-p/p_o)}$	$\frac{q}{p/p_o}$
7.2349	99.88	2.76	361.88	30157.00	0.00276
3.138	43.33	0.944	459.00	809.96	0.00217
1.079	14.90	0.572	260.49	306.09	0.00384
0.553	7.63	0.486	157.09	170.00	0.00636
0.261	3.60	0.543	66.32	68.79	0.01508
0	0	0.186	----	----	----

[a] Note: p_o = 7.2435 mmHg at 6.435°C

Table 24. Adsorption isotherm data for water vapor on E-glass powder, first run [a]

p, mmHg	p/p_o, x10^{-2}	q, x10^{-3}	$\frac{p/p_o}{q}$	$\frac{p/p_o}{q(1-p/p_o)}$	$\frac{q}{p/p_o}$
0.039	0.566	0.129	43.87	44.12	0.0228
0.130	1.85	0.272	68.07	69.35	0.0147
0.647	9.19	0.372	246.86	271.84	0.00405
1.606	22.82	0.387	589.71	764.08	0.00169
3.151	44.78	0.487	919.57	1665.28	0.00109
3.790	53.87	0.544	330.20	2146.55	0.00101
4.460	63.38	0.630	1006.03	2747.22	0.00099
5.409	76.87	0.802	958.17	4102.54	0.00104
5.796	82.37	0.945	871.21	4941.63	0 00115
5.864	83.34	1.271	655.70	3935.80	0.00152
6.172	87.73	1.576	556.66	4533.08	0.00179
6.429	91.38	1.827	500.16	5801.69	0.00200
6.452	91.71	2.203	416.29	5018.69	0.00240
6.655	94.59	3.080	307.11	5677.76	0.00325
6.622	94.11	3.402	276.63	4696.62	0.00361
6.741	95.81	4.244	225.75	5385.35	0.00443
6.841	97.22	5.175	187.86	6765.02	0.00532
6.910	98.21	6.035	162.73	9111.65	0.00614

[a] Note: P_o = 7.036 mmHg at 6.05°C

Table 25. Desorption isotherm data for water vapor on E-glass powder, first run[a]

p, mmHg	p/p_o, $\times 10^{-2}$	q, $\times 10^{-3}$	$\frac{p/p_o}{q}$	$\frac{p/p_o}{q(1-p/p_o)}$	$\frac{q}{p/p_o}$
6.777	96.318	4.212	228.67		0.00473
6.218	88.379	1.862	474.645	4084.38	0.00210
5.606	79.677	1.375	579.469	2851.29	0.00172
5.190	73.763	1.261	584.595	2229.51	0.00171
4.635	65.881	1.175	560.689	1643.33	0.00178
3.662	52.04	1.037	501.832	1046.35	0.00199
2.312	32.85	0.960	342.187	509.58	0.00292
1.285	18.267	0.945	193.199	236.38	0.00517
0.399	5.68	0.845	67.219	71.27	0.01488
0.252	3.50	0.845	42.367	43.94	0.0236

[a]Note: p_o = 7.036 mmHg at 6.05°C

Table 26. Adsorption isotherm data for water vapor on E-glass pellet, first run[a]

p, mmHg	$p/p_o, \times 10^{-2}$	$q, \times 10^{-3}$	$\frac{p/p_o}{q}$	$\frac{p/p_o}{q(1-p/p_o)}$	$\frac{q}{p/p_o}$
0.002	0.02	0.242	0.83	0.83	1.21
0.092	0.99	0.204	48.53	49.01	0.206
0.246	2.66	0.332	80.12	82.31	0.01248
0.285	3.08	0.319	96.55	99.62	0.01035
0.565	6.12	0.332	184.34	196.35	0.00542
0.783	8.47	0.408	207.59	226.81	0.00481
1.061	11.48	0.421	272.68	308.05	0.00367
1.633	17.66	0.459	384.75	467.27	0.00259
2.413	26.10	0.574	454.70	615.29	0.00219
2.979	32.22	0.638	505.01	745.08	0.00198
4.434	47.96	0.727	659.69	1267.67	0.00151
6.173	66.77	0.816	818.26	2462.41	0.00122
7.776	84.12	1.174	716.48	4510.43	0.00139
7.944	85.92	1.569	547.63	3890.56	0.00182
8.095	87.56	1.582	553.47	4449.17	0.00180
8.556	92.55	1.913	483.78	6491.07	0.00206
8.573	92.73	2.015	460.20	6330.10	0.00217
8.844	95.66	2.181	438.61	10106.13	0.00227
8.820	95.40	2.462	387.49	8423.69	0.00258

[a] Note: p_o = 9.245 mmHg at 10.06°C

Table 27. Desorption isotherm data for water vapor on E-glass pellet, first run[a]

P, mmHg	p/p_o, $\times 10^{-2}$	q, $\times 10^{-3}$	$\frac{p/p_o}{q}$	$\frac{p/p_o}{q(1-p/p_o)}$	$\frac{q}{p/p_o}$
7.997	86.51	1.78	485.988	3601.52	0.00206
6.987	75.57	1.44	524.83	2148.84	0.00190
6.074	65.70	1.34	490.30	1429.50	0.00204
5.308	57.42	1.31	438.31	1029.36	0.00228
4.437	47.99	1.22	393.42	756.53	0.00254
3.326	35.98	1.17	307.51	480.33	0.00325
1.945	21.04	1.07	196.65	249.06	0.00508.
1.527	16.52	1.05	157.32	188.45	0.00636
1.133	12.25	1.07	114.53	130.53	0.00873
0.344	3.72	0.98	38.02	39.49	0.02630
0	0	0.41	----	----	----

[a] Note: p_o = 9.245 mmHg at 10.06°C

Table 28. Adsorption isotherm data for water vapor on E-glass pellet, second run[a]

P, mmHg	$p/p_o, \times 10^{-2}$	$q, \times 10^{-3}$	$\frac{p/p_o}{q}$	$\frac{p/p_o}{q(1-p/p_o)}$	$\frac{q}{p/p_o}$
0.0986	0.56	0.089	63.14	63.50	0.0158
0.0926	0.528	0.191	27.64	27.79	0.0362
0.276	1.57	0.229	68.73	69.83	0.0145
0.435	2.48	0.318	78.02	80.00	0.0128
1.065	6.075	0.446	136.21	145.02	0.00734
1.704	9.72	0.523	185.85	205.86	0.00538
3.514	20.04	0.663	302.34	378.13	0.00331
4.371	24.93	0.688	362.41	482.792	0.00276
5.319	30.34	0.727	417.36	599.15	0.00239
6.727	38.37	0.778	493.24	800.37	0.00203
7.853	44.79	0.854	524.55	950.23	0.00191
8.935	50.97	0.944	539.93	1101.24	0.00185
10.144	57.87	1.020	567.31	1346.45	0.00176
11.125	63.463	1.-70	593.11	1623.32	0.00169
12.413	70.810	1.173	603.66	2068.06	0.00165
13.184	75.21	1.301	578.08	2379.71	0.00173
14.533	82.90	1.441	575.31	3365.01	0.00174
15.043	85.81	1.735	494.60	3486.29	0.00202
15.918	90.80	2.360	384.76	4184.02	0.00260
15.836	90.34	2.309	391.23	4048.37	0.00256

Table 28. (Continued)

P, mmHg	$p/p_o, \times 10^{-2}$	$q, \times 10^{-3}$	$\frac{p/p_o}{q}$	$\frac{p/p_o}{q(1-p/p_o)}$	$\frac{q}{p/p_o}$
16.717	95.362	3.533	269.92	5819.71	0.00370
16.808	95.88	3.942	234.23	5905.06	0.00411
16.822	95.96	3.840	249.90	6187.14	0.00400
17.015	97.06	5.396	179.87	6122.45	0.00556
17.097	97.530	5.268	185.13	7495.41	0.00540
17.151	97.838	6.544	149.51	6915.26	0.00669
17.169	97.94	6.646	147.37	7157.28	0.00678
17.262	98.47	7.233	136.14	8903.94	0.00734
17.491	99.78	9.083	109.85	49260.21	0.00910

[a]Note: p_o = 17.53 mmHg at 19.99°C

Table 29. Desorption isotherm data for water vapor on E-glass pellet, second run[a]

p, mmHg	p/p_o, x10^{-2}	q, x10^{-3}	$\frac{p/p_o}{q}$	$\frac{p/p_o}{q(1-p/p_o)}$	$\frac{q}{p/p_o}$
15.05	85.88	2.26	380.00	2691.22	0.00263
14.02	79.96	1.72	464.884	2319.78	0.00215
13.70	78.18	1.57	497.962	2282.13	0.00201
12.67	72.28	1.45	498.496	1798.46	0.00200
11.78	67.24	1.31	511.712	1561.95	0.00195
11.17	63.72	1.29	494.713	1363.56	0.00202
10.25	58.46	1.22	477.655	1150.00	0.00209
9.11	51.98	1.15	452.779	942.87	0.00221
8.51	48.53	1.02	475.823	924.54	0.00210
7.32	41.78	1.06	394.896	678.28	0.00253
6.36	36.27	1.03	351.103	550.91	0.00285
5.43	31.01	0.98	351.784	457.72	0.00316
4.35	24.83	0.98	252.810	336.30	0.00395
3.72	21.20	0.99	213.105	270.45	0.00469
2.88	16.41	0.90	181.348	216.95	0.00551
2.36	13.50	0.81	165.404	191.21	0.00604
0.81	4.60	0.79	58.266	61.07	0.01716
0.40	2.29	0.76	29.987	30.69	0.03335

[a]Note: p_o = 17.53 mmHg at 19.99°C

Table 30. Adsorption isotherm data for water vapor on E-glass pellet, third run[a]

p, mmHg	p/p_o, $\times 10^{-2}$	q, $\times 10^{-3}$	$\frac{p/p_o}{q}$	$\frac{p/p_o}{q(1-p/p_o)}$	$\frac{q}{p/p_o}$
0.054	0.307	0.06	51.17	51.32	0.0195
0.065	0.375	0.089	42.13	42.29	0.0237
0.097	0.556	0.153	36.34	36.54	0.0275
0.136	0.778	0.204	38.14	38.43	0.0262
0.248	1.414	0.318	44.46	45.10	0.0225
0.352	2.01	0.344	58.43	59.63	0.0171
0.621	3.544	0.408	86.86	90.05	0.0115
1.007	5.747	0.433	132.72	140.82	0.0075
1.368	7.80	0.459	169.93	184.31	0.0059
1.796	10.245	0.484	211.67	235.83	0.0047
2.385	13.607	0.535	254.33	294.39	0.0039
3.215	18.338	0.561	326.88	400.28	0.0030
3.931	22.427	0.586	382.71	493.34	0.0026
4.574	26.09	0.637	409.57	554.15	0.0024
5.555	31.69	0.689	459.94	673.31	0.0021

[a]Note: p_o = 17.53 mmHg at 19.99°C

Table 31. Adsorption isotherm data for water vapor on E-glass pellet, fourth run[a]

p,mmHg	p/p_o,x10^{-2}	q,x10^{-3}	$\frac{p/p_o}{q}$	$\frac{p/p_o}{q(1-p/p_o)}$	$\frac{q}{p/p_o}$
0.063	0.357	0.200	17.85	17.91	0.0560
0.153	0.875	0.269	32.53	32.81	0.0307
0.355	2.028	0.399	50.83	51.88	0.0196
1.342	7.656	0.503	152.21	164.83	0.00657
2.498	14.249	0.568	250.86	292.55	0.00398
3.398	19.383	0.594	326.31	404.77	0.00247
5.175	29.521	0.672	439.30	623.31	0.00160

[a]Note: p_o = 17.53 mmHg at 19.99°C

<u>E-glass-benzene vapor system</u>

Table 32. Adsorption isotherm data for benzene vapor on E-glass pellet, first run[a]

p,mmHg	p/p_o,10^{-2}	q,x10^{-3}	$\frac{p/p_o}{q}$	$\frac{p/p_o}{q(1-p/p_o)}$	$\frac{q}{p/p_o}$
1.430	1.98	0.236	80.51	87.07	0.01242
2.983	3.99	0.275	145.09	151.12	0.00689
4.929	6.59	0.335	196.71	210.59	0.00508
6.558	8.77	0.361	242.93	266.29	0.00412
8.207	10.97	0.375	292.53	328.58	0.00342

Table 32. (Continued)

p,mmHg	p/p_o,10^{-2}	q,$x10^{-3}$	$\frac{p/p_o}{q}$	$\frac{p/p_o}{q(1-p/p_o)}$	$\frac{q}{p/p_o}$
10.261	13.72	0.393	349.11	404.62	0.00286
11.954	15.98	0.393	406.61	483.95	0.00246
13.480	18.02	0.393	458.52	559.31	0.00218
15.254	20.39	0.393	518.83	651.71	0.00193
16.798	22.46	0.406	553.20	713.44	0.00181
18.565	24.82	0.406	611.33	813.15	0.00163
20.039	26.79	0.419	639.38	873.35	0.00156
21.644	28.93	0.419	690.45	971.65	0.00145
23.340	31.20	0.419	744.63	1082.31	0.00134
27.578	36.87	0.419	879.95	1393.87	0.00113
32.307	43.19	0.419	1030.78	1814.76	0.00097
36.376	48.63	0.419	1160.62	2259.33	0.00086
37.743	50.46	0.419	1204.29	2430.95	0.00083
38.954	52.07	0.419	1242.72	2592.78	0.00080
40.420	54.04	0.419	1289.74	2806.21	0.000.75
41.789	55.87	0.419	1333.41	3021.55	0.00075
43.140	57.67	0.419	1376.37	3251.53	0.00073
44.574	59.59	0.419	1422.19	3519.41	0.00070
45.907	61.37	0.419	1464.68	3791.55	0.00068
50.670	67.74	0.419	1616.71	5011.49	0.00062
50.966	68.13	0.419	1626.01	5102.02	0.00061

Table 32. (Continued)

p,mmHg	$p/p_o, 10^{-2}$	$q, \times 10^{-3}$	$\frac{p/p_o}{q}$	$\frac{p/p_o}{q(1-p/p_o)}$	$\frac{q}{p/p_o}$
52.046	69.58	0.433	1606.93	5282.47	0.00062
53.442	71.44	0.433	1649.88	5776.90	0.00061
54.774	73.22	0.433	1690.99	6314.39	0.00059
56.123	75.03	0.433	1732.79	6939.50	0.00058
57.127	76.37	0.446	1712.33	7246.43	0.00060
58.255	77.88	0.459	1696.73	7670.58	0.00059
57.954	77.47	0.472	1641.31	7285.01	0.00061
59.604	79.68	0.485	1642.88	8085.07	0.00061
60.202	80.48	0.498	1616.06	8279.02	0.00062
62.741	83.88	0.511	1641.48	10182.9	0.00061
63.530	84.93	0.524	1620.80	10755.1	0.00062
63.941	85.48	0.537	1591.80	10970.4	0.00063
66.686	89.15	0.616	1447.24	13338.6	0.00069
67.664	90.44	0.603	1499.83	15688.6	0.00068
69.623	93.07	0.655	1420.91	20503.8	0.00070
69.957	93.52	0.708	1320.90	20415.8	0.00076
70.492	94.24	0.760	1240.00	21527.8	0.00081
74.568	99.68	4.170	239.04	74700.2	0.00418

[a]Note: p_o = 74.803 mmHg at 19.866°C

Table 33. Adsorption isotherm data for benzene vapor on E-glass pellet, second run[a]

p, mmHg	$p/p_o, \times 10^{-2}$	$q, \times 10^{-3}$	$\frac{p/p_o}{q}$	$\frac{p/p_o}{q(1-p/p_o)}$	$\frac{q}{p/p_o}$
0.202	0.297	0.262	11.336	11.369	0.088215
0.639	0.940	0.171	54.971	55.492	0.018191
2.015	2.963	0.210	141.095	145.403	0.007087
3.640	5.353	0.262	204.313	215.868	0.004894
5.252	7.725	0.262	294.847	319.531	0.003391
6.918	10.175	0.262	388.358	432.350	0.002574
8.945	13.156	0.262	502.137	578.206	0.001991
11.413	16.787	0.262	640.725	769.982	0.001560
13.512	19.873	0.262	758.511	946.636	0.001318
14.991	22.049	0.262	841.565	1079.607	0.001188
17.403	25.596	0.262	976.946	1313.029	0.001023
23.471	34.522	0.262	1317.633	2012.330	0.000759

[a]Note: p_o = 67.99 mmHg at 18.00°C

Table 34. Adsorption isotherm data for benzene vapor on E-glass pellet, third run[a]

p, mmHg	p/p_o, x10^{-2}	q, x10^{-3}	$\frac{p/p_o}{q}$	$\frac{p/p_o}{q(1-p/p_o)}$	$\frac{q}{p/p_o}$
1.832	2.694	0.171	157.54	161.899	0.006347
4.424	6.506	0.210	309.81	331.347	0.003227
6.203	9.122	0.223	409.06	450.108	0.002444
8.033	11.813	0.234	506.02	574.401	0.001980
10.300	15.147	0.223	679.237	800.421	0.001472
11.952	17.579	0.234	751.239	911.477	0.001331
14.364	21.126	0.223	947.354	1201.007	0.001055
16.488	24.250	0.223	1087.444	1435.549	0.000919
18.537	27.264	0.231	1180.259	1622.573	0.000847
20.574	30.260	0.223	1356.950	1945.728	0.000736
22.802	33.538	0.223	1503.946	2262.934	0.000664
26.972	39.670	0.223	1778.923	2948.655	0.000562
31.034	45.645	0.210	2173.571	3998.475	0.000460
34.829	51.226	0.210	2439.333	5000.683	0.000409
39.101	57.510	0.210	2738.571	6445.214	0.000365
43.294	63.677	0.210	3032.238	8348.673	0.000329
47.687	70.138	0.210	3339.904	11185.213	0.000299
50.296	73.975	0.223	3317.264	12748.903	0.000301
53.069	78.054	0.223	3500.179	15946.147	0.000285

Table 34. (Continued)

p, mmHg	$p/p_o, \times 10^{-2}$	$q, \times 10^{-3}$	$\frac{p/p_o}{q}$	$\frac{p/p_o}{q(1-p/p_o)}$	$\frac{q}{p/p_o}$
54.599	80.304	0.231	3476.363	17646.515	0.000287
58.038	85.362	0.289	2953.70	20175.563	0.000338
61.667	90.700	0.342	2652.04	28516.632	0.000367
62.661	92.162	0.460	2003.52	25555.124	0.000499
63.900	93.984	0.552	1702.61	28282.53	0.000587
64.662	95.105	0.605	1571.98	32081.29	0.000636
65.543	96.401	0.750	1285.34	35704.07	0.000778
67.476	99.244	3.330	298.03	39214.47	0.003355
67.990	100	3.883	257.53		

[a] Note: p_o = 67.99 mmHg at 17.998°C

Geometric Surface Area Calculations for Fiberglas-E

Radius measurement from microscope photo

Instrument: Ultraphot II

Magnify power: 20 x 40

Flux: 8.6

Exposure time: 7 min. (auto)

Diameter: 8 mm/800 = 0.01 mm = 10 μ

<u>Surface area calculation</u>

$$A = 2n\pi r^2 + 2n\pi r l_i$$

$$V = n\pi r^2 l_i = 0.1076 \text{ cm}^3$$

where $l_i = 1.5$ cm, $r = 5\ \mu = 5 \times 10^{-4}$ cm. So, number of fibers

$$n = 0.1076/\pi \times 1.5 \times (5\times10^{-4})^2 = 9.16\times10^4$$

then, surface area

$$A = 2\times9.16\times10^4\times3.1415\times5\times10^{-4}(5\times10^{-4} + 1.5)$$

$$= 431.8 \text{ cm}^2$$

since weight of the sample = 0.27976 gram the specific surface of E-glass fiber:

$$\Sigma = 1550 \text{ cm}^2/\text{gm}$$

$$= 0.155 \text{ m}^2/\text{gm}.$$

Adsorption Energy Change Data

<u>E-glass-water vapor system</u>

The values of adsorption energy change, $-\Sigma \Delta F$, were obtained using Equation 48. The results presented here were derived from the adsorption isotherm data.

Table 35. Adsorption energy change of E-glass due to adsorption of water vapor

p/p_o	Adsorption energy change ($-\Sigma\Delta F$), erg/gmx10^6					
	Sample form Iso-temp. ^oC	Fiber 20.05	Fiber 6.05	Powder 6.05	Pellet 10.06	Pellet 19.99
0.025		0.86	0.81	0.88	0.74	1.14
0.050		1.07	0.99	1.07	1.01	1.48
0.100		1.30	1.24	1.30	1.32	1.91
0.200		1.64	1.56	1.63	1.71	2.47
0.300		1.86	1.77	1.84	1.99	2.85
0.400		2.03	1.93	2.04	2.22	3.15
0.500		2.19	2.09	2.14	2.42	3.40
0.600		2.34	2.23	2.27	2.60	3.64
0.700		2.49	2.37	2.39	2.76	3.86
0.800		2.62	2.50	2.53	2.93	4.08
0.900		2.77	2.64	2.72	3.14	4.38
1.000		2.98	2.84	3.26	3.48	4.94

E-glass-benzene vapor system

Adsorption energy changes for the benzene adsorption on E-glass pellet were obtained at two temperatures.

Table 36. Adsorption energy changes of E-glass pellet due to adsorption of benzene vapor

p/p_o	Adsorption energy change ($-\Sigma\Delta F$), erg/gmx10^5		
	Iso-temp. ^oC	19.86	18.00
0.025		1.58	1.07
0.050		2.15	1.46
0.100		2.88	1.90
0.200		3.64	2.36
0.300		4.22	2.63
0.400		4.59	2.81
0.500		4.88	2.95
0.600		5.11	3.06
0.700		5.31	3.16
0.800		5.49	3.27
0.900		5.69	3.38
1.000		6.10	3.72

Heats of Adsorption and Entropies of Adsorption Data

E-glass-water vapor system

Table 37. Calculated film thickness of water vapor adsorbed on E-glass fiber

t, Å	P/P_o 6.05	P/P_o 20.05	P, mmHg 6.05	P, mmHg 20.05	f 6.05	f 20.05	q_f[a] 6.05	q_f[a] 20.05
2.00	0.004	0.005	0.029	0.093	1.1207	1.1148	2.148	2.137
2.25	0.008	0.011	0.060	0.184	1.1238	1.1177	2.423	2.410
2.50	0.051	0.058	0.308	1.017	1.1307	1.1251	2.709	2.696
2.75	0.125	1.140	0.879	2.455	1.1353	1.1289	2.992	2.975
3.00	0.195	0.210	1.372	3.682	1.1373	1.1307	3.270	3.251
3.25	0.280	0.300	1.970	5.261	1.1388	1.1322	3.547	3.526
3.50	0.335	0.350	2.357	6.137	1.1397	1.1330	3.823	3.800
3.75	0.465	0.483	3.272	8.470	1.1411	1.1343	4.101	4.076
4.00	0.486	0.503	3.419	8.821	1.1413	1.1346	4.375	4.349
4.25	0.508	0.525	3.574	9.206	1.1415	1.1348	4.649	4.622
4.50	0.551	0.568	3.877	9.960	1.1419	1.1350	4.925	4.895
4.75	0.609	0.624	4.285	10.942	1.1423	1.1353	5.200	5.168
5.00	0.655	0.665	4.608	11.661	1.1426	1.1357	5.475	5.442
5.50	0.720	0.730	5.066	12.801	1.1430	1.1361	6.025	5.988
6.00	0.805	0.814	5.664	14.274	1.1435	1.1366	6.575	6.536
6.50	0.835	0.842	5.875	14.765	1.1437	1.1368	7.124	7.082
7.00	0.850	0.857	5.981	15.028	1.1438	1.1369	7.673	7.627
8.00	0.898	0.902	6.318	15.817	1.1440	1.1370	8.771	8.717
9.00	0.905	0.910	6.367	15.958	1.1440	1.1371	9.867	9.808
10.00	0.909	0.913	6.396	16.010	1.1440	1.1371	10.96	10.90
16.50	0.913	0.918	6.427	16.098	1.1441	1.1371	18.09	17.98
20.00	0.956	0.958	6.726	16.799	1.1442	1.1372	21.93	21.80

[a] Note: $q_f = t \cdot f \cdot \delta_B$

Table 38. Calculated film thickness of water vapor adsorbed on E-glass powdered pellet

t, Å	P/P_o 10.06	P/P_o 19.99	P, mmHg 10.06	P, mmHg 19.99	f 10.06	f 19.99	q_f[a] 10.06	q_f[a] 19.99
0.75	0.004	0.005	0.037	0.084	1.1198	1.1143	0.805	0.801
1.00	0.006	0.008	0.059	0.133	1.1218	1.1163	1.075	1.070
1.25	0.009	0.011	0.083	0.184	1.1252	1.1177	1.348	1.339
1.50	0.015	0.017	0.143	0.307	1.1256	1.1199	1.618	1.610
1.75	0.018	0.021	0.171	0.368	1.1264	1.1207	1.889	1.879
2.00	0.026	0.029	0.240	0.517	1.1279	1.1222	2.162	2.151
2.25	0.058	0.064	0.536	1.122	1.1313	1.1255	2.439	2.427
2.50	0.090	0.097	0.832	1.700	1.1332	1.1273	2.715	2.701
2.75	0.170	0.178	1.572	3.120	1.1361	1.1300	2.994	2.978
3.00	0.221	0.232	2.043	4.076	1.1371	1.1311	3.269	3.252
3.50	0.411	0.424	3.804	7.433	1.1398	1.1338	3.823	3.803
4.00	0.514	0.525	4.750	9.203	1.1403	1.1347	4.373	4.350
4.50	0.630	0.640	5.824	11.219	1.1418	1.1355	4.924	4.897
5.00	0.701	0.709	6.481	12.437	1.1421	1.1360	5.473	5.443
5.50	0.766	0.773	7.086	13.551	1.1426	1.1364	6.023	5.990
6.00	0.801	0.807	7.401	14.147	1.1427	1.1366	6.571	6.536
6.50	0.837	0.842	7.738	14.760	1.1429	1.1367	7.120	7.081
7.00	0.849	0.854	7.854	14.970	1.1430	1.1368	7.668	7.626
8.00	0.883	0.887	8.168	15.549	1.1431	1.1370	8.764	8.717
9.00	0.898	0.902	8.307	15.812	1.1432	1.1370	9.860	9.807
10.00	0.906	0.910	8.380	15.952	1.1432	1.1371	10.956	10.900
20.00	0.957	0.958	8.847	16.794	1.1434	1.1373	21.916	21.799

[a]Note: $q_f = t \cdot f \cdot \delta_B$

Table 39. Calculated heats of adsorption for water vapor adsorbed on E-glass fiber

q_f	P, mmHg 20.05	6.05	P_1/P_2	ln P_1/P_2	ΔH_a^a kcal/mole	q_d^a, kcal/mole 20.05	6.05
2	0.10	0.02	5.17	1.646	19.12	18.54	18.57
2.5	0.40	0.10	4.00	1.386	16.16	15.58	15.60
3	2.50	0.83	3.01	1.102	12.80	12.12	12.25
3.5	5.20	1.80	2.89	1.060	12.32	11.73	11.76
4	7.15	2.63	2.72	1.001	11.63	11.05	11.07
4.5	8.90	3.30	2.70	0.993	11.54	10.96	10.98
5	10.60	4.00	2.65	0.974	11.32	10.73	10.76
5.5	12.10	4.65	2.60	0.955	11.09	10.51	10.54
6	13.35	5.20	2.57	0.943	10.96	10.38	10.40
7	14.73	5.83	2.53	0.928	10.78	10.20	10.23
8	15.50	6.13	2.53	0.928	10.78	10.20	10.23
9	15.84	6.30	2.51	0.920	10.69	10.11	10.13
10	15.98	6.36	2.51	0.920	10.69	10.11	10.13
12	16.00	6.37	2.51	0.920	10.69	10.11	10.13
14	16.01	6.37	2.51	0.920	10.69	10.11	10.13
16	16.01	6.38	2.51	0.920	10.69	10.11	10.13
18	16.08	6.40	2.51	0.920	10.69	10.11	10.13
20	16.38	6.51	2.52	0.924	10.74	10.15	10.18
22	16.98	6.76	2.51	0.920	10.69	10.11	10.13

[a]Note: $\Delta H_a = RT_1T_2/(T_1 - T_2) \ln P_1/P_2$

$q_d = \Delta H_a - RT$

Table 40. Calculated heats of adsorption for water vapor adsorbed on E-glass pellet

q_f	P, mmHg 19.99	10.06	P_1/P_2	ln P_1/P_2	ΔH_a kcal/mole	q_d, kcal/mole 19.99	10.06
1	0.10	0.03	3.33	1.203	19.99	19.40	19.42
2	0.47	0.20	2.35	0.854	14.19	13.61	13.62
2.5	1.00	0.48	2.00	0.722	12.00	11.42	11.44
3	3.06	1.54	1.99	0.688	11.44	10.86	10.88
3.5	5.70	2.90	1.97	0.678	11.26	10.68	10.70
4	8.06	4.20	1.92	0.652	10.83	10.25	10.27
4.5	9.90	5.10	1.94	0.663	11.01	10.43	10.45
5	11.52	5.90	1.95	0.668	11.10	10.52	10.55
5.5	12.65	6.60	1.92	0.652	10.83	10.25	10.27
6	13.50	7.06	1.92	0.651	10.83	10.25	10.27
7	14.70	7.66	1.92	0.652	10.83	10.25	10.27
8	15.30	8.00	1.91	0.647	10.75	10.17	10.19
9	15.68	8.20	1.91	0.647	10.75	10.17	10.19
10	15.87	8.33	1.91	0.647	10.75	10.17	10.19
12	15.92	8.38	1.90	0.642	10.67	10.08	10.10
14	15.94	8.39	1.90	0.642	10.67	10.08	10.10
16	15.95	8.40	1.90	0.642	10.67	10.08	10.10
18	16.00	8.41	1.90	0.642	10.67	10.08	10.10
20	16.27	8.50	1.91	0.647	10.75	10.17	10.19
22	16.86	8.90	1.89	0.636	10.57	9.98	10.00

Table 41. Gibbs free energy and entropy of adsorption for water vapor adsorbed on E-glass fiber

q_f	t, Å 20.05	t, Å 6.05	ΔH_a kcal/mole	$-\Delta H$, kcal/mole 20.05	$-\Delta H$, kcal/mole 6.05	P/P_o 20.05	P/P_o 6.05	$-\Delta G$, kcal/mole 20.05	$-\Delta G$, kcal/mole 6.05	$-\Delta S$, e.u. 20.05	$-\Delta S$, e.u. 6.05
2	1.87	1.86	19.125	8.584	8.45	0.006	0.004	3.01	3.03	19.00	19.43
2.5	2.33	2.32	16.10	5.43	5.56	0.023	0.008	2.20	2.65	11.00	10.44
3	2.77	2.75	12.80	2.26	2.13	0.143	0.118	1.13	1.18	3.85	3.39
3.5	3.22	3.21	12.32	1.78	1.64	0.296	0.256	0171	0.76	3.64	3.18
4	3.68	3.66	11.63	1.09	0.96	0.408	0.374	0.52	0.55	2.47	2.31
4.5	4.14	4.11	11.54	1.00	0.86	0.507	0.469	0.39	0.42	2.05	1.59
5	4.59	4.57	11.32	0.78	0.64	0.604	0.568	0.29	0.31	1.65	1.18
5.5	5.05	5.02	11.09	0.55	0.42	0.690	0.661	0.22	0.23	1.16	0.69
6	5.51	5.47	10.96	0.42	0.28	0.761	0.725	0.16	0.18	0.88	0.38
7	6.42	6.38	10.78	0.24	0.11	0.840	0.828	0.10	0.10	0.48	0.02
8	7.34	7.29	10.78	0.24	0.11	0.881	0.871	0.07	0.07	0.10	-0.38
9	8.26	8.21	10.69	0.15	0.02	0.903	0.895	0.06	0.06	0.31	-0.16
10	9.17	9.12	10.69	0.15	0.02	0.911	0.904	0.05	0.05	0.33	-0.14
12	11.01	10.94	10.69	0.15	0.02	0.912	0.905	0.05	0.05	0.33	-0.13
14	12.84	12.77	10.69	0.15	0.02	0.913	0.905	0.05	0.05	0.33	-0.13
16	14.68	14.59	10.69	0.15	0.02	0.913	0.907	0.05	0.05	0.33	-0.13
18	16.51	16.41	10.69	0.15	0.02	0.917	0.909	0.05	0.05	0.34	-0.12
20	18.35	18.24	10.69	0.19	0.06	0.934	0.925	0.04	0.04	0.53	0.08
22	20.18	20.06	10.69	0.15	0.02	0.968	0.961	0.02	0.02	0.44	-0.01

Table 42. Gibbs free energy and entropy of adsorption for water vapor adsorbed on E-glass pellet

q_f	t, Å 19.99	t, Å 10.06	ΔH_a kcal/mole	$-\Delta H$, kcal/mole 19.99	$-\Delta H$, kcal/mole 10.06	P/P_o 19.99	P/P_o 10.06	$-\Delta G$, kcal/mole 19.99	$-\Delta G$, kcal/mole 10.06	$-\Delta S$, e.u. 19.99	$-\Delta S$, e.u. 10.06
1	0.93	0.93	19.98	9.44	9.35	0.006	0.003	3.03	3.22	21.88	21.63
2	1.86	1.85	14.19	4.46	4.37	0.027	0.025	2.11	2.06	8.03	8.13
2.5	2.32	2.30	12.40	1.86	1.76	0.057	0.054	1.67	1.64	0.65	0.43
3	2.77	2.75	11.74	1.20	1.11	0.175	0.168	1.02	1.04	0.63	0.23
3.5	3.22	3.20	11.26	0.72	0.63	0.325	0.314	0.65	0.67	0.24	0
4	3.68	3.66	10.83	0.29	0.20	0.460	0.454	0.45	0.44		0
4.5	4.13	4.11	11.02	0.47	0.38	0.565	0.552	0.33	0.33	0.49	0.16
5	4.59	4.57	11.10	0.56	0.46	0.657	0.638	0.24	0.25	1.07	0.74
5.5	5.05	5.02	10.83	0.29	0.20	0.722	0.714	0.19	0.19	0.35	0.02
6	5.51	5.48	10.83	0.29	0.20	0.762	0.764	0.16	0.15	0	0
7	6.42	6.39	10.83	0.29	0.20	0.838	0.828	0.10	0.11	0.65	0.47
8	7.34	7.30	10.75	0.21	0.11	0.873	0.865	0.08	0.08	0.44	0.12
9	8.26	8.21	10.75	0.21	0.11	0.894	0.887	0.06	0.07	0.49	0.16
10	9.17	9.13	10.75	0.21	0.11	0.905	0.901	0.06	0.06	0.51	0.19
12	11.01	10.95	10.67	0.13	0.04	0.908	0.906	0.05	0.05	0.24	0
14	12.85	12.78	10.67	0.13	0.04	0.909	0.907	0.05	0.05	0.24	0
16	14.68	14.60	10.67	0.13	0.04	0.910	0.908	0.05	0.05	0.24	0
18	16.51	16.43	10.67	0.13	0.04	0.913	0.910	0.05	0.05	0.25	0
20	18.35	18.25	10.67	0.21	0.11	0.928	0.919	0.04	0.05	0.56	0.23
22	20.18	20.07	10.57	0.03	-0.03	0.962	0.963	0.02	0.02	0.01	0

E-glass-benzene vapor system

Table 43. Calculated film thickness of benzene vapor adsorbed on E-glass pellet

t, Å	p/p_o 18.00	p/p_o 19.86	p, mmHg 18.00	p, mmHg 19.86	f 18.00	f 19.86	q_f[a] 18.00	q_f[a] 19.86
2	0.0125	0.0133	0.849	0.995	1.110	1.107	1.811	1.807
2.25	0.0138	0.0147	0.918	1.099	1.111	1.108	2.038	2.034
2.50	0.0152	0.0162	1.033	1.212	1.111	1.109	2.267	2.261
2.75	0.0170	0.0180	1.156	1.346	1.112	1.109	2.494	2.488
3.00	0.0185	0.0197	1.258	1.473	1.112	1.109	2.722	2.715
3.25	0.0216	0.0230	1.468	1.720	1.113	1.110	2.951	2.943
3.50	0.0255	0.0267	1.734	1.997	1.114	1.111	3.181	3.172
3.75	0.0295	0.0315	2.006	2.356	1.115	1.112	3.410	3.402
4.00	0.0360	0.0380	2.447	2.842	1.116	1.113	3.641	3.631
4.50	0.0730	0.0770	4.963	5.759	1.120	1.117	4.110	4.100
4.75	0.1000	0.1050	6.799	7.854	1.122	1.118	4.348	4.334
5.00	0.160	0.166	10.878	12.417	1.124	1.121	4.584	4.572
5.25	0.305	0.310	20.744	23.188	1.127	1.124	4.828	4.815
5.50	0.730	0.740	49.632	55.553	1.132	1.129	5.079	5.066
6.00	0.798	0.800	54.256	59.879	1.132	1.129	5.542	5.529
6.50	0.860	0.865	57.791	64.703	1.132	1.130	6.006	5.991
7.00	0.890	0.894	59.151	66.873	1.133	1.130	6.469	6.453
8.00	0.950	0.954	64.590	71.361	1.133	1.130	7.396	7.376
9.00	0.960	0.963	65.270	72.034	1.133	1.130	8.321	8.299
10.00	0.980	0.892	66.630	73.455	1.133	1.130	9.247	9.222

[a] $q_f = tf\delta_b$

Table 44. Calculated heats of adsorption for benzene adsorbed on E-glass pellet

q_f	p, mmHg 18.00	p, mmHg 19.86	p_1/p_2	$\ln p_1/p_2$	ΔH_a^a kcal/mole	q_d^b, kcal/mole 18.00	q_d^b, kcal/mole 19.86
2.0	0.071	0.084	1.20	0.182	16.625	16.047	16.043
2.5	0.900	0.107	1.19	0.178	16.224	15.746	15.742
3.0	1.30	1.55	1.19	0.174	15.859	15.281	15.277
3.5	2.20	2.60	1.18	0.169	15.467	14.889	14.885
4.0	3.90	4.60	1.18	0.165	15.094	14.516	14.512
4.5	10.0	11.5	1.15	0.140	12.760	12.182	12.178
5.0	49.0	55.5	1.13	0.124	11.356	10.778	10.774
5.5	54.5	61.0	1.12	0.113	10.326	9.748	9.742
6.0	57.6	64.2	1.11	0.109	9.998	9.420	9.416
7.0	63.0	69.6	1.11	0.104	9.515	8.937	8.933
8.0	65.0	72.0	1.11	0.102	9.360	8.782	8.778
9.0	65.9	72.8	1.10	0.101	9.187	8.609	8.605
10.0	66.3	73.3	1.10	0.100	9.114	8.536	8.532
18.5	67.1	73.9	1.10	0.098	8.932	8.354	8.350

$^a\Delta H_a = RT_1T_2/(T_1 - T_2)\ln p_1/p_2$

$^b q_d = \Delta H_a - RT$

Table 45. Gibbs free energy and entropy of adsorption for benzene adsorbed on E-glass pellet

q_f	t, Å 18.00	t, Å 19.86	ΔH_a kcal/mole	$-\Delta H$, kcal/mole[a] 18.00	$-\Delta H$, kcal/mole[a] 19.86	p/p_o 18.00	p/p_o 19.86	$-\Delta G$, kcal/mole 18.00	$-\Delta G$, kcal/mole 19.86	$-\Delta S$, e.u. 18.00	$-\Delta S$, e.u. 19.86
1	1.05	1.06	17.05	8.87	8.89	0.01	0.01	2.72	2.71	21.10	21.08
1.5	1.60	1.63	16.80	8.62	8.64	0.01	0.01	2.68	2.64	20.38	20.47
2	2.17	2.18	16.63	8.44	8.46	0.01	0.01	2.53	2.50	20.30	20.25
2.5	2.68	2.70	16.22	8.04	8.06	0.02	0.02	2.36	2.34	19.51	19.53
3	3.20	3.23	15.86	7.68	7.70	0.02	0.02	2.26	2.23	18.59	18.66
3.5	3.77	3.81	15.47	7.28	7.31	0.03	0.03	1.96	1.96	18.28	18.24
4	4.24	4.28	15.09	6.91	6.93	0.06	0.06	1.66	1.66	18.03	17.99
4.5	4.81	4.85	12.76	4.52	4.60	0.13	0.15	1.16	1.12	11.73	11.87
5	5.35	5.39	11.36	3.17	3.20	0.73	0.73	0.18	0.18	10.27	10.28
5.5	6.00	6.04	10.33	2.14	2.17	0.80	0.81	0.13	0.13	6.91	6.94
6	6.46	6.51	10.00	1.81	1.84	0.87	0.87	0.08	0.08	5.95	5.99
7	7.51	7.58	9.52	1.33	1.35	0.94	0.94	0.04	0.04	4.44	4.49
8	8.60	8.69	9.36	1.18	1.20	0.96	0.97	0.02	0.92	3.96	4.01
9	9.71	9.80	9.19	1.00	1.02	0.97	0.98	0.02	0.02	3.39	3.45
10	10.80	10.90	9.11	0.93	0.95	0.99	1.00	0.01	0.01	3.17	3.23
18.5	20.01	20.12	8.93	0.74	0.77	1.00	1.00	0.00	0.00	2.55	2.61

[a] Heat of condensation was calculated from the following equation (4):

$$\Delta H_l = 5922.4R - 6.194RT$$

Sorption Rate Data

Table 46. Adsorption rate data for water vapor adsorbed on IR-activated E-glass pellet at 20°C

t, min.	Q, mg	q, mg/mg	$q_f/(q_f-q)$	n molec./gm	dn/dt molec./gm.min.
0.5	0.0880	0.00029	1.0223	9.63×10^{18}	1.93×10^{19}
1	0.1232	0.00040	1.0315	1.35×10^{19}	7.71×10^{18}
2	0.1808	0.00059	1.04695	1.98×10^{19}	6.31×10^{18}
3	0.240	0.00078	1.06329	2.63×10^{19}	6.48×10^{18}
4	0.3072	0.00100	1.08247	3.36×10^{19}	7.36×10^{18}
5	0.3744	0.00122	1.10236	4.10×10^{19}	7.36×10^{18}
6	0.440	0.00143	1.12249	4.82×10^{19}	7.28×10^{18}
8	0.552	0.00180	1.15862	6.04×10^{19}	6.13×10^{18}
10	0.6144	0.00200	1.17978	6.73×10^{19}	3.42×10^{18}
12	0.7488	0.00244	1.22807	8.20×10^{19}	7.36×10^{18}
18	1.00096	0.00329	1.33404	1.10×10^{20}	4.76×10^{18}
24	1.2096	0.00394	1.42857	1.32×10^{20}	3.65×10^{18}
30	1.3728	0.00447	1.51625	1.50×10^{20}	2.98×10^{18}
36	1.536	0.00500	1.61538	1.68×10^{20}	2.98×10^{18}
42	1.6896	0.00550	1.72131	1.85×10^{20}	2.80×10^{18}
48	1.8368	0.00598	1.83673	2.01×10^{20}	2.69×10^{18}
54	1.9648	0.00640	1.95046	2.15×10^{20}	2.33×10^{18}
60	2.064	0.00672	2.04878	2.26×10^{20}	1.81×10^{18}
90	2.609	0.00850	2.83463	2.85×10^{20}	1.99×10^{18}
120	2.94242	0.00958	3.70044	3.22×10^{20}	1.21×10^{18}

Table 47. Adsorption rate data for water vapor adsorbed on non IR-activated E-glass pellet at 20°C

t, min	Q, mg	q, mg/mg	$q_f/(q_f-q)$	n molec./gm	dn/dt molec./gm.min.
0.5	0.080	0.00026	1.3195	8.78×10^{18}	1.75×10^{19}
1	0.141	0.00046	1.05763	1.54×10^{19}	1.33×10^{19}
2	0.243	0.00079	1.10390	2.66×10^{19}	1.12×10^{19}
3	0.344	0.00112	1.15357	3.76×10^{19}	1.10×10^{19}
4	0.416	0.00135	1.19188	4.55×10^{19}	7.87×10^{18}
5	0.480	0.00156	1.22814	5.25×10^{19}	7.00×10^{18}
6	0.5376	0.00175	1.26271	5.88×10^{19}	6.30×10^{18}
8	0.6160	0.00200	1.31301	6.738×10^{19}	4.287×10^{18}
10	0.7232	0.00235	1.3865	7.910×10^{19}	5.86×10^{18}
12	0.7920	0.00258	1.44196	8.663×10^{19}	3.76×10^{18}
18	0.9808	0.00319	1.61178	1.07×10^{20}	3.44×10^{18}
24	1.1280	0.00367	1.77473	1.23×10^{20}	2.68×10^{18}
30	1.2560	0.00408	1.94578	1.37×10^{20}	2.33×10^{18}
36	1.3680	0.00445	2.12500	1.49×10^{20}	2.04×10^{18}
42	1.4672	0.00477	2.31375	1.60×10^{20}	1.81×10^{18}
48	1.5600	0.00507	2.52344	1.71×10^{20}	1.69×10^{18}
54	1.6416	0.00534	2.74194	1.79×10^{20}	1.48×10^{18}
60	1.7152	0.00558	2.97422	1.876×10^{20}	$1.3r\times10^{18}$
90	2.000	0.00650	4.42466	2.187×10^{20}	1.04×10^{18}
120	2.192	0.00713	6.59184	2.397×10^{20}	7.00×10^{17}
180	2.427	0.00789	16.47959	2.654×10^{20}	4.29×10^{17}
240	2.520	0.00820	40.3750	2.756×10^{20}	1.69×10^{17}
300	2.568	0100835	161.5000	2.808×10^{20}	8.75×10^{16}

Table 48. Adsorption rate data for water vapor adsorbed on IR-activated E-glass pellet at 18°C

t, min	Q, mg	q, mg/mg	$q_f/(q_f-q)$	n molec./gm	dn/dt molec./gm.min.
0.5	0.052	0.00017	1.0327	5.69×10^{18}	1.14×10^{19}
1	0.088	0.00028	1.0565	9.64×10^{18}	7.88×10^{18}
2	0.156	0.00051	1.1048	1.71×10^{19}	7.44×10^{18}
3	0.184	0.00060	1.1260	2.01×10^{19}	3.07×10^{18}
4	0.212	0.00069	1.1480	2.32×10^{19}	3.07×10^{18}
5	0.252	0.00082	1.1810	2.76×10^{19}	4.38×10^{18}
6	0.288	0.00094	1.2124	3.15×10^{19}	3.94×10^{18}
8	0.340	0.00111	1.2607	3.72×10^{19}	2.85×10^{18}
10	0.392	0.00127	1.3131	4.29×10^{19}	2.85×10^{18}
12	0.444	0.00144	1.3700	4.86×10^{19}	2.85×10^{18}
18	0.576	0.00187	1.5393	6.31×10^{19}	2.41×10^{18}
24	0.684	0.00223	1.7125	7.49×10^{19}	1.97×10^{18}
30	0.792	0.00258	1.9296	8.67×10^{19}	1.97×10^{18}
36	0.892	0.00290	2.1862	9.77×10^{19}	1.82×10^{18}
42	0.972	0.00318	2.4610	1.07×10^{20}	1.53×10^{18}
48	1.052	0.00342	2.7770	1.15×10^{20}	1.38×10^{18}
54	1.120	0.00365	3.1374	1.22×10^{20}	1.24×10^{18}
60	1.160	0.00378	3.3967	1.27×10^{20}	7.30×10^{17}
90	1.300	0.00423	4.7791	1.42×10^{20}	5.10×10^{17}
120	1.372	0.00447	6.0441	1.50×10^{20}	2.63×10^{17}
180	1.440	0.00469	8.0588	1.58×10^{20}	1.24×10^{17}
240	1.4920	0.00486	10.8158	1.63×10^{20}	9.49×10^{16}
300	1.5360	0.00500	15.2222	1.68×10^{20}	8.03×10^{16}

Table 49. Adsorption rate data for water vapor adsorbed on non IR-activated E-glass pellet at 18°C

t, min	Q, mg	q, mg/mg	$q_f/(q_f-q)$	n molec./gm.	dn/dt molec./gm. min.
0.5	0.0432	0.00014	1.04135	4.73×10^{18}	9.46×10^{18}
1	0.06160	0.00020	1.06002	6.74×10^{18}	4.03×10^{18}
2	0.0768	0.00025	1.07595	8.41×10^{18}	1.66×10^{18}
3	0.120	0.00039	1.12397	1.31×10^{19}	4.73×10^{18}
4	0.1472	0.00048	1.15646	1.61×10^{19}	2.98×10^{18}
5	0.184	0.00060	1.20354	2.01×10^{19}	4.03×10^{18}
6	0.2056	0.00067	1.23300	2.25×10^{19}	2.36×10^{18}
8	0.2584	0.00084	1.31148	2.83×10^{19}	2.89×10^{18}
10	0.3104	0.00101	1.39918	3.39×10^{19}	2.84×10^{18}
12	0.3408	0.00111	1.45610	3.73×10^{19}	1.66×10^{18}
18	0.4456	0.00145	1.69365	4.88×10^{19}	1.91×10^{18}
24	0.5256	0.00171	1.93457	5.75×10^{19}	1.46×10^{18}
30	0.6088	0.00198	2.27045	6.67×10^{19}	1.52×10^{18}
36	0.6760	0.00220	2.64078	7.40×10^{19}	1.22×10^{18}
42	0.7392	0.00241	3.11927	8.09×10^{19}	1.15×10^{18}
48	0.7992	0.00260	3.76731	8.75×10^{19}	1.09×10^{18}
54	0.8520	0.00277	4.61017	9.33×10^{19}	9.63×10^{17}
60	0.87040	0.00283	5.0000	9.53×10^{19}	3.36×10^{17}
90	1.0088	0.00328	13.73737	1.10×10^{20}	5.05×10^{17}
120	1.0488	0.00341	27.75510	1.15×10^{20}	1.46×10^{17}
180	1.0576	0.00344	35.78947	1.16×10^{20}	1.60×10^{16}
240	1.0696	0.00348	59.13043	1.17×10^{20}	2.19×10^{16}
300	1.0760	0.00350	90.66667	1.18×10^{20}	1.17×10^{16}

Table 50. Adsorption rate data for water vapor adsorbed on IR-activated E-glass pellet at 18.9°C

t, min	Q, mg	q, mg/mg	$q_f/(q_f-q)$	n molec./gm	dn/dt molec./gm.min.
0.5	0.056	0.00018	1.0160	6.132×10^{18}	1.23×10^{19}
1	0.104	0.00034	1.0302	1.139×10^{19}	1.05×10^{19}
2	0.152	0.00049	1.0447	1.664×10^{19}	5.256×10^{18}
3	0.192	0.00062	1.0571	2.102×10^{19}	4.38×10^{18}
4	0.232	0.00075	1.0699	2.540×10^{19}	4.38×10^{18}
5	0.264	0.00086	1.0803	2.89×10^{19}	3.504×10^{18}
6	0.296	0.00096	1.0909	3.241×10^{19}	3.50×10^{18}
8	0.456	0.00148	1.1473	4.993×10^{19}	4.38×10^{18}
10	0.456	0.00148	1.1473	4.993×10^{19}	4.38×10^{18}
12	0.536	0.00174	1.1777	4.869×10^{19}	4.38×10^{18}
18	0.744	0.00242	1.2649	8.147×10^{19}	3.79×10^{18}
24	0.920	0.00299	1.3495	1.007×10^{20}	3.21×10^{18}
30	1.088	0.00354	1.4415	1.191×10^{20}	3.06×10^{18}
36	1.240	0.00404	1.5363	1.358×10^{20}	2.77×10^{18}
42	1.352	0.00440	1.6145	1.480×10^{20}	2.04×10^{18}
48	1.424	0.00464	1.6692	1.559×10^{20}	1.31×10^{18}
54	1.528	0.00497	1.7549	1.673×10^{20}	1.89×10^{18}
60	1.621	0.00528	1.8393	1.775×10^{20}	1.69×10^{18}
90	2.000	0.00651	2.2886	2.190×10^{20}	1.38×10^{18}
120	2.264	0.00737	2.7577	2.479×10^{20}	9.63×10^{17}
180	2.640	0.00859	3.8947	2.891×10^{20}	6.86×10^{17}
240	2.928	0.00953	5.6923	3.206×10^{20}	5.25×10^{17}
300	3.096	0.01008	7.7894	3.390×10^{20}	3.06×10^{17}

Table 51. Adsorption rated data for water vapor adsorbed on non IR-activated E-glass pellet at 18.9°C

t, min.	Q, mg	q, mg/mg	$q_f/(q_f-q)$	n molec./gm	dn/dt molec./gm.min.
0.5	0.060	0.00020	1.0386	6.57×10^{18}	1.31×10^{19}
1	0.116	0.00038	0.0775	1.27×10^{19}	5.23×10^{18}
2	0.164	0.00053	1.1133	1.79×10^{19}	5.25×10^{18}
3	0.209	0.00068	1.1494	2.29×10^{19}	4.99×10^{18}
4	0.252	0.00082	1.1853	2.76×10^{19}	4.64×10^{18}
5	0.292	0.00095	1.2212	3.19×10^{19}	4.38×10^{18}
6	0.324	0.00105	1.2515	3.54×10^{19}	3.50×10^{18}
8	0.428	0.00139	1.3615	4.68×10^{19}	5.69×10^{18}
10	0.492	0.00160	1.4394	5.38×10^{19}	3.50×10^{18}
12	0.548	0.00178	1.5150	6.00×10^{19}	3.06×10^{18}
18	0.676	0.00220	1.7222	7.40×10^{19}	2.33×10^{18}
24	0.796	0.00259	1.9755	8.71×10^{19}	2.19×10^{18}
30	0.888	0.00289	2.2265	9.72×10^{19}	1.68×10^{18}
36	0.980	0.0032	2.5506	1.07×10^{20}	1.68×10^{18}
42	1.052	0.0034	2.8786	1.15×10^{20}	1.31×10^{18}
48	1.1104	0.0036	3.2137	1.21×10^{20}	1.06×10^{18}
54	1.1560	0.00376	3.5351	1.26×10^{20}	8.32×10^{17}
60	1.1960	0.00389	3.8750	1.31×10^{20}	7.30×10^{17}
90	1.3080	0.00426	5.3026	1.43×10^{20}	4.08×10^{17}
120	1.3840	0.0045	7.0701	1.51×10^{20}	2.77×10^{17}
180	1.4400	0.0047	9.3721	1.57×10^{20}	1.02×10^{17}
240	1.4800	0.0048	12.2121	1.62×10^{20}	7.30×10^{16}
300	1.5440	0.0050	23.7059	1.69×10^{20}	1.17×10^{17}